Summer 2017

A Computational Investigation of BODIPY Excited State Properties and Photosensitization of Molecular Oxygen

Keenan Komoto

Western Washington University, komotok@wwu.edu

A Computational Investigation of BODIPY Excited State Properties and Photosensitization of Molecular Oxygen

by

Keenan Komoto

Accepted in Partial Completion
of the Requirements for the Degree
of

Master of Science

Kathleen L. Kitto, Dean of the Graduate School

ADVISORY COMMITTEE

Chair, Dr. Tim Kowalczyk

Dr. Robert Berger

Dr. Steven R. Emory

MASTER'S THESIS

In presenting this thesis in partial fulfillment of the requirements for a masters degree at Western Washington University, I grant to Western Washington University the non-exclusive royalty-free right to archive, reproduce, distribute, and display the thesis in any and all forms, including electronic format, via any digital library mechanisms maintained by WWU.

I represent and warrant this is my original work, and does not infringe or violate any rights of others. I warrant that I have obtained written permissions from the owner of any third party copyrighted material included in these files.

I acknowledge that I retain ownership rights to the copyright of this work, including but not limited to the right to use all or part of this work in future works, such as articles or books.

Library users are granted permission for individual, research and non-commercial reproduction of this work for educational purposes only. Any further digital posting of this document requires specific permission from the author.

Any copying or publication of this thesis for commercial purposes, or for financial gain, is not allowed without my written permission.

Keenan Komoto

June 16th, 2017

A Computational Investigation of BODIPY Excited State Properties and Photosensitization of Molecular Oxygen

A Thesis
Presented to
The Faculty of
Western Washington University

In Partial Fulfillment
Of the Requirements for the Degree
Master of Science

by
Keenan Komoto
June 2017

Abstract

Cancer has long been a significant problem that has affected our world's population for years and continues to this day. With the number of cases expected to increase annually there is a societal pressure to find effective treatment methods for eliminating cancer. Current forms of cancer treatment tend to cause detrimental effects to the human body and are usually quite expensive and long lasting, some costing upwards of $30,000 over an 8 week period. A more recently established form of cancer treatment known as photodynamic therapy is an effective treatment option for ridding cancers that lie on or just below the surface of the skin. Photodynamic therapy is usually done as an outpatient procedure, on average costing between $2,500-3,000 and can eliminate all traces of cancer in as little as a single visit. A major drawback to this form of cancer treatment is the lack of efficient photosensitizers, the light absorbing organic compounds which initiate the destruction of cancer cells. Our research is based on establishing a computational strategy for predicting the effectiveness of new photodynamic therapy photosensitizers. We focus our study on a set of photosensitizers known as boron-dipyrromethene (BODIPY) dyes. These dyes are fluoresecent compounds used throughout a variety of photochemical applications such as photovoltaics, biological imaging, and more recently photodynamic therapy. We apply computational chemistry methods to calculate electronic properties we can use to rate the performance of these photosensitizers. First, we begin with a fundamental understanding of what photodynamic therapy is and the components that make up the treatment method. Then we move to descriptions of the computational methods we implement, inlcuding density functional theory (DFT), time-dependent density functional theory (TDDFT), restricted open-shell Kohn-Sham method (ROKS), and constrained density functional theory (CDFT). Next we investigate the parallelity between the S_1 excited state potential energy surfaces predicted by TDDFT and ROKS. Finally, we investigate the singlet oxygen $^1O_2$ photosensitization characteristics of a particular BODIPY derivative. This study will help future scientists approach the issue of finding the top candidate photosensitizers for use in photodynamic therapy through a rational design process rather than a repetitive trial and error based approach.

Acknowledgements

I would first like to thank my research advisor, Dr. Tim Kowalczyk. Tim has given me almost too much of his time over the past 3 years. I am forever grateful for the incredible amount of commitment, knowledge, and support that he has given me.

Thank you to my thesis committee, Dr. Steven R. Emory and Dr. Robert Berger for the guidance and willingness to speed-read my thesis within a short time period before my defense. Big thanks to my past Chemistry professors for making me fall in love with Chemistry.

A great thanks to WWU the Department of Chemistry, AMSEC, and the Institute for Energy Studies for the support and funding that allowed for the accomplishment of this research. Thanks to all the faculty and administrators down in the office have been invaluable to me.

To my fellow lab mates who became some of my closest friends here at Western, thank you for the support and sanity checks while we were grinding away on these computers. Viktor Laszlo, Natalya Garcia, Linda Grabill, and Amanda Weis, you are some of my closest colleagues and I am grateful for every moment spent with all of you. To the rest of the lab, Khoa, Zoe, Nicole, Josh, Geoff, Alyssa, Hillary, Alessandro, Jack, Anna, and Emily, thank you for keeping the lab a fun and enjoyable work environment. To the other graduate students, thank you for all the group outings, midday jogs, and conversations we had to vent about research.

Finally, to my family and loved ones. There are no words to describe how supportive all of you have been during my time here at Western. Everyday you lift me up and inspire me to work as hard as I possibly can. Mom, your unstoppable support, love, and care that you give to me is insurmountable. I am incredibly grateful for how you and dad raised me. Thanks is simply not enough for all that you have done for me. Dad, you have shown me the definition of what hard work is, I would not be graduating with my Master's degree if it weren't for the mentality you gave me. I can't thank you enough for alwyas giving me your full support and providing me with everything I could ever ask for. Melissa, you give me the advice I need to hear when I need it, however harsh it may be. You have been a true friend and sibling to me. I am proud to have grown up with you through all the sunny farm days, travelling adventures, and time spent at home. Thank you for always being there for me and supporting me through anything. Michael, your kindness and encouragement has had an incredibly positive influence on my life. I am proud to be in the same family as you. Thank you for being a true brother to me and for being a role model I can look up to. Grandma Komoto, and Grandma & Grandpa Johnston, you are always there for me and I am thankful every single day that I have you in my life (also I promise to visit more now that my thesis is done!). Isabella, the one who has dealt with me the most during this process. The incredible amount of support and love you have given me is more than I could ever ask for. Thank you for standing by my side through all the stress and pressure, and for showing me how to look at the world with a rosy outlook. It means the world to me. Garik, my longtime best friend (and favorite cousin), you bring adventure to my life, and your blunt criticism never fails to make me laugh. Thanks for all the laughs and at times "dangerous" adventures that make me question our sanity. Here is to many more adventures. Lastly, to all of my family and loved ones, this thesis is dedicated to you.

Contents

List of Figures

List of Tables

1 Introduction

A significant problem has plagued the world's population for centuries, and has continued to affect us to this day. There were an estimated 1.7 million cases of cancer diagnosed in the United States during 2016, according to the National Cancer Institute.[2] With the number of cases expected to increase annually, scientists and medical professionals are working towards finding effective interventions to cancer. There are several treatment options currently in use such as chemotherapy, radiation therapy, and surgery. While these methods do work, they tend to be expensive and more often than not cause detrimental effects to the human body. Patients endure months to years of chemotherapy and radiation, with undesireable side effects.[3–6] There are some methods to cope with the side effects,[7] but it is not enough to cover all the issues that come with chemotherapy. The cost for these types of treatments can be an issue for those without sufficient insurance coverage, especially for individuals who require multiple visits.[8] The cost and after-effects of surgery can be as unfavorable as the other options, even if multiple visits are not required.[9] Though surgery has the ability to clear certain cancerous tumors from a region and prevent metastasis,[10] it may cause permanent damage to one's body,[11] and surgery may also need to be combined with other remedies to avoid recurrence.[12]

In light of these unattractive options, there is a societal pressure to find methods that cause minimal harm while still eliminating cancer from the body. One promising method is photodynamic therapy (PDT). PDT is a relatively non-invasive form of cancer treatment which involves administering a PDT agent (photosensitizer) intravenously into a region where the cancer cells are present. A light of specific wavelength is then shined on that region which initiates a photochemical reaction that destroys cancer cells (Figure 1.1).

This method is used to treat cancers which lie on or just below the surface of the skin since most of the clinically available PDT agents are only able to absorb light at short wavelengths.[13–15] Light of longer wavelengths, such as infrared (IR), are able to penetrate deeper than light of shorter wavelengths. Currently this form of cancer treatment is being

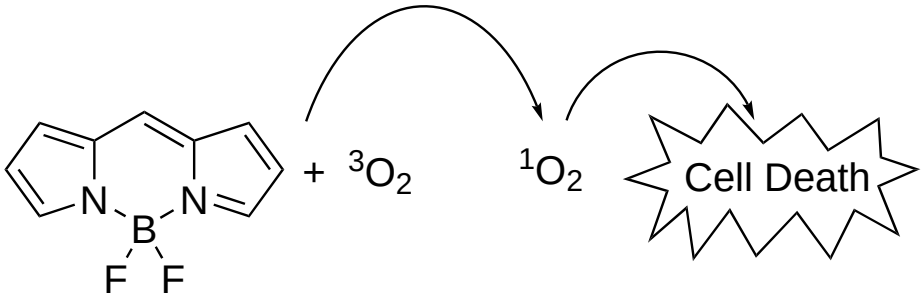

Figure 1.1: Simplified schematic of the process of PDT. Triplet oxygen ($^3O_2$) is the electronic ground state of oxygen, while singlet oxygen ($^1O_2$) is the highly reactive form of oxygen.

tested as a method

to treat cancers of the skin, prostate, brain, lungs, mouth, and other areas that can be made accessible by light. PDT does exhibit some of the same adverse side effects as other treatment methods such as nausea, skin sensitivity, scarring, and swelling, but these tend to be less severe compared to other treatment options.[16] The primary side effect of PDT tends to be sensitivity to light. For several weeks after the treatment after the treatment, patients need to limit their exposure to the outdoors and take extra precautions to avoid bright sources of light.[13–15] The side effects of PDT resolve more rapidly than those of more extended treatment methods such as chemotherapy.[6,16] PDT does minimal damage to healthy tissue surrounding the treatment site in comparison to other treatment methods due to its high specificity. PDT is a rapidly growing field, bolstered by the increasing amount of research and funding being dedicated to its development.

1.1 The What, Why and How of Photosensitizers

PDT operates by illuminating the targeted area with light of a specific wavelength, inducing photochemical reactions that destroy cancer cells within the region. In order to achieve this elimination, PDT uses a chemical known as a "photosensitizer". Photosensitizers (PS) are molecules which can absorb light to become energetically excited, and then use that energy to react, fluoresce, or transfer energy to other molecules. In PDT, light of a specific wavelength electronically excites the PS which then reacts with nearby oxygen (O_2) molecules to form

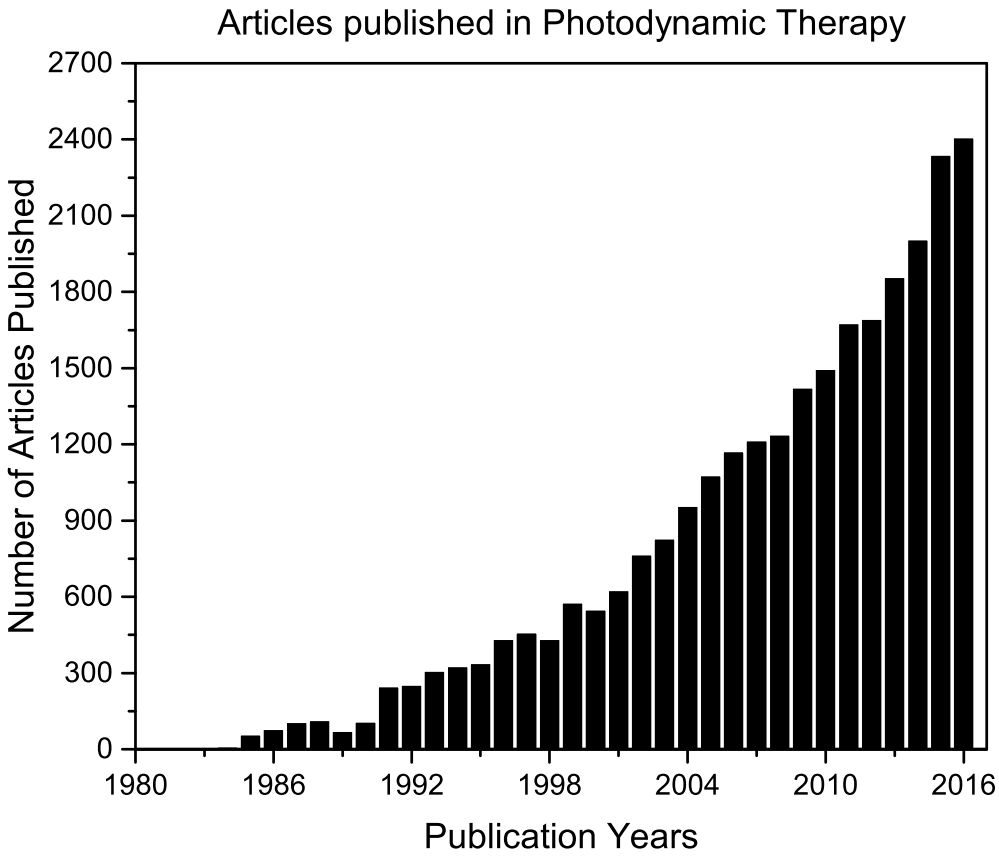

Figure 1.2: Number of articles involving PDT published over the last 30+ years

singlet oxygen ($^1O_2$). $^1O_2$ is an electrophilic, highly reactive form of oxygen that damages critical components of cells, both cancerous and healthy. Though damage to healthy tissue is not a desirable trait for cancer treatments, PDT is able to target a specific region, causing minimal damage to healthy cells. The precision of PDT is due to the half-life of $^1O_2$ being so small $(0.6 \times 10^{-6} \mu s)$[17] that the amount of healthy tissue damaged is limited to only those cells that lie in close proximity to the illuminated area. Precision is also dependent on how small of an area the light can be concentrated or accessed.

When designing a new PS for singlet oxygen photosensitization, one must first consider the process that a PS undergoes to generate $^1O_2$. The principal photochemical process that occurs to generate $^1O_2$ is initiated by the ^{1}PS ground state absorbing incoming light. The

absorption of light causes the ground state ^{1}PS to become excited into its S_1 excited state (^{1}PS*). Once excited, intersystem crossing occurs to generate the ^{3}PS state. The ^{3}PS state then transfers its energy to $^3O_2$ to form ^{1}PS and $^1O_2$ electronic states. Lastly, $^1O_2$ proceeds to damage cell components via oxidation, inducing apoptosis, and the leftover PS and clears the body in a few weeks.[1] This type of reaction resulting in the production of $^1O_2$ is known as a type II reaction. Type II reactions may also consists of the formation of an oxidized PS and a superoxide ion, created by the PS transferring an electron to an oxygen molecule. There

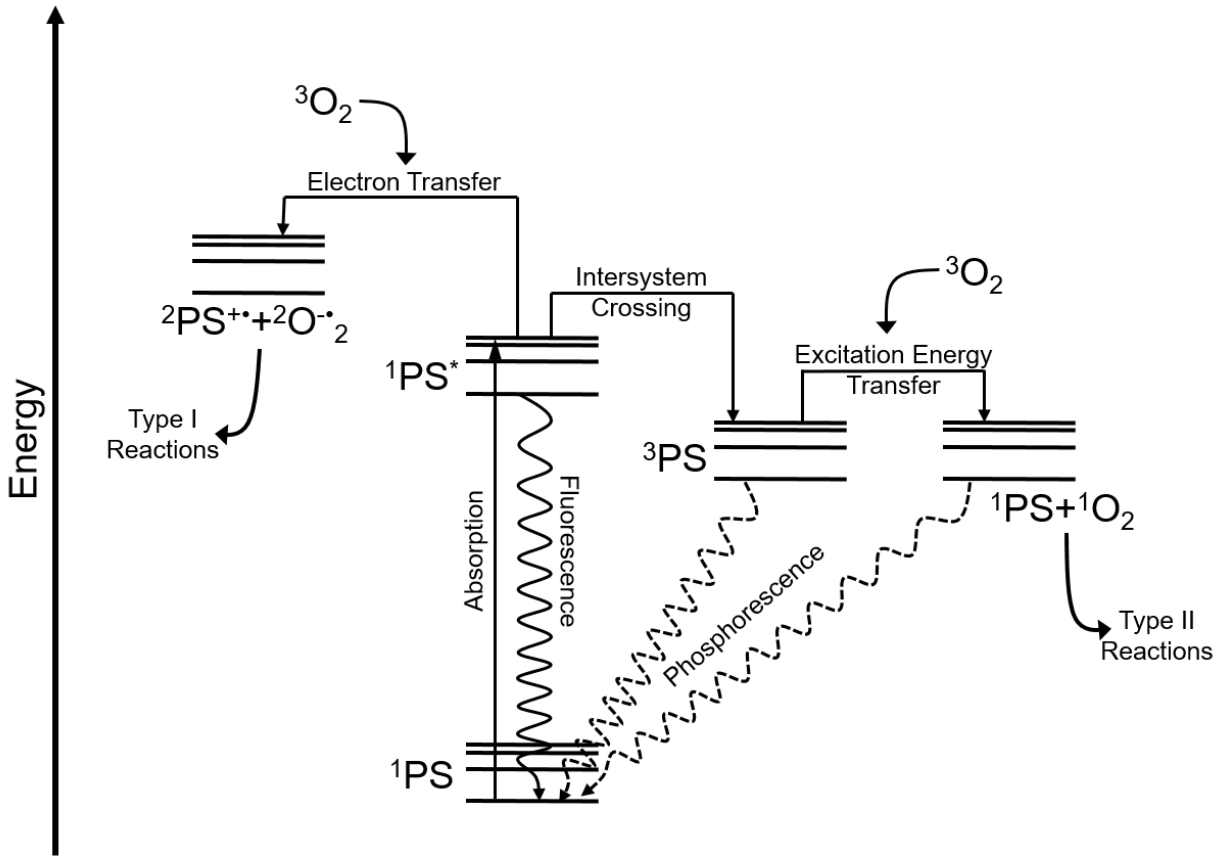

Figure 1.3: Jablonski diagram for the different electronic states involved in PDT.

is the possibility that the excited PS (^{1}PS*) may transfer an electron to $^3O_2$ immediately from the S_1 excited state (^{1}PS*) to form a doublet/doublet cation/anion state ($^2PS^{\bullet+}\ ^2O_2^{\bullet-}$). This alternate process is known as a type I reaction. Type I reactions yield radical ions due to either hydrogen atom or electron transfer. Both of these photochemical processes are illustrated in the Jablonski diagram provided in Figure 1.3.

1.2 The Photosensitizers

When designing a PS for PDT, the ultimate concern is how well it will perform in reducing cancer cells. A major concern should be placed on the quantum yield of $^1O_2$ since it is the necessary component to eliminate cancer cells.

$$\Phi_{^1O_2} = \frac{^1O_2 \text{ molecules generated}}{\text{absorbed photons}} \tag{1.1}$$

Though a high quantum yield of $^1O_2$ is a primary qualification for PS, there are many other properties that one should consider. Several studies have assessed desirable traits to consider when choosing PS that are to be used in PDT.[1,18] In order for a PS to be successful, one must consider both chemical and clinical traits in the design process. Some of the most important properties to consider when designing PS are described in Table 1.1.[19,20]

Table 1.1: Properties to consider when designing PS.

Chemical Properties
High quantum yield of triplet state formation and high triplet state energy
High singlet-to-triplet intersystem crossing efficiencies
Efficient and high yielding synthesis
Simple and stable compounds that are well characterized and have a constant composition
High quantum yield of singlet oxygen
Photophysical Properties
Strong absorption (High extinction coefficient in red or near infrared region (620-850nm))
Deep tissue penetration
Minimal photobleaching (decomposition of dye due to light)
Clinical Properties
Minimal side-effects (*e.g.* skin photosensitivity and pain)
High retention/aggregation in diseased tissue
Rapid clearance from body after treatment
Minimum dark toxicity (negligible cytotoxicity in absence of light)
Soluble in biological media

There are several different PS currently being used in the field of PDT. One of the first and most popular ones is porfimer sodium (Photofrin, see Figure 1.4). Photofrin brought PDT to a worldwide audience[21] and set the stage for all modern PS used in oncologic PDT. After clinical trials Photofrin was approved for treating bladder, skin, lung and esophageal tumors. One of the best qualities of Photofrin is the fact that it accumulates to a greater degree in tumors than in healthy tissue, which minimizes the destruction of healthy tissue (assuming that not so much of the PS is injected that it overflows into healthy tissue as

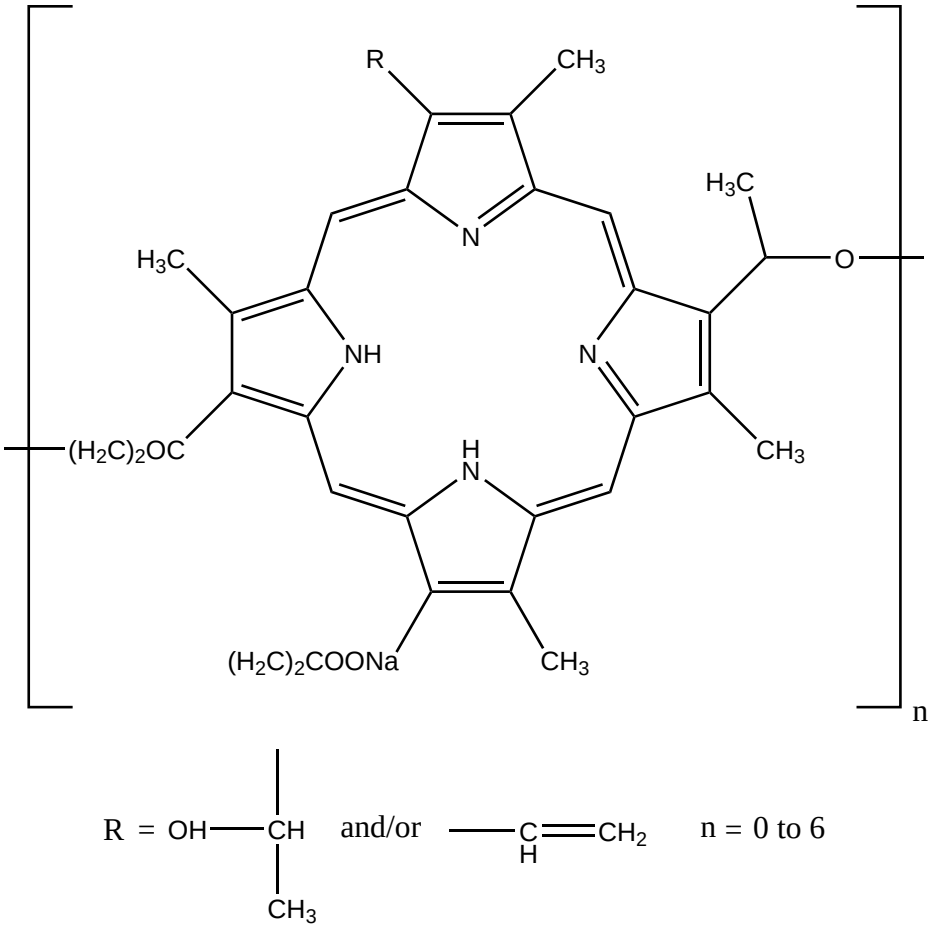

Figure 1.4: Structure of Photofrin

well). One drawback is that Photofrin has a low absorbance at 630nm, thereby requiring an extended period of irradiation from a higher energy source to activate it. The weaknesses of Photofrin gave rise to the research and development of more efficient PS. Studies have proposed other

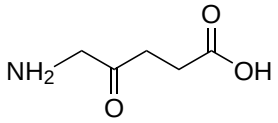

(a) ALA

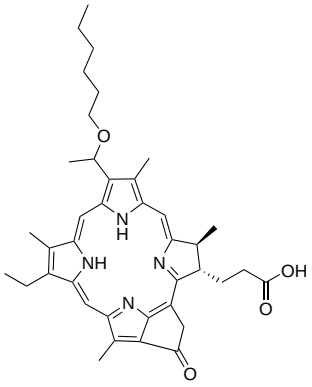

(b) HPPH

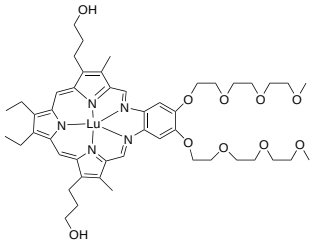

(c) Motexafin-Lutetium

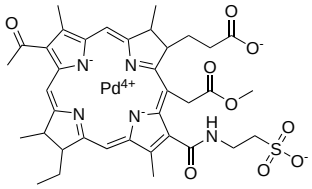

(d) Padeliporfin

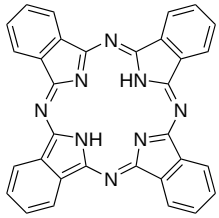

(e) Phthalocyanine

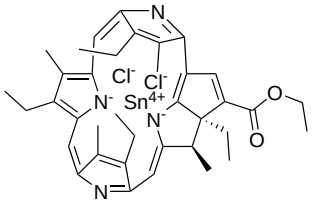

(f) Rostaporfin

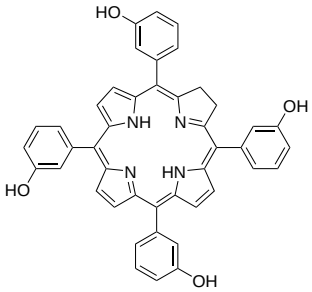

(g) Temoporfin

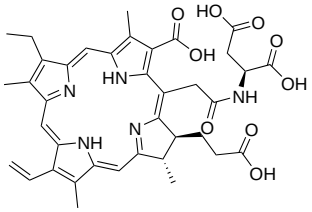

(h) Talaporfin

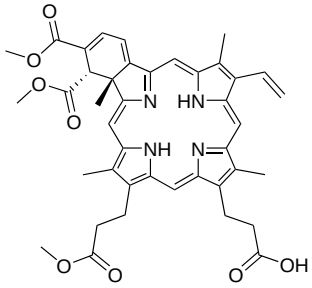

(i) Verteporfin

Figure 1.5: Structues of PS reviewed by Sibata et al.[1]

porphyrin and non-porphyrin related PDT agents for clinical use, but many fell short of optimal status due to: administration issues, high photobleaching rates, synthetically inaccessible, or having low light-to-dark toxicity ratios (i.e. PS will not be harmful until light beam is applied).[22–27] Many PS which perform excellently have been investigated and thoroughly reviewed by Sibata et al.[1]

1.3 BODIPY Dyes

A new class of photoactive organic compounds has emerged known as boron-dipyrromethene (BODIPY) dyes. Discovered in 1968 by Treibs and Kreuzer,[28] these fluorescent dyes have found use across a vast range of applications,[29] and possess many ideal properties for applications as PS in PDT.[19] The diversity of applications for which BODIPY dyes are used can be attributed to how easily one can tune the photophysical, spectroscopic and chemical properties via moderately simple synthetic methods.[30,31] BODIPY dyes are currently being used in applications that primarily involve fluorescence and excitation energy transfer.

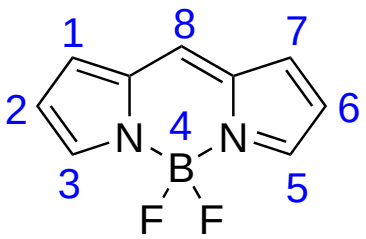

Figure 1.6: The structure of the BODIPY chromophore

BODIPY dyes are quite stable in biological environments, being mostly unaffected by the surrounding pH and polarity, and they can be attached to proteins which aggregate in specific parts of the body. For imaging, BODIPY dyes strongly absorb light and emit sharp fluorescence peaks with high fluorescence quantum yields. The ability to synthesize water-soluble BODIPY derivatives able to permeate into biological cells and target tumor cells made them attractive candidates for use as PS in PDT. Burgess et al. published work summarizing the properties of halogenated & aza-/non-halogenated BODIPY dyes for use in PDT.[19] In the time since Burgess' review of BODIPY dyes for PDT, there have been many studies

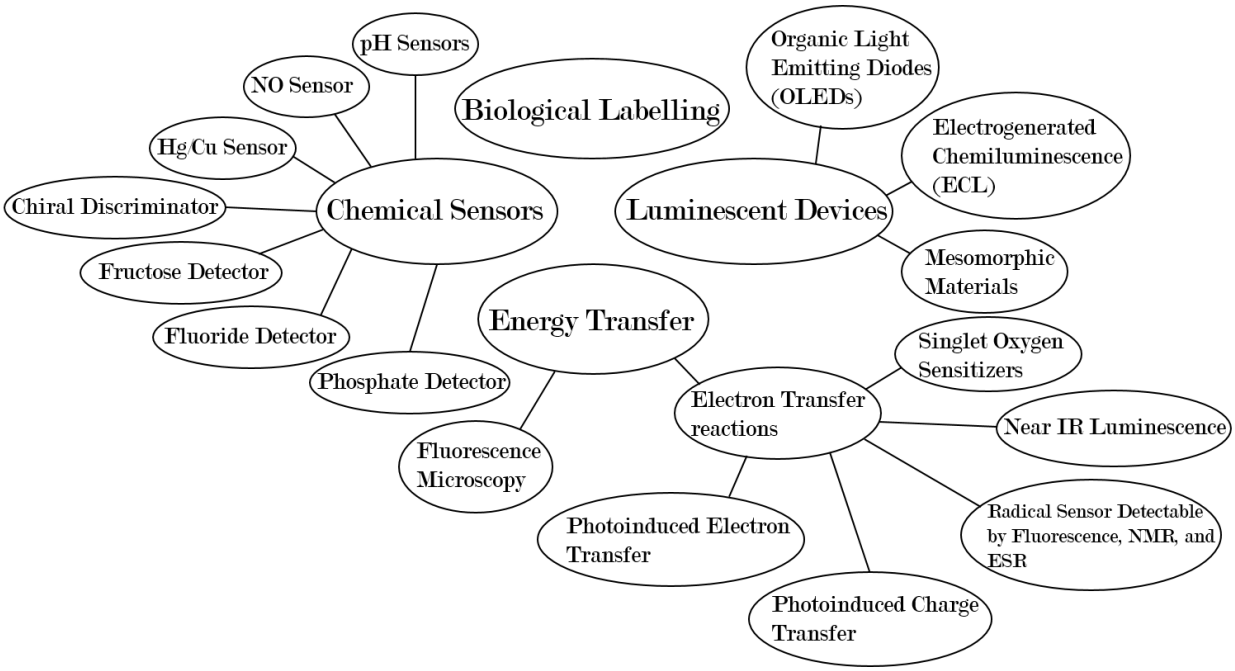

Figure 1.7: Applications of BODIPY dyes.

investigating the use of BODIPY dyes as PS. Several studies have found that BODIPY dyes are able to eliminate cancer cells when being used as a PS for treating breast cancer.[32,33] Though there are a variety of applications that BODIPY derivatives can be used for, one of the most promising is their use in PDT. For the rest of this work we will be focusing on the properties of BODIPY derivatives as they relate to PDT and the production of singlet oxygen, while simultanenously examining the computational chemistry methods that are used to predict their photophysical properties (covered in Chapter 2).

1.4 Preface

All of the research performed in this thesis was accomplished using computational chemistry methods. Computational chemistry is a branch of chemistry that uses computer models to understand chemical systems. These methods are rooted in the fundamental laws of chemistry and physics. A fundmental calculation in computational chemistry is solving the Schrödinger equation for a specific chemical system. There are many computational methods that range from highly accurate ones which are quite computationally expensive (such as

ab initio methods) to simple and cheap methods (such as molecular mechanics). Density functional theory (DFT) is the foundation for many of the calculations in this study. DFT is much more accurate than molecular mechanics methods, but is generally less accurate than *ab initio* methods. DFT is a middle ground for calculating molecular properties with reasonable accuracy without sacrificing exorbitant amounts of time or computational power. Extensions of ground state DFT permit the calculation of a variety of properties for chemical systems. DFT based calculations are able to predict many of the properties that can be physically measured or observed in a lab. DFT can provide very accurate results for geometries, energies, and dynamics in comparison to those properties obtained via experimental methods (depending on the experimental conditions that the values were measured at). The majority of values calculated in this thesis are energies (excitation, emission, coupling, vibrational, etc.). Aside from energies, we also calculate and interpret the structures and dynamics to better understand PDT functionality.

The major questions we address in this work are as follows:

- What are the benefits and limitations to time-dependent and time-independent density functional methods for dye photophysics?
- What electronic excited state properties are most important for photosensitizer optimization?
- What are the singlet oxygen generation properties for a specific BODIPY dye?
  - How do we calculate the singlet oxygen generation properties for this BODIPY dye?
- What advantages exist for using time-independent density functional methods over time-dependent ones?

To address these questions, we perform calculations to compare time-dependent/time-independent density functional methods directly for BODIPY dyes. We examine how these

methods perform for calculating excited state properties and then compare the results to experimental values and to each other to distinguish which method (if either) is more accurate and how they differ from each other. We computationally examine the individual states that a PS and oxygen molecule occupy during the process of generating singlet oxygen. By calculating each of these individual states and the couplings between the states we are able to estimate the rate at which singlet oxygen would be generated for a specific BODIPY chromophore. Finally we examine in more detail why a time-independent density functional method can be effective when investigating electronic excited states. With this thesis we hope to provide useful information to those who are designing PS for use in PDT. We also hope to give insightful knowledge about the benefits and limitations of time-dependent and time-independent density functional methods to those who are developing such methods. This thesis provides an examination of how we can calculate quantifiable measures of PS quality and how accurate those values can be. Our findings can help researchers develop streamlined methods for sorting through a variety of PS to be used in PDT, significantly cutting down on time spent conducting experiments on potential PS that may end up being ineffective. This thesis brings new information about the density functional based methods, the photophysical properties of BODIPY dyes, and the singlet oxygen generation characteristics that will support researchers and industry professionals in the field of PDT and density functional based method development.

1.5 The Structure of This Thesis

The structure of this thesis is divided into 4 sections. Chapter 2 describes the different computational methods used during the course of this thesis work. Chapter 3 compares two computational methods in relation to BODIPY dyes' excited state energies. Chapter 4 presents the calculated properties associated with the singlet oxygen generation of BODIPY dyes. Finally, Chapter 5 closes with the validation of restricted open-shell Kohn-Sham method for electronic states involving charge transfer.

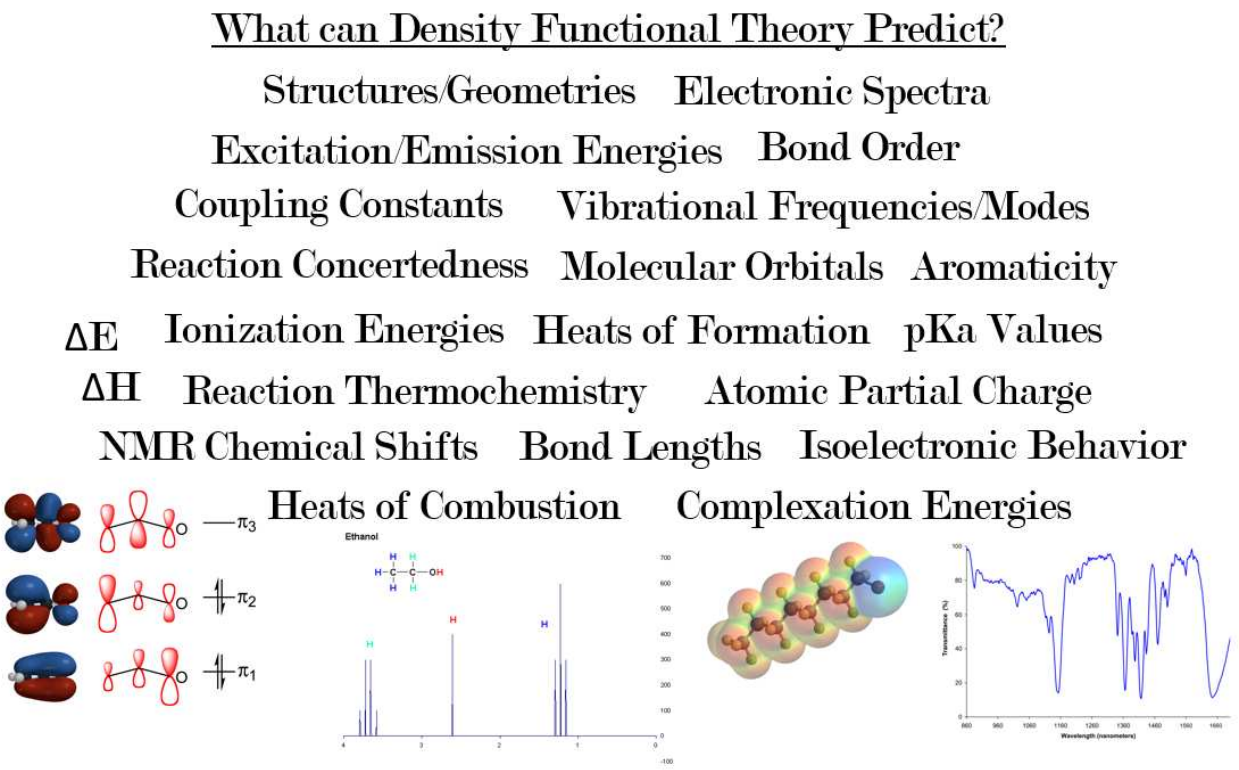

Figure 1.8: Types of chemical properties that can be calculated by DFT based methods.

In Chapter 2, we cover the fundamentals of the 4 major methods used during this research: Density functional theory (DFT), the restricted open-shell Kohn-Sham method (ROKS), time-dependent density functional theory (TDDFT), and constrained density functional theory (CDFT). The basis from which these methods were created are discussed, highlighting the fundamental characteristics that differentiate these methods from one another. Also covered in this chapter is the range of chemical properties each method calculates. Then we describe how each method is invoked in practice and which parameters are required to perform a calculation using each of these methods.

Chapter 3 investigates the parallelity between two excited state potential energy surfaces (PES) of a singular BODIPY chromophore (synonymous for our purposes with BODIPY "dye"). First covered is the vertical excitation energies from the S_0 ground state to the S_1 excited state for a set of BODIPY derivatives where experimental values were previously obtained. Then discussed is the process of generating a S_1 excited state PES via molecular

dynamics (MD) sampling utilizing ROKS and TDDFT, and then calculating the opposing methods' S_1 energy to compare the PES directly. We found that ROKS MD sampling provides a description of the PES where the TDDFT and ROKS PES are quite parallel but has an energy gap between them, while TDDFT MD sampling describes a portion of the PES where the two PES have a very similar energy but they are not nearly as parallel to each other. Then we delve into what exactly was causing the deviations in parallelity between the two PES for the same molecule. This is accomplished by analzing the results of vibrational energy calculations performed on a BODIPY derivative and determining the vibrational modes that differed most from each other across the two methods (ROKS and TDDFT). We found that TDDFT and ROKS have a strong correlation in their excitation and emission energies, showing that they predict similar shifts in absorption/emission spectra. Also it was found that TDDFT overestimates the vertical excitation energy, while ROKS underestimates this energy though to a lesser margin. This section's work is geared towards providing useful information to those who are focused on optimizing the BODIPY framework. This work also contributes useful information to those who are developing time-independent excited state DFT strategies, giving them an understanding of the methods strengths and weaknesses.

In Chapter 4 we present a study focused on investigating the interaction between a single BODIPY dye and an oxygen molecule. We began with a look at the preferred configurations of oxygen molecules about the dye, where we found that oxygen molecules aggregate above/below the plane of the BODIPY dye, or along the outer edges of the plane, classified as face-on and side-on configurations, respectively. We presented a method for a qualitative assessment of the singlet oxygen generation characteristics by using the couplings as *pseudo* rate values. We then looked at the electronic states which are involved in the photochemical excitation of the BODIPY dye and sequence of electronic transitions that lead to the formation of singlet oxygen generation and the competing pathways. Being able to accurately compute the different electronic states we moved to computing the couplings between directly connected electronic states (i.e. electronic states that are able to transition from

one to the other). The distribution of couplings revealed that the transition leading to the formation of singlet oxygen was more favorable than the competing pathway of forming a set of radicals. Further analysis of the couplings showed that oxygen molecules which adopted a face-on configuration to the plane of the dye would also adopt an orientation parallel to the plane of the dye, as well as hold a higher coupling value. We conclude with an analysis of our alternative scheme for computing the electronic couplings, which show little to no correlation with the full computations. This study sets the foundational work for a future protocol which performs high-throughput analysis of many candidate PS for use in PDT. We also provide useful information to those attempting to constrain multi-molecule systems with varying electronic states and the couplings between them.

2 Computational Methods

Computational chemistry is a branch of chemistry that uses a combination of physical theories and mathematics to calculate properties of atoms and subatomic particles via the computer. Computational quantum chemistry is primarily based around solving the Schrödinger equation.

$$\hat{H}\Psi = E\Psi \tag{2.1}$$

Using this equation small scale calculations of molecular properties can be performed by hand, but as the system gets larger with the number of atoms increasing it becomes unreasonable to work through the math by hand. The computational power provided allows us to calculate the properties of large systems containing many atoms and/or molecules in a shorter amount of time. Early computational methods include the Thomas-Fermi and Hartree-Fock (HF) methods. The HF method approximates the wavefunction of a system using a single Slater determinant, ignoring the effects of electron correlation. The Thomas-Fermi method is based on the electronic density alone, and is only perfectly accurate in the limit of infinite nuclear charge. Kohn-Sham Density Functional Theory (DFT) is a method based on the electronic density of a system, which replaces the approximate kinetic energy of the Thomas-Fermi method with an exact kinetic energy for non-interacting electrons, plus a correction term called the exchange-correlation functional. DFT is able to handle larger systems with improved accuracy in comparison to the two former methods. While DFT is exact in principle, the accuracy of the calculations are primarily based on which functional is used. Due to the advances made in computational methods and the development of highly accurate functionals, we are able to calculate the electronic properties of chemical systems of varying sizes with reasonable accuracy.

In order to calculate photochemical processes, we require the use of several computational methods. DFT is the fundamental method on which most other methods we use are based. The other methods we use are time-dependent DFT (TDDFT), restricted open-shell

Kohn-Sham (ROKS) method, and constrained DFT (CDFT). TDDFT and ROKS are both excited state methods which can be used to calculate properties of the S_1 excited state for the BODIPY dyes in our study. CDFT constrains electronic charge and spins on specific atoms, molecules, or molecular fragments. We use CDFT to calculate the energies for specific electronic states (singlet, doublet, triplet, cation, anion, etc.) that are involved in the generation of $^1O_2$. In this chapter we cover how each of the different computational methods functions, as well as how they are used to calculate the properties of BODIPY derivatives.

2.1 Density Functional Theory

DFT is a computational method that calculates the electronic ground state energy of a chemical system. DFT is formulated in terms of the electronic density. This is contrary to methods considered to be ancestors of DFT (i.e. Hartree-Fock-Slater methods) which are based on the many-electron wavefunction. Being in principle exact, the accuracy of Kohn-Sham DFT is based on the appropriate exchange correlation (XC) energy functional being used. The problem is that there is not one XC functional that obtains universally high accuracy for all types of chemical systems. There are many different XC functionals being developed for specific goals and types of molecular systems. Modern XC functionals obtain moderate accuracy with DFT calculations. Correlated wavefunction methods obtain a higher level of accuracy than DFT, but are much more computationally expensive (take a lot of computer power and time) and are only reasonable in systems that have very few atoms (in some cases, less than 10 atoms). With DFT being a moderately accurate method, we are able to calculate the ground state energies for chemical systems of many atoms with reasonable accuracy and computational expense.

Fundamentals of DFT

DFT operates based on the electronic ground state density $\rho(r)$ which uniquely determines the external potential $v(r)$.[34] The determination also works vice versa, allowing us to deter-

mine the ground state density.

$$\rho(r) \leftrightarrow v(r) \tag{2.2}$$

The Hamiltonian has the form of

$$\hat{H} \equiv \hat{T} + \hat{V} + \hat{U} \tag{2.3}$$

where

$$\hat{T} \equiv -\frac{1}{2}\sum_{j} \nabla_j^2 \tag{2.4}$$

$$\hat{V} \equiv \sum_{j} v(r_j) \tag{2.5}$$

$$\hat{U} = \frac{1}{2}\sum_{i \neq j} \frac{1}{\mid r_i - r_j \mid} \tag{2.6}$$

in atomic units. Since $\rho(r)$ determines $v(r)$ as well as the number of electrons, it determines the full Hamiltonian $\hat{H}$ and implicitly all properties determined by $\hat{H}$. A variational principle for the energy as a function of density can be developed given the theorem by Hohenberg and Kohn.[34] The variational principle is defined as:

$$E_{v(r)} \geq E_{v(r)}[\rho_0(r)] \equiv E \tag{2.7}$$

where $\rho_0(r)$ is the density of the ground state and E is the energy of the ground state. When we run DFT calculations we are using the computer as an aid to solve for E. These calculations show that there is a more solvable auxiliary system of non-interacting electrons that has the same density as a system of interacting electrons, allowing us to correctly represent the density without explicitly evaluating all many-body interactions.

How we use DFT

DFT is a tool that we use in order to calculate the ground state energies of chemical systems. Figure 2.1 shows a schematic of two potential energy surfaces (PES), one for the ground

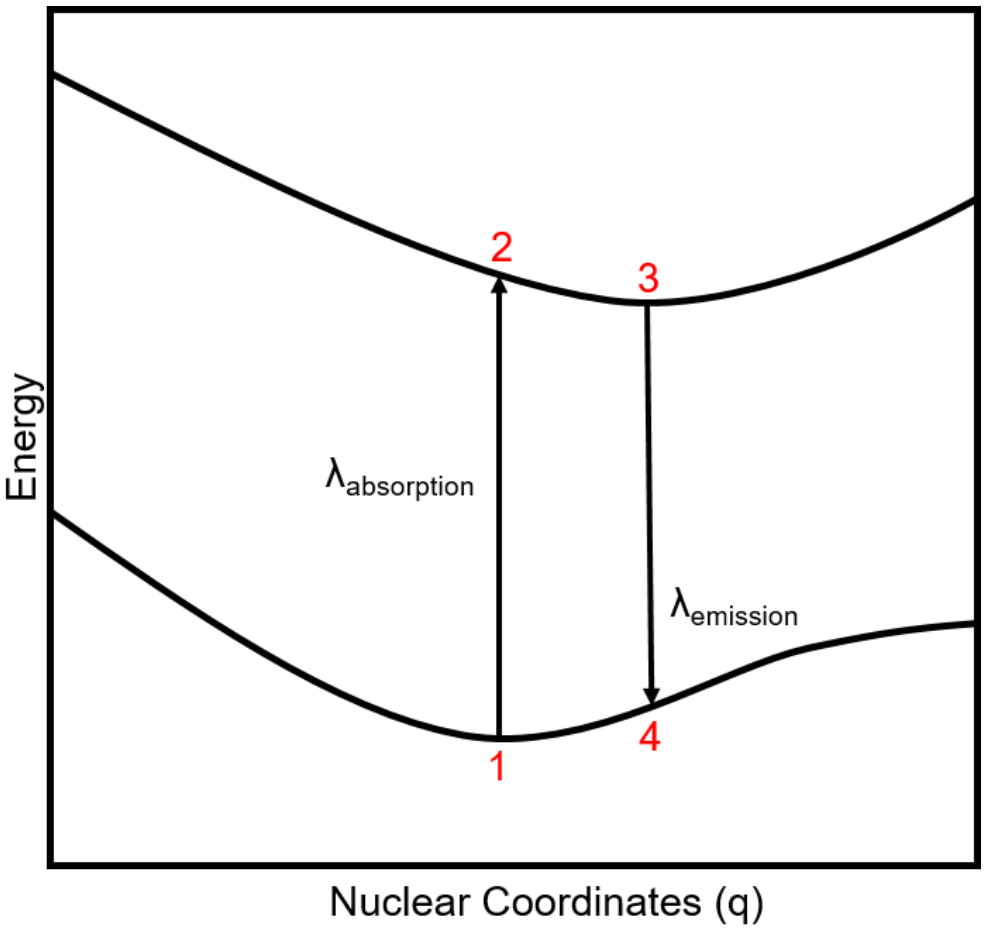

Figure 2.1: Schematic diagram of two potential energy surfaces. The ground state PES (S_0) and the excited state PES (S_1).

state (S_0) and one for the lowest singlet excited state (S_1). Nuclear coordinates simply determine the 3-dimensional conformation that a molecule adopts in space. DFT calculations approximate the most stable ground state energy of a system, which is labeled position 1 in Figure 2.1. When molecular coordinates are constructed by hand, they are rarely in the most stable state, so we perform geometry optimizations which bring the molecule to the lowest energy conformation (position 1) which is the most stable conformation that the

molecule can adopt. Without reliable methods to achieve this conformation we would end up with inaccurate values for the energy. It is important for us to obtain the most stable ground state energy and 3-dimensional arrangement of atoms in space (nuclear coordinates) because we base subsequent excited state calculations on the energies from ground-state DFT. When exciting molecules, our calculations simulate vertical excitations on one set of nuclear coordinates (position 1 to position 2). As seen in Figure 2.1, as the nuclear coordinates change, so does the total energy of the system. So as long as we obtain a reliable S_0 ground state energy and nuclear coordinates from DFT, then we can perform analogous excited state calculations with full confidence that excitation energies are computed relative to the correct reference.

2.2 Time-Dependent Density Functional Theory

Time-dependent density functional theory (TDDFT) is a computational method used to calculate, among other properties, the electronic excitation and emission energies of molecules. This method is widely accepted and used throughout the field of quantum chemistry, particularly in the realm of electronic excited states. However, TDDFT tends to fail for excited states with charge transfer or double-excitation character. TDDFT has proven to be an accurate method for calculating the electronic excitation energies for a variety of systems.[35,36] We perform TDDFT calculations in order to compare the calculated transition energies to those obtained from time-independent density functional based methods, as well as to experimentally obtained values (energies physically measured in an experimental lab). Since TDDFT is based on traditional DFT, the accuracy of the calculations greatly depends on the specific XC functional that is used in the calculations. Choosing an XC functional is completely dependent on the type of system under study. With our systems containing a relatively small number of atoms (40-60 atoms) we have found fairly accurate results using the B3LYP and ωB97X-D functionals.[37] Our use of TDDFT is geared towards having a reliable method to compare against the ROKS method and verifying that ROKS can perform

just as well if not better than a more well established and accurate method.

Fundamentals of TDDFT

Derived from traditional DFT, TDDFT operates by replacing the many-body Schrödinger equation

$$i\frac{\partial}{\partial t}\Psi(\{r\},t) = \hat{H}(\{r\},t)\Psi(\{r\},t) \tag{2.8}$$

with a series of time-dependent Kohn-Sham (TDKS) equations.

$$i\frac{d\phi_j(\mathrm{r},t)}{dt} = \left(-\frac{\nabla^2}{2} + v_s[n](\mathrm{r},t)\right)\phi_j(\mathrm{r},t) \tag{2.9}$$

This substitution is allowed due to the Runge-Gross theorem which shows that a specific time-dependent density results from a single time-dependent external potential.[38] The many-body Schrödinger equation represents a many-electron problem, which is quite time consuming and computationally expensive to solve numerically, while the TDKS equations replace this with a set of single-particle equations that are solved much more easily and quickly. The TDKS equations describe a system of N non-interacting electrons that change over time with an external potential, and produces the same density as a system of interacting electrons. Without the electron-electron interactions explicitly evaluated, the TDKS equations become much faster to solve, especially for larger systems. We start with a system of non-interacting electrons, apply an external potential to that system, then calculate the density of the interacting system using the Kohn-Sham orbitals. The only fundamental approximation made throughout a TDDFT calculation is that in the time-dependent Kohn-Sham potential

$$v_{\mathrm{KS}}[n](\mathbf{r},t) = v_{\mathrm{ext}}(\mathbf{r},t) + v_{\mathrm{Hartree}}[n](\mathbf{r},t) + v_{\mathrm{xc}}[n](\mathbf{r},t) \tag{2.10}$$

there is a separation of the known external and hartree potentials ($v_{ext}, v_{Hartree}$) from the XC functional term (v_{xc}) which is approximated in the same manner as in Kohn-Sham DFT.

We are able to use TDDFT to study the electron's response to an electric field perturbation using linear response theory.[39] From this response we are able to identify the excitation and emission energies. In practice TDDFT, just like other methods, is implemented as a generalized eigenvalue problem to solve for the electronic properties of molecular systems.

How we use TDDFT

In our research we use TDDFT to calculate the excitation and emission energies for a set of BODIPY dyes. Referring back to Figure 2.1, TDDFT calculations gives us the energy difference between points 1 & 2 (excitation energy) and points 3 & 4 (emission energy). Note that the values given are not the exact energies at each point along the PES illustrated in Figure 2.1, but instead we get energy differences. If we want the separate points then we would need to run subsequent calculations or do some simple math using previous (ground state DFT) calculations to solve for the unknown points. We primarily use TDDFT to compare its performance to ROKS on BODIPY derivatives. We also compare TDDFT to experimental values[40] to further the comparison between TDDFT and ROKS. The goal is to compare the performance of ROKS to this well-known, established method for calculating excitation and emission energies for a set of BODIPY dyes.

2.3 Restricted Open-Shell Kohn-Sham

The Restricted open-shell Kohn-Sham (ROKS) method is a computational method used for calculating excited states of molecules. While being less established than TDDFT, ROKS is a method that could potentially provide valuable information about charge transfer states, double excitations, and Stokes shifts that cannot be accurately predicted by TDDFT calculations. Advantages of ROKS over TDDFT will be discussed in Chapter 3. One disadvantage of ROKS is that it is only able to calculate the excitation energy of molecules in the lowest singlet excited state; the method in its current implementation is not able to calculate the energy for other excited states. Another issue associated with excited state methods is known

as variational collapse. Variational collapse occurs during the self-consistent field (SCF) convergence when an excited state orbital occupation pattern returns to the ground state determinant. Delta self-consistent field DFT (ΔSCF-DFT), a similar excited state method to ROKS, is prone to variational collapse unless the maximum overlap method (MOM) is included.[41] Using MOM still does not guarantee convergence on the excited state. An advantage of ROKS over other excited state methods is that ROKS provides a straightforward method for optimizing the Kohn-Sham orbitals in excited electronic configurations. ROKS's ability to avoid variational collapse makes it a reliable computational method for S_1 excited states.

Fundamentals of ROKS

To calculate the ROKS energy for a singlet excited state, we use a two-determinantal equation

$$E_s^{\mathrm{ROKS}} = 2E_m[\phi_i] - E_t[\phi_i] \tag{2.11}$$

where s is the singlet excited state, m is the mixed spin or broken-symmetry determinant, and t is the triplet determinant. Note that the mixed and triplet determinants are both constructed from the same set of orbitals. Using this single set of orbitals eliminates the problem of the spin purification procedure in ΔSCF being approximate. Before solving for the ROKS energy, we must first solve for the single-determinant energies. To do so we solve the following equation

$$\mathbf{FC} = \mathbf{C}\epsilon \tag{2.12}$$

in a series of three steps. ($\mathbf{F}$ is the effective Fock matrix, $\mathbf{C}$ is the molecular orbital coefficients, and ϵ is the orbital energies. We first build mixed and triplet density matrices from a set of Kohn-Sham orbitals, build matrices for the mixed and triplet determinants from those densities, then we construct the effective ROKS Fock matrix F and solve for ϵ self consistently. Finally we substitute the single-determinant energies to solve for E_s^{ROKS}.

How we use ROKS

As with TDDFT, we use ROKS to calculate the excited state energies of the BODIPY dyes we are studying. Primarily we set out to investigate the similarities and differences in the performance of ROKS and TDDFT when calculating the excitation and emission energies for BODIPY derivatives. Within this thesis we are looking to determine whether ROKS is a viable method to study BODIPY dyes. We also look at ROKS' ability to calculate the $^1O_2$ generation characteristics of a BODIPY dye. Unlike TDDFT, ROKS provides exact values for different positions in Figure 2.1. Instead of calculating energy differences, ROKS gives energies for each of the positions 2, and 3. The different approach ROKS takes to calculating the excited state energies of molecules gives it an advantage over TDDFT in specific cases, and we hope to exploit those advantages during the course of this thesis.

2.4 Constrained Density Functional Theory

Constrained density functional theory (CDFT) is a computational method that provides a direct route to the diabatic ionic-like states as well as the charge transfer excited states of chemical systems using the Kohn-Sham SCF procedure. Constraints of the systems are expressed in terms of charge and spin on atoms, molecules, or molecular fragments. CDFT is especially useful when looking at specific electronic states that are otherwise not computable by other computational methods. CDFT allows us to dig deeper into chemical systems and completely understand the mechanics of specific chemical reactions and processes.

Fundamentals of CDFT

In the most simple form of CDFT where we wish to compute the electronic ground state of a system subject to the constraint that there are N electrons in a volume of Ω, we add a Lagrange multiplier into the traditional DFT energy functional.

$$E(N) = \min_{\rho} \max_{V} \left[E[\rho(\mathbf{r}] + V \left(\int_{\Omega} \rho(\mathbf{r}) \mathrm{d}^3\mathbf{r} - N \right) \right] \tag{2.13}$$

We can also calculate systems with a variety of different constraints, such as charge variation, magnetization, and magnetization orientation.[42] If we aggregate all of the different constraints available then we can develop an equation which incorporates all of the different constraints currently computable.

$$W[\rho, V : N] \equiv E[\rho] + V\left(\Sigma_\sigma \int \mathrm{w}^\sigma(\mathbf{r})\rho^\sigma(\mathbf{r})\mathrm{d}^3r - N\right) \tag{2.14}$$

$$E(N) = \min_{\rho} \max_{V} W[\rho, V : N] \tag{2.15}$$

CDFT can perform several complicated calculations involving core excitations, localized excitons, charge localization and fluctuation, electron transfer, electronic coupling, low-lying spin states, parameterizing model Hamiltonians, and more.[42] We are concerned with the use of CDFT for constraining charge and spin on molecules and studying the charge transfer states of molecules.

How we use CDFT

With CDFT we are able to perform calculations on chemical systems with molecules that each have a different spin and/or charge. In the process of a BODIPY dye generating $^1O_2$ the dye and the oxygen molecule go through a series of different electronic states (see Figure 1.3). We use CDFT to calculate each individual electronic state involved in the generation process. We also use CDFT to compute the couplings between each of the different electronic states. The couplings are necessary in order to find the rate at which $^1O_2$ is generated for a specific BODIPY dye. This study is set to show that ROKS can perform more closely to CDFT (the correct description for the behavior of a molecular system) while TDDFT is not able to correctly describe the system.

Some key aspects of CDFT to keep in mind when performing CDFT calculations include:[42]

- Constraining larger fragments will give more consistent results

- Constraining charge and spin together is preferable when possible
- There are many ways to constrain the same state
- When donor and acceptor molecules are very close to each other, CDFT may fail

CDFT proves to be an accurate and effective method for calculating individual electronic states, charge transfer states, and couplings for the chemical systems we are interested in.

We have covered the methods that we use throughout this study, giving a fundamental understanding of how each method functions and how these methods are incorporated into our research. We now begin to explore the results that are obtained from these methods as they apply to the photophysics and photosensitizing potential of BODIPY derivatives.

3 Investigating the Parallelity between Excited State Potential Energy Surfaces from Time-independent and Time-dependent DFT

The design and characterization of organic chromophores for applications including chemical sensing,[43,44] sensitization of photovoltaic devices,[45,46] and photodynamic therapy[47] increasingly integrates computational modeling into the design and development process. Important contributions of computational modeling to chromophore design range from detailed mechanistic studies, which can complement experimental characterization and guide the further refinement of design criteria,[48] to virtual high-throughput screening of candidate structures[49,50]

Among the most thoroughly investigated and utilized chromophore scaffolds, the BODIPY chromophore **1** (Figure 3.1) is especially valued for its high photoabsorption cross-section, sharp emission profile, high fluorescence quantum yield, biocompatibility, and facile derivatization.[51,52] Extensive theoretical modeling of BODIPY dyes has assisted in the design of modular molecular architectures based on the BODIPY chromophore for directed excitation energy transfer,[53,54] triplet-triplet annihilation,[55] and sensitization of $^1O_2$.[56–58] Lincoln and co-workers used molecular orbital calculations based on density functional theory (DFT) as a theoretical bridge to rationalize simple rules based on Hammett constants for predicting excited-state redox potentials of substituted BODIPY dyes.[59] The influence of alkyl substitutions on the planarity, HOMO-LUMO gap, Stokes shift, and fluorescence quantum yield of substituted BODIPYs has also been probed computationally.[60,61]

To model the excited state properties of BODIPY derivatives and other larger chromophores, time-dependent density functional theory[62] (TDDFT) is often employed for its advantageous computational scaling relative to multireference *ab initio* methods[63] and because its strengths and weaknesses for standard chromophore scaffolds have been thoroughly characterized.[64] The TDDFT description of the BODIPY chromophore, and of cyanine dyes

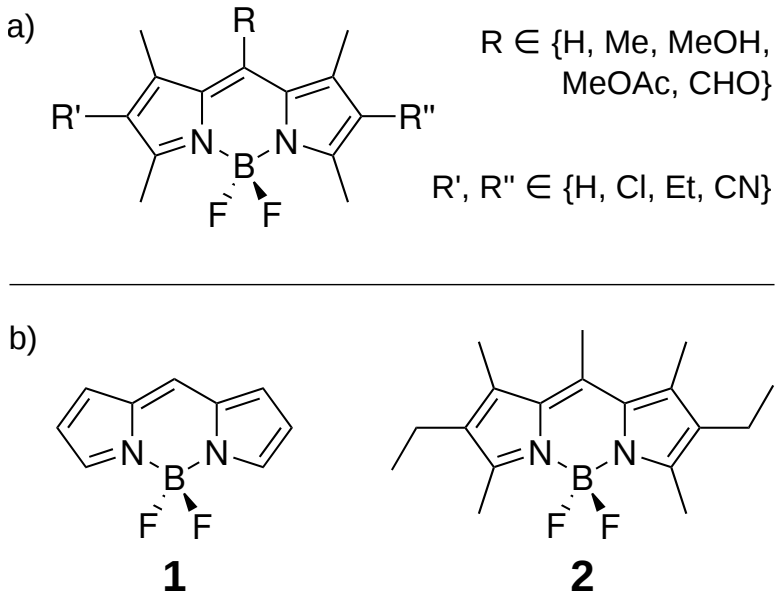

Figure 3.1: (a) Summary of BODIPY derivatives employed in the comparison of TDDFT and ROKS excitation/emission energies. (b) Structures of the BODIPY core **1** and of the BODIPY derivative **2** selected for detailed excited-state PES characterization.

more broadly, has been scrutinized in the literature due to a systematic overestimation of the lowest singlet excitation energy with some commonly used exchange-correlation functionals.[65,66] This error has been attributed to multireference character of the low-lying excited states with additional contributions from double excitations and from the approximate treatment of electron correlation.[67] A hybrid strategy combining configuration-interaction singles (CIS) and TDDFT systematically shifts the excitation energy such that errors relative to experiment are more in line with those observed for other dyes.[68] For modeling nonadiabatic dynamics, standard TDDFT approaches can also yield a qualitatively incorrect description of the conical intersections through which nonradiative relaxation typically occurs.[69]

Relative to TDDFT, time-independent approaches to excited states in DFT such as Δ-self-consistent-field (ΔSCF) DFT,[70–72] the restricted open-shell Kohn-Sham (ROKS) approach,[73,74] constricted variational DFT,[75,76] and orthogonality-constrained DFT[77] remain less thoroughly benchmarked or applied for modeling essential chromophores such as BODIPY. Recent implementations and benchmarking of time-independent excited-state DFT methods with modern exchange-correlation functionals has revealed that their accuracy is

similar to that of TDDFT for a given choice of exchange-correlation functional.[74,76,77] These methods are poised to play a greater role in simulations of excited-state processes, especially in situations where existing TDDFT approaches fail.[78] However, the performance of ROKS and related methods away from critical points, i.e. the minima of the S_0 and S_1 potential energy surfaces (PES), is relatively unexplored. A notable exception in the case of BODIPY is Briggs and co-workers' characterization[79] of BODIPY absorption and emission in water using a ΔSCF-based quantum mechanics / molecular mechanics (QM/MM) approach, with non-Aufbau orbital occupations enforced via the maximum overlap method.[41] The simulated spectra reproduced key features of both CASPT2 and experimental spectra, thus demonstrating the potential utility of time-independent excited state DFT for Born-Oppenheimer molecular dynamics (MD) in excited states.

For time-independent excited state DFT to be suitable for photochemical applications, firm theoretical justification of the methods' approximations and evidence that its accuracy in practice is adequate for the target application are both needed. Progress on the first criterion has been made recently with the proven existence of an excited-state analogue to the exact exchange-correlation functional of Kohn-Sham DFT.[80,81] This work aims to contribute to the second criterion, examining the practical utility of time-independent excited state DFT through a detailed comparison of TDDFT and ROKS descriptions of the S_1 PES of a representative BODIPY chromophore. The influence of the local environment (e.g. solvent effects) on excited state properties can be substantial[82–84] and should be included when aiming to explain observations in condensed phases;[85] however in this study we ignore these contributions in order to focus on exclusively on differences in the excited state PES of the isolated chromophore.

The central goal of this portion of this thesis is to characterize the nonparallelity of linear-response TDDFT and variational ROKS excited state potential energy surfaces for a representative, widely used organic chromophore. If TDDFT and ROKS predicted an energy for the S_1 state of a chromophore which differed systematically by a certain fixed value ΔE,

we would describe the TDDFT and ROKS PES as parallel with displacement ΔE. In practice, the different approximations entering into the TDDFT and ROKS descriptions of the S_1 state cause the two PES to differ in a more complicated manner which can nevertheless be decomposed into a fixed offset ΔE plus correction terms, analogous to the decomposition of a statistical error into systematic and random components. Figure 3.2 provides a simplified visual representation of the energy gap and nonparallelity of two approximations to a single PES. To make this sort of comparison quantitative, the simple alkyl-substituted BODIPY derivative **2** shown in Figure 3.1b was selected for a detailed comparison of the TDDFT and ROKS descriptions of its S_1 PES via excited-state molecular dynamics (MD) sampling and analysis of sampled configurations.

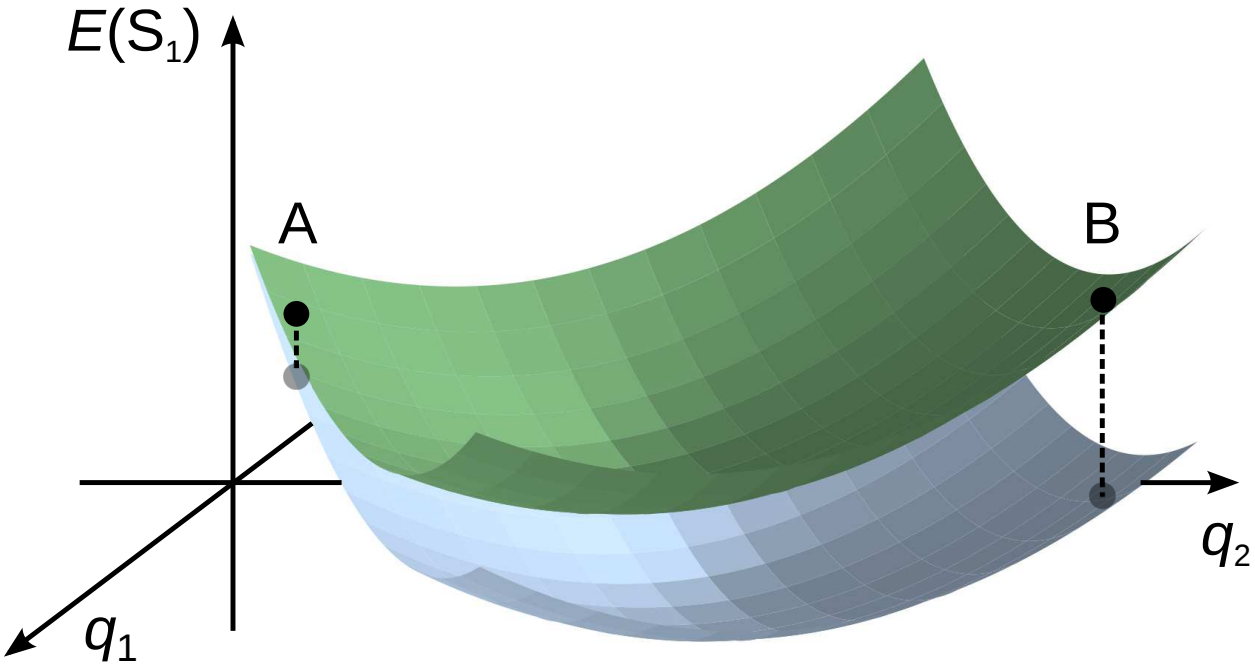

Figure 3.2: Schematic illustrating possible nonparallelity of the TDDFT and ROKS S_1 PES along representative degrees of freedom. There may be regions where the two PES have similar values despite significant differences in parallelity (point A) and other regions where the PES are quite parallel despite significant differences in energy (point B).

The remainder of this section is organized as follows. First we describe the details of our excited state energy, geometry optimization, molecular dynamics, and vibrational frequency calculations. Vertical excitation and emission energies obtained from ROKS and

from TDDFT for a representative set of BODIPY derivatives are then compared against experimental spectra and against one another. Next, to probe the shapes of the ROKS and TDDFT PES in greater detail, we perform excited-state MD sampling in the S_1 excited state of the BODIPY derivative **2** using ROKS and TDDFT and compare both the agreement of the two PES at sampled configurations as well as differences in the sampled configurations themselves. A representation of sampled configurations in the basis of excited state normal modes is pursued to visualize and interpret major differences between the ROKS and TDDFT representations of the PES. Finally, we present our conclusions and identify implications of the work for modeling of chromophore absorption and emission properties via excited-state DFT methods.

3.1 Computational Details

The full set of BODIPY derivatives was generated and pre-optimized with the Avogadro molecular editor[86] prior to full DFT geometry optimization. Energies, geometries, and vibrational frequencies, unless otherwise stated, were computed with the B3LYP exchange-correlation functional[87] and 6-31G(d) basis set. The selection of a functional was based on its use in other theoretical treatments of BODIPY dyes, for ease of comparison.

In contrast to the situation for linear-response TDDFT, applications of the ROKS approach to low-spin excited states are still relatively scarce. Therefore we will briefly review some essential features of ROKS excited states. In the ROKS approach, the variational principle is applied to an energy expression which depends on one or more excited determinants constructed from a single set of Kohn-Sham orbitals $\{\phi_i\}$.[73,74,88] For the S_1 excited state of a closed-shell molecule, two determinants are required: a "mixed" or broken-symmetry configuration m with two unpaired electrons of opposite spin, and a triplet configuration t with the unpaired electrons spin-parallel. Variational minimization of the ROKS energy

expression for the lowest singlet excited state,

$$E^{\mathrm{ROKS}} = 2E_m\left[\{\phi_i\}\right] - E_t\left[\{\phi_i\}\right]$$

yields the S_1 energy and wavefunction in ROKS. The method overcomes the tendency of ΔSCF orbital optimization to collapse to the ground state, but it can sometimes exhibit artificial energy-lowering due to mixing between the two open-shell orbitals.[74,89] This issue can be diagnosed by calculating the wavefunction overlap between the mixed-spin and ground-state determinants and corrected through level-shifting techniques. Details of the implementation used in this work are described in Ref. 74. ROKS excited states are distinct from the use of a restricted open-shell formalism for ground-state DFT calculations on open-shell systems, which has been discouraged on both theoretical and practical grounds.[90]

ROKS calculations of the S_1 excited state were performed without a level shift, as the wavefunction overlap diagnostic indicated that level shifting was unnecessary. For TDDFT calculations, the Tamm-Dancoff approximation (TDA) was used to pre-converge TDDFT roots,[91] but the final excitation energy calculations employ the complete Casida equations. The four lowest roots in the singlet manifold were converged to ensure that the lowest root was obtained in all cases. ROKS and TDDFT $S_1 \rightarrow S_0$ emission energies were computed at the corresponding ROKS and TDDFT optimized S_1 geometries. For the TDDFT excited state geometry optimizations, where state-switching can occur during the optimization, we confirmed that the character of the S_1 excited state was retained continuously along each optimization. All ground-state DFT and excited-state TDDFT and ROKS calculations were performed with the Q-Chem 4.2 package.[92]

Born-Oppenheimer MD simulations on the S_1 excited state of **2** were carried out in the *NVE* ensemble. For both ROKS and TDDFT MD, ten independent MD simulations were performed starting at the B3LYP/6-31G(d) S_0 optimized geometry and with initial velocities independently sampled from the Maxwell-Boltzmann distribution at 300 K. The time step

was set to 40 a.u. to ensure energy conservation, and the smaller 3-21G basis set was employed for computational efficiency. For both sets of trajectories, measures were taken to mitigate the likelihood of termination due to convergence failure: for ROKS, a level shift of 0.2 Hartree was pre-emptively employed, while the convergence criterion for TDDFT roots was pre-emptively slightly loosened to 10^{-5} Hartree.

Snapshots from the production MD simulations were collected at every 20th timestep to mitigate correlation between sampled configurations. The ROKS and TDDFT excitation energies were then computed for each snapshot at the B3LYP/6-31G(d) level of theory. Note that this comparison entails a re-evaluation of the excitation energy obtained from the RO-B3LYP/3-21G or TD-B3LYP/3-21G MD simulation using the larger 6-31G(d) basis set.

Vibrational frequencies were calculated at the ground state and excited-state (TDDFT and ROKS) optimized geometries of **2**. In the case of ROKS, frequencies were obtained using analytic first derivatives but numerical second derivatives with a displacement of 10^{-3} Å. The resulting normal mode displacements were used to express MD snapshots in terms of distortions from the optimized S_1 geometry.

3.2 Results and Discussion

Vertical Excitation and Emission of BODIPY Derivatives

As an initial probe of differences between ROKS and TDDFT descriptions of the BODIPY S_1 state, we calculated the vertical excitation and emission energies for the set of BODIPY derivatives indicated in Figure 3.1a. Scatterplots of excitation and emission energies from ROKS and from TDDFT are presented against maxima of the experimental absorption and emission spectra[59] in Figure 3.3. Relative to experiment, we observe a systematic overestimation of the excitation energy by TDDFT on the order of 0.4 eV, fully consistent with previous observations for the BODIPY chromophore.[68] Conversely, ROKS underestimates the excitation energy relative to experiment by approximately 0.15 eV on average.

In the absence of solvent corrections, TDDFT and ROKS excitation energies show only

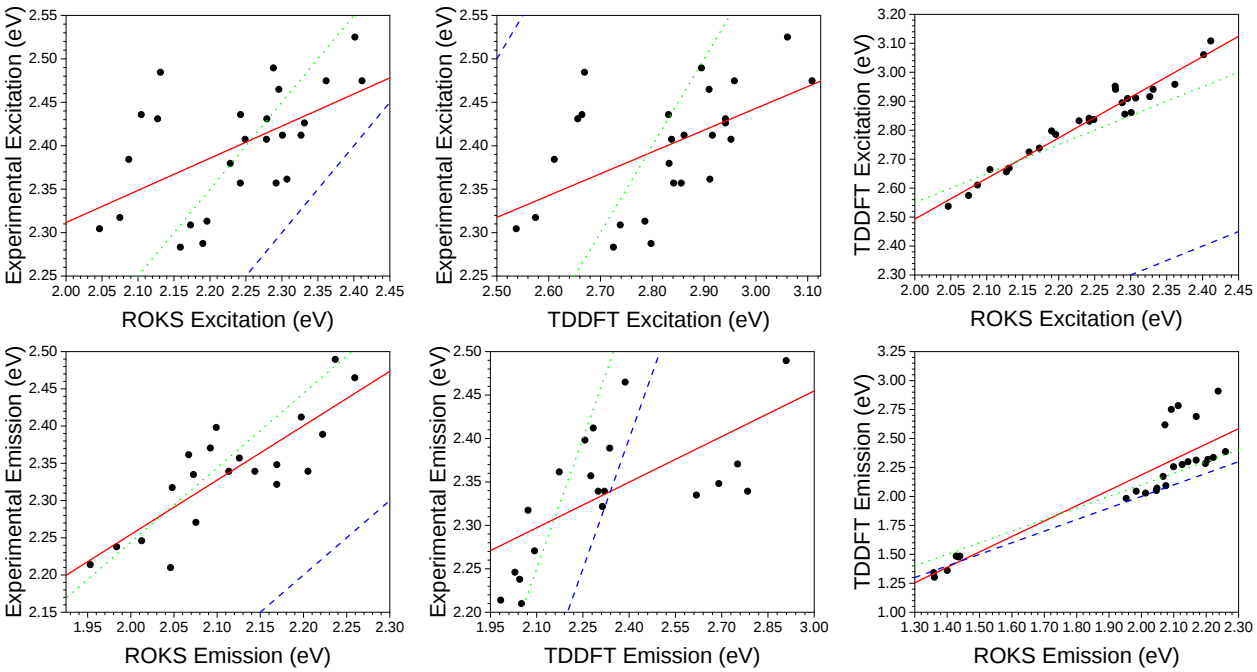

Figure 3.3: Vertical excitation ($S_0 \rightarrow S_1$) and emission ($S_1 \rightarrow S_0$) energies of BODIPY derivatives from ROKS and TDDFT compared against maxima of experimental absorption and emission spectra. The best linear fit (solid red line), best linear fit assuming a slope of 1 (dotted green line), and hypothetical perfect agreement (dashed blue line) are provided for reference.

a loose correlation with experimental absorption maxima (TDDFT: $r = 0.81$, ROKS: $r = 0.83$). However, the correlation between ROKS and TDDFT excitation energies is quite strong ($r = 0.98$), notwithstanding the enormous average gap (> 0.5 eV) between them. This gap originates in the known overestimation of the S_1 excitation energy in BODIPY dyes by TDDFT with global hybrid functionals[68] and is exacerbated by an apparent underestimation of excitation energies by ROKS, which has been observed in other studies, especially with pure exchange-correlation functionals.[74,89,93] The favorable correlation between ROKS and TDDFT excitation energies indicates that the two approaches make very similar predictions of shifts in excitation energy due to derivatization of the BODIPY core, at least within the set of derivatives examined here.

Overall, ROKS and TDDFT capture similar trends in the excitation energy as the substituents are varied. Provided that the systematic under- or overestimation of the excitation

energy is accounted for,[68] the two methods appear similarly well suited for use in computational screening of BODIPY derivatives based on static, optimized geometries.

Turning attention to the emission energy (bottom row of Figure 3.3), the correlation between TDDFT and ROKS would be strong if not for the handful outliers for which TDDFT predicts an anomalously small decrease in the S_1 energy due to geometry relaxation in the excited state. Three of these five apparent outliers in the comparison of TDDFT and ROKS emission energies bear only -H in the R′ and R″ positions. The dominant orbital contributions to the TDDFT transition vector in these cases does not differ substantially from those of the other BODIPY derivatives, so it is not possible to ascribe the error to a qualitative change of character of the excited state along the relaxation pathway. The influence of these outliers is evident on the best-fit line relating TDDFT emission energies to experiment, where they have a significant effect on the slope and result in a poor correlation coefficient ($r = 0.64$). In contrast, the ROKS emission energies lack such outliers and maintain closer agreement with experimental emission energies across the set of BODIPY derivatives ($r = 0.83$).

Table 3.1: Mean error (ME), mean absolute error (MAE), and root-mean-square deviation (RMSD) of ROKS and TDDFT absorption/emission relative to experiment. All energy errors are reported in eV.

	ROKS		TDDFT	
	Abs.	Em.	Abs.	Em.
ME	−0.161	−0.224	0.431	0.016
MAE	0.161	0.176	0.431	0.431
RMSD	0.181	0.202	0.447	0.210

ROKS and TDDFT emission energies are in much closer agreement with one another than the corresponding vertical excitation energies. This observation – along with the fact that TDDFT overestimates the excitation energy in BODIPY dyes while ROKS underestimates them – suggests that TD-B3LYP will tend to overestimate Stokes shifts of BODIPY dyes, while RO-B3LYP is more likely to underestimate them. Just from the excited-state energies at these two geometries alone (the S_0 and S_1 optimized geometries), it is clear that the TDDFT and ROKS descriptions of the S_1 PES cannot be exactly parallel: if they were,

then the average gap between TDDFT and ROKS excitation energies would be identical to the average gap between TDDFT and ROKS emission energies. In the next section, we characterize nonparallelity of the TDDFT and ROKS models of the S_1 excited state for a representative BODIPY chromophore.

Nonparallelity of TDDFT and ROKS Potential Energy Surfaces

The propagation of molecular dynamics on the S_1 PES is an important step in extracting rates and quantum yields of photophysical processes from electronic structure simulations. Naturally, the quality of the predictions is only as good as the quality of the PES. Therefore, we aim to compare features of the S_1 PES obtained from TDDFT against time-independent approaches like ROKS, with particular attention to differences which may impact the prediction of excited-state properties. In this section we compare TDDFT and ROKS models of the S_1 PES for the BODIPY chromophore **2** (Figure 3.1) through MD sampling of both surfaces and analysis of molecular motions associated with the most significant differences between the two PES.

Molecular Dynamics Sampling From the ground-state optimized geometry, we initiated excited-state Born-Oppenheimer MD simulations on both the ROKS and TDDFT representations of the S_1 PES as described in the Computational Details. To compare the two PES at a consistent collection of geometries, the S_1 energy of snapshots obtained from TDDFT MD is recomputed using ROKS, and vice versa. Any nonparallelity of the PES will manifest not only in fluctuations in the energy difference $\Delta E = E(\text{ROKS}) - E(\text{TDDFT})$; it will also affect the region of configuration space sampled by the MD. Both of these effects are discussed below.

Scatterplots of the S_1 energy obtained from ROKS and from TDDFT for configurations sampled from the two approaches are presented in Figure 3.4. If the two methods were in perfect agreement, then the energies for all sampled configurations would lie on the dashed

blue lines representing a perfect correspondence between the ROKS and TDDFT energy. In particular, any deviation of the best-fit line from unit slope would indicate nonparallelity between the two PES. However, as shown in the previous section, TDDFT consistently predicts higher S_1 energies than ROKS for BODIPY chromophores; this trend is evident in the constant offset of roughly 0.5 eV for configurations sampled from ROKS MD, shown in Figure 3.4a. However, the configurations obtained from ROKS MD sampling show a strong correlation between ROKS and TDDFT energies, indicating that the ROKS and TDDFT representations of the PES are quite parallel in the region sampled by ROKS.

The configurations sampled by TDDFT MD (Figure 3.4b) reveal two key differences relative to the ROKS-sampled configurations. First, the correlation between TDDFT and ROKS energies is significantly weaker for configurations sampled by TDDFT. Furthermore, the significant offset between TDDFT and ROKS energies is absent among the configurations sampled by TDDFT MD; roughly as many configurations have a higher energy according to ROKS than according to TDDFT. Together, these observations suggest that our TDDFT MD has sampled a qualitatively different region of the S_1 PES compared to ROKS MD. While ROKS MD appears to sample a region of configuration space where the ROKS and TDDFT S_1 PES are approximately parallel but significantly displaced, TDDFT MD has sampled a region characterized by a smaller displacement but greater nonparallelity. Here, the configurations sampled by ROKS MD retain the large energy gap between TDDFT and ROKS S_1 energies observed for the S_0 optimized geometry in Figure 3.3, while configurations sampled by TDDFT MD show a smaller gap more consistent with the S_1 optimized geometry. These observations suggest that TDDFT MD evolved toward the S_1 minimum early in the simulations and sampled configurations mostly near this minimum, whereas ROKS MD evolved much more slowly toward the S_1 minimum, sampling mostly structures near the S_0 minimum. These qualitative differences illustrate the potentially compounding effect of nonparallelity error on finite sampling of high-dimensional PES: errors in the shape of the PES can bias MD away from important configurations, introducing further error into

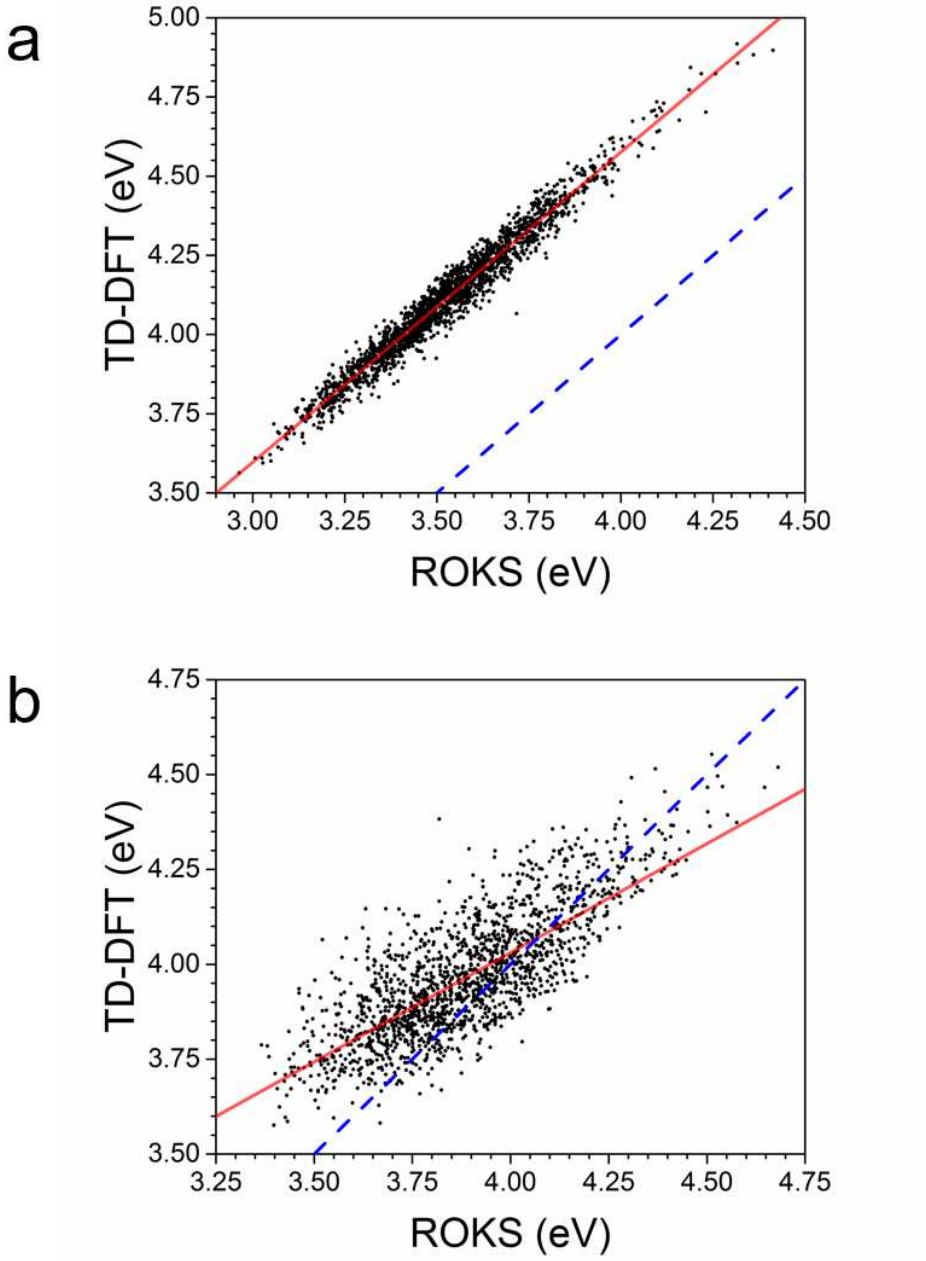

Figure 3.4: Scatterplot of TDDFT and ROKS energies for configurations sampled from (a) ROKS and (b) TDDFT MD simulations. The solid red line is a linear fit, while the dashed blue represents perfect agreement between ROKS and TDDFT.

ensemble averages of molecular properties.

It is instructive to interpret the observed differences between configurations sampled by ROKS and TDDFT in the context of Figure 3.2 as a means of visualizing regions of the PES sampled by the two methods. The ROKS MD simulation appears to have sampled a region represented by Point B in Figure 3.2, where the two PESs are highly parallel but have a large gap in energy, while the TDDFT MD simulation sampled a region akin to Point A, where the two PESs have little gap in energy, but they deviate from parallelity. To better understand these differences in the PESs and their implications for BODIPY photophysics, we proceeded to analyze the sampled configurations in terms of molecular motions along which two PESs differed most substantially.

Normal mode analysis of sampled configurations The extent of correlation between TDDFT and ROKS energies for the S_1 state across sampled configurations provides a useful global view of similarities and differences between the two PES. However, in order to determine how these differences might influence predictions of photophysical or photochemical rearrangements in the excited state, it is necessary to identify those molecular motions along which TDDFT and ROKS disagree the most. The normal vibrational modes of **2** in the S_1 excited state form a convenient basis for describing these internal motions.

To identify the normal modes along which the two PES differ most significantly, the Cartesian coordinates of each sampled configuration from the MD trajectories were recast in terms of displacements from the equilibrium S_1 geometry along the normal vibrational modes,

$$\mathbf{x}_i = \mathbf{x}_0 + \mathbf{Q}\mathbf{c}_i \tag{3.1}$$

where $\mathbf{x}$ and $\mathbf{x}_0$ are the Cartesian coordinates of sampled configuration i and of the equilibrium geometry, respectively, $\mathbf{Q}$ is a matrix of normal mode displacements, and $\mathbf{c}_i$ are the undetermined weights of the different normal modes that map the equilibrium structure to the displaced configuration i. Eq. 3.1 is nominally underdetermined because of global

translation and rotation, so we constrain the first two nuclei to their correct positions in the target configuration and solve Eq. 3.1 for the positions of the remaining nuclei. More sophisticated approaches based on principal component analysis have been applied to identify key motions that modulate the excitation energy based on ground-state MD;[94] we adopt the simpler approach outlined above in order to focus on key motions along which TDDFT and ROKS excitation energies differ.

The choice of which two nuclei to fix is a potential source of bias in the reconstruction of snapshot configurations from normal mode displacements. To address this concern, we compared the weights $\mathbf{c}_i$ obtained for a representative snapshot with those obtained from a different choice of fixed nuclei, observing negligible differences in the dominant modes.

Normal mode displacements which contributed most substantially to the sampled configurations from ROKS MD and from TDDFT MD are summarized in Table 3.2. Remarkably, the same three modes emerged as most dominant in both the TDDFT and ROKS MD-sampled configurations, despite the qualitative differences in sampling observed in the previous section. Two of the three modes are very low-frequency modes primarily associated with the side chains on the BODIPY core, although in ROKS this mode also shows some bending of the plane of the BODIPY chromophore. The third mode is in the ring-breathing region of the IR spectrum and includes changes in the B–N bond lengths. While the large weights for the low-frequency modes could be explained by the shallowness of the PES along such modes, the third mode cannot be rationalized in this way. We suspected instead that this mode is one of the key modes along which the BODIPY chromophore relaxes from the initial S_0 optimized geometry toward equilibrium S_1 geometries. We confirmed this hypothesis by subjecting the S_0 optimized geometry to the same normal mode analysis and identifying this mode as one of the three modes with largest weight along the displacement connecting the two minima.

In order to understand how differences between TDDFT and ROKS sampling of the S_1 PES might affect predictions of excited state dynamics, we sorted the normal mode displace-

Table 3.2: Frequency, character, and weight (element of $\mathbf{c}_i$ in Eq. 3.1) of the most significant normal mode displacements sampled in TDDFT and ROKS MD.

TDDFT MD

Mode	Frequency (cm^{-1})	Vib. Mode Description	Average Weight		Difference
			ROKS	TDDFT	
12	161	methyl twisting, ethyl rocking	0.39887	0.39829	5.8×10^{-4}
15	192	methyl, ethyl twisting	0.35908	0.35856	5.2×10^{-4}
75	1227	chromophore B-N and C=C stretch	0.35699	0.35655	4.4×10^{-4}

ROKS MD

Mode	Frequency (cm^{-1})	Vib. Mode Description	Average Weight		Difference
			ROKS	TDDFT	
12	159	methyl twisting, ethyl rocking	0.39553	0.39621	6.8×10^{-4}
15	183	out of plane bending, BF_2 wagging	0.35774	0.35842	6.8×10^{-4}
75	1245	chromophore B-N and C=C stretch	0.35475	0.35540	6.5×10^{-4}

ments by their average weights among snapshots from TDDFT MD and from ROKS MD and then identified the modes whose average contributions differed the most. Among the snapshots sampled by TDDFT MD, the two modes along which the ROKS and TDDFT PES deviate most significantly are reported in Table 3.3. Both of the modes are low-frequency motions predominantly affecting the alkyl side groups rather than the chromophore itself. This finding indicates that the molecular motions contributing dominantly to the nonparallelity of TDDFT and ROKS in MD sampling of the S_1 state of **2** are side chain motions, not distortions of the central BODIPY chromophore. For computationally assisted design of BODIPY-based functional molecules and materials, where understanding the influence of side chains on photophysical properties is crucial, our analysis shows that the simulated dynamics of these side chains after photoexcitation can be highly sensitive to the choice of excitation model (here, TDDFT or ROKS) for the S_1 PES, even if the exchange-correlation functional is the same.

Table 3.3: Frequencies, character, and contribution weights of normal mode displacements along which TDDFT and ROKS energies most significantly deviate.

TDDFT MD

Mode	Frequency (cm^{-1})	Vib. Mode Description	Average Weight		Difference
			ROKS	TDDFT	
10	149	methyl twisting	0.02245	0.02108	1.4×10^{-3}
13	180	ethyl, methyl twisting	0.10768	0.10892	1.2×10^{-3}

ROKS MD

Mode	Frequency (cm^{-1})	Vib. Mode Description	Average Weight		Difference
			ROKS	TDDFT	
10	142	methyl twisting	0.00945	0.00994	4.9×10^{-4}
13	171	ethyl, methyl twisting	0.11807	0.11793	1.4×10^{-4}

To provide a low-dimensional representation of the differences between the TDDFT and ROKS S_1 PES, we projected each PES onto the normal mode displacements whose contributions to sampled TDDFT and ROKS configurations differed most significantly (Figure

3.5). These projections were constructed by evaluating the TDDFT and ROKS single-point energies at different degrees of displacement along the normal mode displacement vector $\mathbf{q}$, with the degree of displacement controlled by an angular variable θ. Coordinates $\mathbf{x}$ for each sampled displacement were determined relative to the optimized geometry $\mathbf{x}_0$ according to the formula $\mathbf{x} = \mathbf{x}_0 + \mathbf{q}\ \sin\theta$.

Nonparallelity of the TDDFT and ROKS PES along all four selected modes is evident in the changing gap between TDDFT and ROKS energies in Figure 3.5. Along three of the four selected modes, the difference between TDDFT and ROKS energies decreases as the molecule distorts; the exception is mode 18, for which the TDDFT energy becomes even higher relative to ROKS along the distortion. There is a noticeable asymmetry in the nonparallelity of the two PES with respect to the direction of the distortion. For example, the TDDFT and ROKS PES are sufficiently nonparallel to cross during extension along mode 21 ($\theta > 0$), but a compression of the same magnitude along the same mode does not induce a similar crossing.

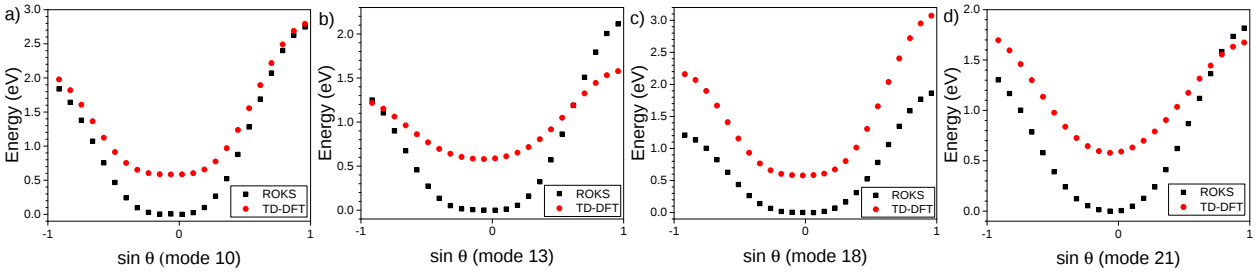

Figure 3.5: Comparison of S_1 PES projections for **2** onto normal modes along which TDDFT and ROKS sampled configurations most significantly differ. The angular coordinate θ traces periodic vibrational motion along the corresponding mode with $\sin\theta = 0$ for the minimum energy configuration and $\sin\theta = \pm 1$ for the turning points along the mode.

While these significant differences in the shape of the TDDFT and ROKS PES may be somewhat mitigated by the use of more sophisticated functionals,[95,96] differences are likely to persist due to the fundamentally different approaches – time-independent and variational versus time-dependent linear response – used to model the S_1 state. Both approaches invoke approximations beyond the choice of exchange-correlation functional. For example, TDDFT-

based excited-state MD simulations generally rely on the adiabatic approximation.[97] ROKS indirectly relies on an adiabatic approximation as discussed for the related ΔSCF approach in Ref. 72, but the ROKS formulation employed here also invokes a two-determinant Kohn-Sham ansatz which may be inadequate, for example, in systems with significant double-excitation character.[98,99]

3.3 Conclusion

In this section we identified both similarities and significant practical differences in the TDDFT and ROKS descriptions of vertical excitation and emission energies of BODIPY dyes. In contrast to the known overestimation of the lowest singlet vertical excitation energy by TDDFT with the B3LYP functional, the ROKS approach systematically underestimates this excitation energy, though by a lesser margin. Nevertheless, TDDFT and ROKS vertical excitation and emission energies calculated across a range of substituted BODIPY dyes exhibit a strong correlation, indicating that the two approaches predict similar shifts in absorption and emission spectra due to chemical substitution along the periphery of the chromophore.

By sampling the S_1 excited state PES of a selected BODIPY derivative through both TDDFT and ROKS MD simulations, we determined that the two approaches exhibit qualitatively different sampling behavior which is likely to impact ensemble-averaged estimates of excited-state properties. ROKS samples a region of the S_1 PES where the ROKS and TDDFT descriptions of the PES are parallel but offset by roughly 0.5 eV; in contrast, TDDFT samples configurations with a smaller offset but more substantial differences in the local shape of the PES.

The excited-state characterization of substituted BODIPYs presented here may help guide the further optimization of chromophores based on the BODIPY framework. Additionally, the explicit comparison of ROKS and TDDFT PES may offer useful insight for users and developers of time-independent excited state DFT strategies. A more complete

understanding of these methods' strengths and shortcomings will increase confidence in the interpretation of simulated spectra and excited-state properties.

4 Photophysics of $^1O_2$ Sensitization by a BODIPY Derivative

As a reminder, this study is focused on the computational characterization of the properties of a set of boron-dipyrromethene (BODIPY) dyes as potential photosensitizers (PS) in photodynamic therapy (PDT). PS are molecules that are able to absorb photons, become energetically excited, and then transfer that energy to promote some target chemical process. In PDT a specific sequence of electronic transitions involving the PS an oxygen molecule leads to the formation of singlet oxygen $^1O_2$, the active component of PDT which causes the destruction of cancer cells. Overall this study aims to shed light on the singlet oxygen sensitization characteristics for the BODIPY dyes in question and to help make accurate distinctions between several derivatives that are under consideration for use as PS in PDT.

Earlier in this thesis we examined and rationalized how the restricted open-shell Kohn-Sham (ROKS) method and time-dependent density functional theory (TDDFT) can accurately describe the S_1 excited states for several BODIPY dyes. Now we can move towards studying how the excited PS ($^1PS^*$) interacts with ground state triplet oxygen ($^3O_2$) and leads to the formation of $^1O_2$. First, it is important to understand the process of how $^1O_2$ is formed and how we can perform calculations to replicate that process. Shown in Figure 1.3 the PS sequentially adopts two electronic states that precede the formation of $^1O_2$: $^1PS^*$, and ^3PS, where ^1PS is the state that results with $^1O_2$. In order to restrict the calculations so that we can compute each individual electronic state we must use constrained density functional theory (CDFT). Without constraints on the electron and spin densities, it would be impossible to accurately compute certain electronic states of BODIPY-O_2 complexes that we are studying. In addition to computing the individual electronic states, we also need to compute the electronic couplings between all of the directly connected states (couplings between $^1PS^*$ and ^3PS, as well as ^3PS and ^1PS). Knowing the couplings will provide us with insight on the transition rates between the electronic states. Understanding the couplings

and transition rates will give us a relative estimate on how efficiently a dye can generate $^1O_2$.

To computationally characterize $^1O_2$ photosensitization by BODIPY we use a single BODIPY dye and one oxygen molecule. Rather than computing the $^1O_2$ generation properties for all 26 of the derivatives summarized in Table A1, we decided to hone in on a specific BODIPY derivative seen in Figure 4.1 to perform all subsequent calculations on.

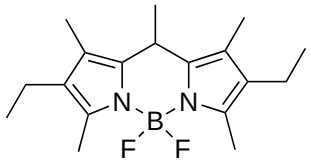

Figure 4.1: Strucutre of 2,6-diethyl-1,3,5,7-tetramethyl-pyrromethene fluoroborate

We decided on specifically the molecule in Figure 4.1, firstly because we had performed the MD simulations on this molecule which gives us a detailed understanding of the description for the S_1 excited state PES for this particular BODIPY derivative. Second, because the structure of this molecule is relatively simple, having two ethyl groups attached on either end of the core's structure (positions 2 and 6 in Table A1) and methyl groups located at the 1, 3, 5, 7, and 8-carbon positions of the core. Having saturated alkyl substituents is more simple than halogens or other inorganic substituents which could complicate the electronic structure of the BODIPY core. The simplicity of molecule 4.1 makes our predictions more precise and less susceptible to unaccounted deviations in our data. Molecule 4.1 is simple enough to be widely representative of BODIPY derivatives but has substituents that add some complexity. At the moment there have been no other studies that have attempted to predict the properties that we are computing, so limiting our calculations to moderately simple cases was the most reasonable approach to tackle this problem. In the future there are plans to broaden this study by looking at how different substituents affect the generation of $^1O_2$.

4.1 Electronic Transitions

Molecules that are able to be electronically excited, fluoresce, and sometimes transfer their energy to form other electronic states are known as fluorophores. There are several relaxation routes that a fluorophore can take after it has been photo-excited. The first possibility is that the fluorophore (in its S_1 excited state) fluoresces directly and drops back down to the ground state (S_0). In fluorescence, 3 primary steps are involved:

- Excitation (refer to Figure 2.1)
  - The fluorophore, in its S_0 ground state, is promoted to the S_1 excited state via an incoming photon of specific energy
- Relaxation of the excited state
  - The fluorophore's conformation slighty changes to adopt the lowest energy conformation in its S_1 excited state (position 3 in Figure 2.1)
- Fluorescence emission
  - A photon of lower energy than the incoming photon that excited the fluorophore is emitted, bringing the molecule back down to the S_0 ground state (position 4)
  - The emitted photon has a lower energy due to the excited state relaxation. The energy difference between the energy provided by the incoming photon and energy emitted is the Stokes shift)

While in the singlet excited state, a process called internal conversion occurs where the molecule relaxes from a higher vibrational level down to the lowest vibrational level. The lowest vibrational level of the singlet excited state is usually the level from which fluorescence occurs.[100] If the excited state lifetime is long enough to prevent the PS from not immediately fluorescing right back down to the S_0 ground state then there is a possibility that the fluorophore can transfer an electron or undergo intersystem crossing entering a state of different

multiplicity. For example, if a PS is excited to its ^{1}PS* excited state then it can go through intersystem crossing to form a high energy triplet state (^{3}PS).[100] From here the PS has the possibility to transfer its excitation energy to another molecule, or it may phosphoresce.

Phosphorescence is a spontaneous emission of energy (in the from of a photon) that is much slower than fluorescence, due to the fact that the transition from the triplet state ^{3}PS to the ground state ^{1}PS is spin-forbidden.[100] When a PS enters the ^{3}PS state, internal conversion occurs generating a state that is lower in energy than the preceding singlet excited state ^{1}PS*. The low energy and multiplicity of the triplet state forbids a radiationless transition back down to the S_1 ground state ^{1}PS. However, radiative transitions are able to bring the ^{3}PS back down to the S_0 ground state because spin-orbit coupling breaks the selection rule. This radiative transition (phosphorescence) occurs much more slowly and over a longer period of time than fluorescence does, though it emits weaker than fluorescence. The efficiency of phosphorescence may be increased by including heavier atoms into the molecule.[101]

Contrary to fluorescence and phosphorescence, which emit a photon when relaxing to the ground state from an excited electronic state, intersystem crossing brings an excited electronic state to a different electronic state (not always another excited state), without emitting any photons. Internal conversion is another process that does not emit any photons, but internal conversion results with a change in vibrational energy rather than a change in electronic states. These processes are known as non-radiative transitions, while fluorescence and phosphorescence are radiative.[102] Internal conversion is a non-radiative transition between two states which have the same multiplicity. In internal conversion, instead of emitting a photon the energy is given off by a molecule's vibrational modes and heat. Intersystem crossing is a non-radiative transition between electronic states which have different multiplicities. Intersystem crossing occurs between a singlet state and triplet state, where the transition can occur in either direction depending on the molecular system in question. This electronic conversion has little to no energy that is gained or lost within the system.

It is very favorable when the vibrational levels of two electronic excited states overlap, and also when there are heavy atoms present (due to the higher spin-orbit coupling).[100]

Having summarized the key relaxation pathways of excited photosensitizers, let's take a deeper look at how singlet oxygen can be formed and how we can predict the singlet oxygen generation properties. First, after a molecule is excited to its lowest singlet excited state ($^1PS^*$) there are two different mechanisms that can occur which lead to different types of products. One pathway that the molecular system can undergo is defined as a Type I mechanism by analog to the definitions of type I and type II photosensitized oxidation by Foote, Gollnick, and Schenck.[103] Type I mechanisms occur when the S_1 excited state molecule directly transfers an electron to a substrate (in our case the substrate is molecular triplet oxygen), which yields a set of radicals ($^2PS^{\bullet+}$ and $^2O_2^{\bullet-}$). Type II mechanisms are when the excited molecule undergoes intersystem crossing from the singlet excited state ($^1PS^*$) forming the triplet state (^3PS), then the triplet state transfers energy to molecular oxygen ($^3O_2$) during a collision between the molecules which generates singlet oxygen. Some photosensitizers can produce up to 10^5 molecules of $^1O_2$ before they degrade.[104] In our study we want to focus on Type II mechanisms which yield the active component of PDT ($^1O_2$).

In order to find the quantum yield of singlet oxygen, we must first know the amount of singlet oxygen molecules that are produced. The primary quantum yield is defined as:

$$\Phi_{^1O_2} = \frac{\text{number of singlet oxygen molecules produced}}{\text{number of photons absorbed}} \tag{4.1}$$

In terms of rates we can define the quantum yield as:

$$\Phi_{^1O_2} = \frac{\text{rate of } ^1O_2 \text{ generation}}{\text{sum of rates for all other processes}} = \frac{k_{^1O_2}}{\sum_i k_i} \tag{4.2}$$

To further quantify the rate, we can invoke Fermi's Golden Rule, which states that during the transition between electronic states, the rate is a constant value during the transition

(i.e. the rate is not time-dependent). This definition is formulated by relating the rate of a state crossing to the electronic coupling matrix element for the process.[105] We are focusing on the following rate equation:

$$\omega_{\mathrm{T}} = \frac{2\pi}{\hbar}\rho(\mathrm{E}_m) \mid \mathrm{V}_{km} \mid^2 \tag{4.3}$$

where ω_{T} is the rate, $\rho(\mathrm{E}_m)$ is the density of states, and V_{km} is the electronic coupling between states k and m. In this study we are not concerned with the absolute rate of the transitions, we are instead focused on the relative rates. To calculate the relative rates we are looking at the ratio between two rate processes:

$$\frac{\omega_{\mathrm{T,m}}}{\omega_{\mathrm{T,n}}} = \frac{\frac{2\pi}{\hbar}\rho(\mathrm{E}_m) \mid \mathrm{V}_{km} \mid^2}{\frac{2\pi}{\hbar}\rho(\mathrm{E}_n) \mid \mathrm{V}_{ln} \mid^2} \tag{4.4}$$

With this ratio we have the $\frac{2\pi}{\hbar}$ cancel each other out resulting in:

$$\frac{\omega_{\mathrm{T,m}}}{\omega_{\mathrm{T,n}}} = \frac{\rho(\mathrm{E}_m) \mid \mathrm{V}_{km} \mid^2}{\rho(\mathrm{E}_n) \mid \mathrm{V}_{ln} \mid^2} \tag{4.5}$$

Also, we do not expect $\rho(\mathrm{E}_m)$ and $\rho(\mathrm{E}_n)$ to deviate substantially from one another. Resulting in the following equation:

$$\frac{\omega_{\mathrm{T,m}}}{\omega_{\mathrm{T,n}}} = \frac{\mid \mathrm{V}_{km} \mid^2}{\mid \mathrm{V}_{ln} \mid^2} \tag{4.6}$$

Where the rates are only dependent on the couplings for each electronic state. Equation 4.6 is now only dependent on the electronic coupling between states. With this new approximate definition of the relative rate we can use the coupling as a *pseudo* rate value to investigate the relative rates of $^1\mathrm{O}_2$ generation, transition between different processes, and between different molecular structures.

Now we must examine how to calculate the couplings V_{km} in equation 4.6 using computational methods. The method used to compute the couplings between different electronic states is CDFT. This description begins with the coupling equation[42] given two electronic

states $\mid \Psi_1\rangle$ and $\mid \Psi_2\rangle$:

$$\mathrm{H}_{12} = \langle \Psi_1 \mid \hat{\mathrm{H}} \mid \Psi_2 \rangle \tag{4.7}$$

where the coupling between the states is the matrix element of the Hamiltonian $\hat{H}$. When describing an electron transfer system, when the molecules are separated from each other the coupling is expected to exponentially decay. A more detailed walk-through of the CDFT method can be found in Kaduk et al.[42] The issue with equation 4.7 is that it is written in terms of wave functions, rather than densities which is what Kohn-Sham DFT provides. So CDFT uses an approximation where each wave function $\mid \Psi_i\rangle$, are eigenstates of $\hat{H}$ as well as the constraining potential $V_i w_i(r)$. Along with this approximation, the wavefunctions are approximated to be their Kohn-Sham surrogates ($\mid \Psi_i\rangle \approx \mid \Phi_i\rangle$) which results in the equation for the CDFT diabatic coupling:

$$\mathrm{H}_{12} \approx \frac{\mathrm{F}_1 + \mathrm{F}_2}{2}\mathrm{S}_{12}^{\mathrm{KS}} - \left\langle \Phi_1 \middle| \frac{\mathrm{V}_1\hat{w}_1(\mathbf{r}) + \mathrm{V}_2\hat{w}_1(\mathbf{r})}{2} \middle| \Phi_2 \right\rangle \tag{4.8}$$

In order to obtain a physically meaningful coupling an orthogonalization is required. The non-orthogonal basis Hamiltonian is transformed into an orthogonal basis using the symmetric Löwdin orthogonalization[42] returning the Hamiltonian in an orthogonal basis:

$$\mathrm{H} = \mathrm{S}^{-\frac{1}{2}}\mathrm{H}\mathrm{S}^{-\frac{1}{2}} \tag{4.9}$$

giving the final couplings (H_{12}) which are the elements of the $\mathbf{H}$ matrix ($[\mathbf{H}]_{12}$).

4.2 Computational Details

In this section we specify how we perform our calculations and obtain the particular electronic states in study. To obtain the specific electronic states we constrain the electrons using CDFT or a combination of charge and multiplicity values. CDFT couplings used the configuration interaction module (CDFT-CI) in Q-Chem with printout of information for the

coupling calculations (overlap, Hamiltonian, population matrix with eigenvectors and eigenvalues, as well as promolecule orbital coefficients and energies). The exchange-correlation functional used was ωB97X-D, along with the 6-31G(d) basis set. In order to meet convergence criteria, calculations were set to a convergence level of either 10^{-5}, 10^{-6}, and in some cases 10^{-8} hartrees, and a threshold value of either 10^{-10} or 10^{-14} to reduce the convergence requirements. In the event of convergence issues we added a ground state calculation prior to the CDFT calculation to read in the molecular orbitals, or as a last resort, to selectively reduce the convergence criteria. Roughly half of the coupling calculations required loosening the convergence criteria, however the restrictions are still reasonably tight, converging energies down to 10^{-5} Hartrees. All calculations were spin-unrestricted. We were able to obtain a few excited electronic state with ROKS,

Table 4.1: Required components for computing each electronic states. See appendix for higher level of details and charge/multiplicity.

Electronic states	CDFT	ROKS	MOM	Initial Ground State
^{1}PS +^{3} O_2	✓			
^{1}PS* + $^3O_2$			✓	✓
^{3}PS + $^3O_2$	✓			
^{1}PS* + $^1O_2$		✓		
^{1}PS + $^1O_2$				
$^2PS^{\bullet+}$ + $^2O_2^{\bullet-}$	✓			

but when computing the coupling between electronic states we were forced to use the maximum overlap method (MOM) in order to reach convergence. When calculating the specific electronic states we used a variety of methods to obtain accurate values for the molecular systems of a single photosensitizer (PS) and oxygen molecule (O_2) as shown in Table 4.1.

Obtaining the couplings between the electronic states is much more logistically cumbersome than computing each individual electronic state. Due to complications with incorpo-

rating ROKS, we were forced to use MOM for all coupling calculations involving an excited state $^1PS^*$. Methods are reported in Table 4.2.

Table 4.2: Required components for computing the couplings between electronic states. See appendix for higher level of details and charge/multiplicity.

Electronic states	CDFT	MOM	Initial Ground State
$^1PS^* + {}^3O_2 \longleftrightarrow {}^2PS^{\bullet+} + {}^2O_2^{\bullet-}$	✓	✓	✓
$^1PS + {}^3O_2 \longleftrightarrow {}^2PS^{\bullet+} + {}^2O_2^{\bullet-}$	✓		✓
$^1PS^* + {}^3O_2 \longleftrightarrow {}^3PS + {}^3O_2$	✓		✓
$^1PS + {}^1O_2 \longleftrightarrow {}^3PS + {}^3O_2$	✓		

We were able to obtain the configurations of the oxygen molecules about the BODIPY dye by performing geometry optimizations on each system. This gave us relatively accurate values for the positions of the oxygen molecules. We obtained the angles of the oxygen molecules by generating a Python script which defined the core of the BODIPY dye as a plane, calculated a vector for the oxygen molecule, and then computed the angle between the oxygen vector and the plane of the dye.

Before being able to converge the coupling calculations between states $^1PS^* + {}^3O_2$ and $^2PS^{\bullet+} + {}^2O_2^{\bullet-}$ we performed an alternative method to calculating the couplings between electronic states. We used CDFT with the same parameters to calculate the couplings between a single oxygen molecule in two different electronic states, and then performed the same computations on a single photosensitizer between electronic states consistent with the states used for O_2. Once calculations were completed we calculated the alternative couplings between them via:

$$\text{Coupling} = \frac{V_{PS}S_{O_2} + V_{O_2}S_{PS}}{2} \tag{4.10}$$

where

V_{PS} = The Hamiltonian off-diagonal matrix elements for the photosensitizer

S_{O_2} = The Overlap off-diagonal matrix elements for the oxygen molecule

V_{O_2} = The Hamiltonian off-diagonal matrix elements for the oxygen molecule

and

S_{PS} = The Overlap off-diagonal matrix elements for the photosensitizer

Calculations required a higher level of CDFT-CI printing in order to obtain both the Hamiltonian off-diagonal matrix elements, as well as the overlap off-diagonal matrix elements. All electronic structure calculations employed the Q-Chem program package.

4.3 Results and Discussion

To begin studying the interaction between a BODIPY dye and an oxygen molecule, we started by generating a variety of geometries for the complex where the oxygen molecule was positioned incrementally around the dye. Once the collection of structures depicted in Figure 4.2 was generated, we performed geometry optimizations on the grid-like orientations and ended up with a new system consisting of conformations the oxygen molecules preferred. From Figures 4.3a and 4.3b we see that the oxygen molecules aggregate around the outer surface of the plane of the BODIPY dye as well as above and below the plane.

We can see that the oxygen molecules which are located around the outer perimeter of the dye have adopted higher energy configurations, while the majority of the molecules that are above/below the plane of the dye tend towards lower energies. There are very few initial configurations that relax towards the space between the face-on and side-on configurations. Oxygen molecules tend to prefer distinct side/top/bottom configurations over angular ones. We suspect that oxygen prefers a face-on configuration about the plane due to the interaction of molecular orbitals between the oxygen molecule. While the repulsion, from pendant

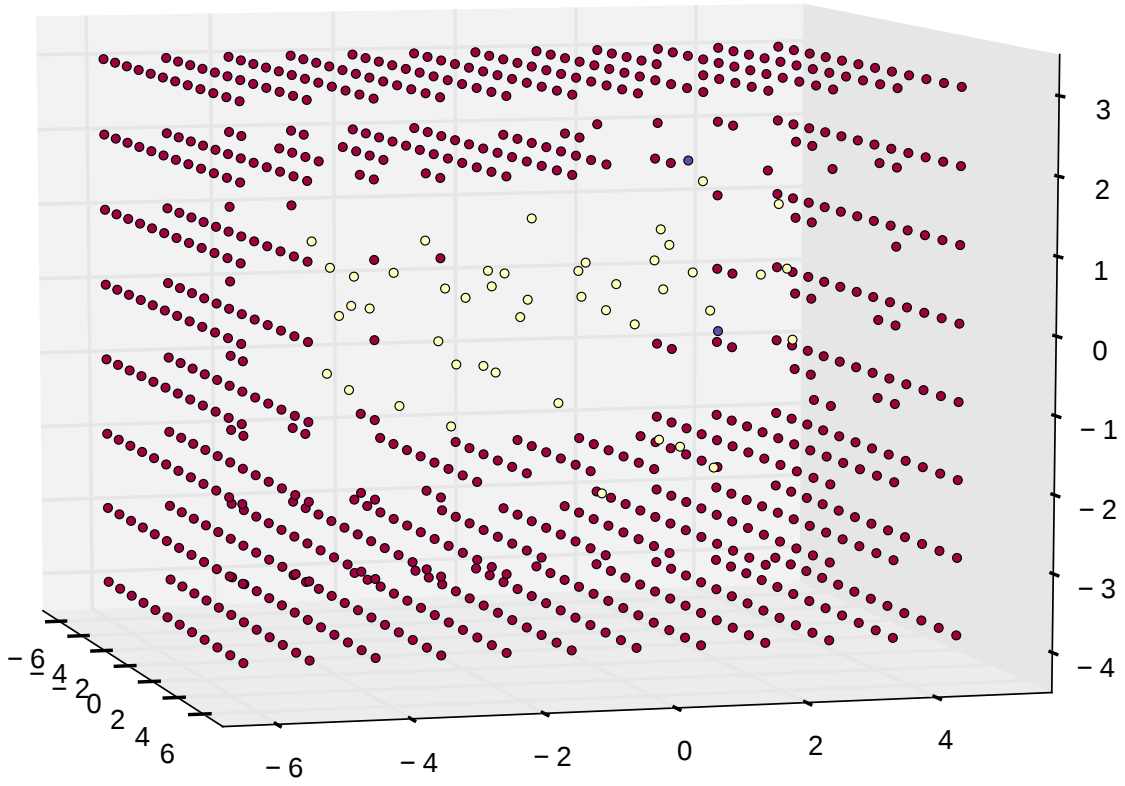

Figure 4.2: Grid of oxygen molecules surrounding a BODIPY dye, generated via Python script. Oxygen molecules were positioned outside of a defined box to not intersect the dye. Yellow and violet dots are atoms of the BODIPY dye, maroon dots are a single oxygen atom (part of an oxygen molecule)

hydrogen atoms, causes other oxygen molecules to adopt a higher energy side-on orientation.

Next, in order to further study the interaction of oxygen with a BODIPY dye, for each optimized structure we calculated the energies for the specific electronic states of the PS+O_2 complex that are involved in PDT.

At first glance the energies seem to match nicely with those energies positioned in the Jablonski diagram in Chapter 1 (Figure 1.3), where we have the ground state system at the lowest energy level, followed by the $^1PS+^1O_2$ and $^3PS+^3O_2$ states, then the $^2PS^{\bullet+}+^2O_2^{\bullet-}$ and $^1PS^*+^3O_2$ states. We see a slight split of the peaks in all the distributions, especially prevelant in the $^2PS^{\bullet+}+^2O_2^{\bullet-}$ state. This is due to the orientation of the oxygen molecules in our sampled configurations being split about evenly between the face-on and side-on configurations. This claim is also backed by the fact that we originally saw a clear split of energies between the optimized systems found in Figure 4.3a and 4.3b. The large split of energies found in the $^2PS^{\bullet+}+^2O_2^{\bullet-}$ state may be due to the radical oxygen molecule located on the side-on configuration, being in much closer proximity to the ethyl groups found on either end of the BODIPY dye, while the face-on configuration oxygen molecules do not have a substituent in such close proximity, resulting in a lower energy. There is an agreement of relative energies between those shown in Figure 4.4 and the Jablonski diagram (Figure 1.3) allowing us to be confident we are computing the correct electronic states. Our primary concern is on the relative energies of the complexes because this study is focused on the photosensitizers ability to generate singlet oxygen which is a process that involves transitions between different electronic states. This process is not dependent on the absolute energy of the systems, but rather the relative energy differences of transitions between the electronic states involved in generating singlet oxygen. Even applying this principle to comparing different photosensitizers side by side, our claims remain sound, because the relative rates are what differentiates one PS as being more or less efficient from another.

Now that we have a stable method for computing the individual electronic states, we calculate the couplings between directly connected electronic states to investigate the rate

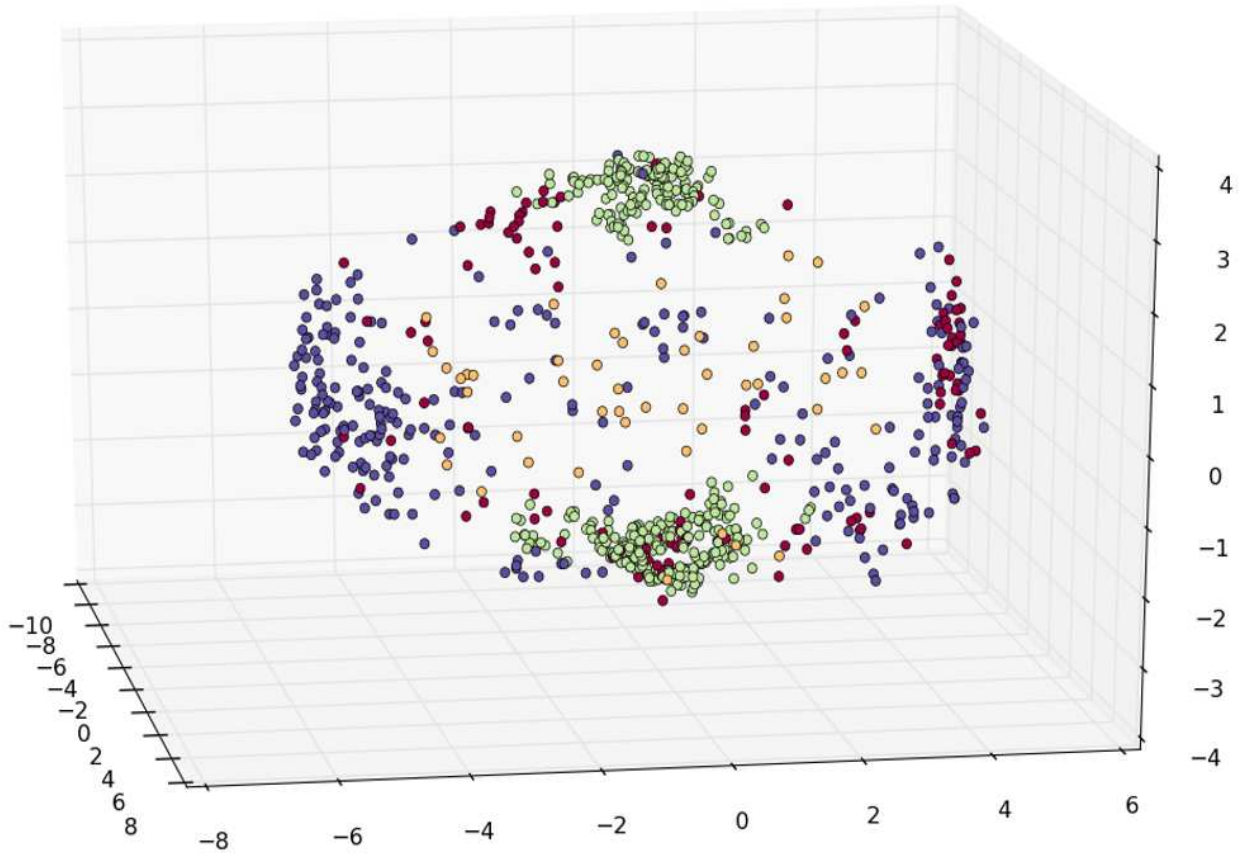

(a) Post-optimization plot of where oxygen molecules aggregated around the BODIPY dye, color coded with energy plot 4.3b where the aqua colored dots are lower energy, violet dots are high energy, the maroon dots are outliers, and the yellow dots are atoms on the BODIPY molecule.

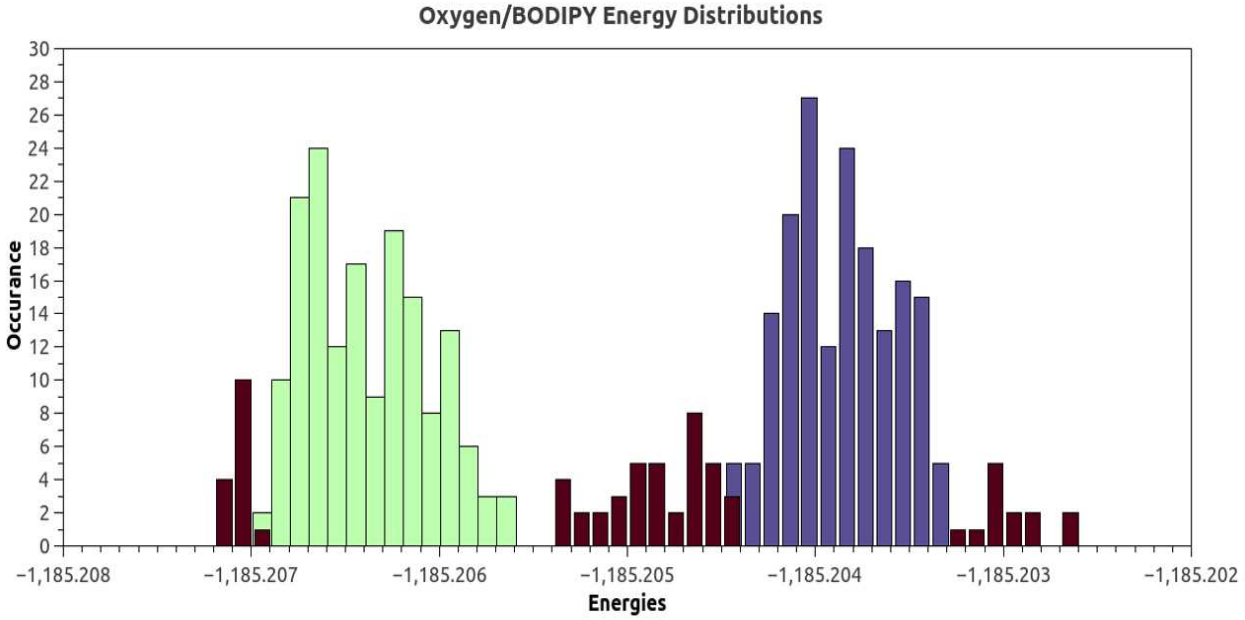

(b) Distribution plot of ground state energies of the BODIPY+O_2 complex, colors are correlated with those of Figure 4.3a.

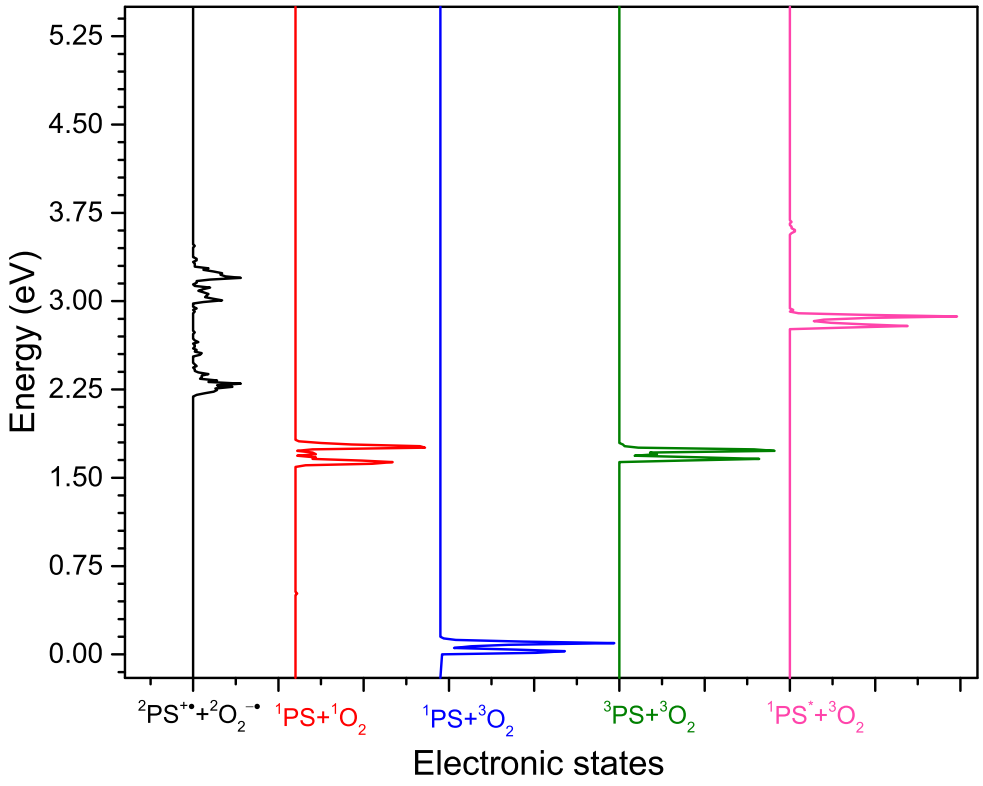

Figure 4.4: Plot of the distributions of energies for the energy of each electronic state. Calculations were performed with a single BODIPY dye and single oxygen molecule within one system. Energies for the states were normalized so that the ground state ($^{1}PS+^{3}O_2$) resides at 0.0eV.

of processes leading to the formation of singlet oxygen and the other processes that compete against them.

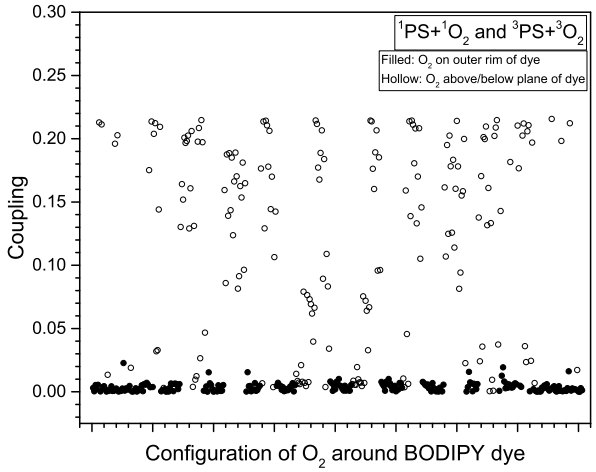

(a) $^1PS+^1O_2$ and $^3PS+^3O_2$

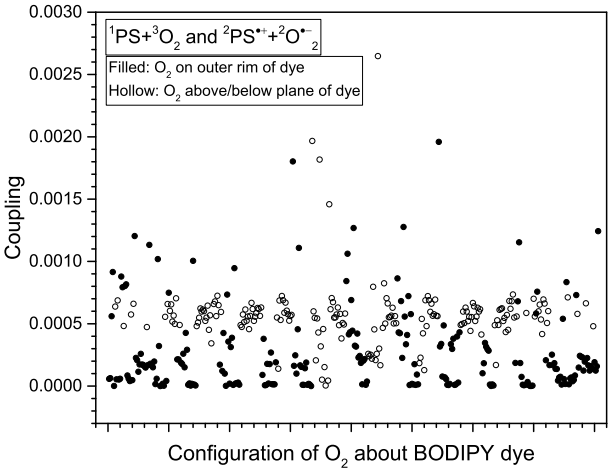

(b) $^1PS+^3O_2$ and $^2PS^{\bullet+}+^2O_2^{\bullet-}$

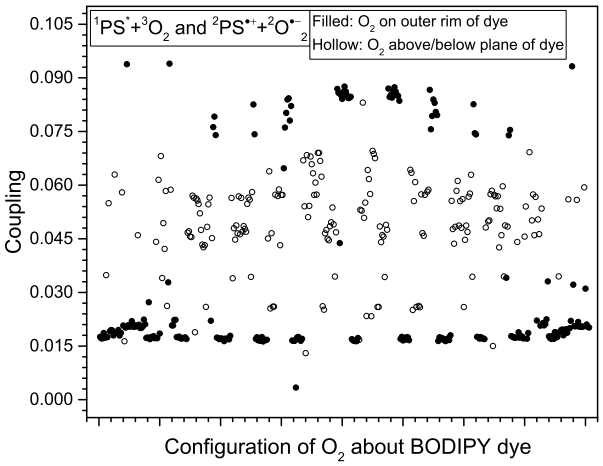

(c) $^1PS^*+^3O_2$ and $^2PS^{\bullet+}+^2O_2^{\bullet-}$

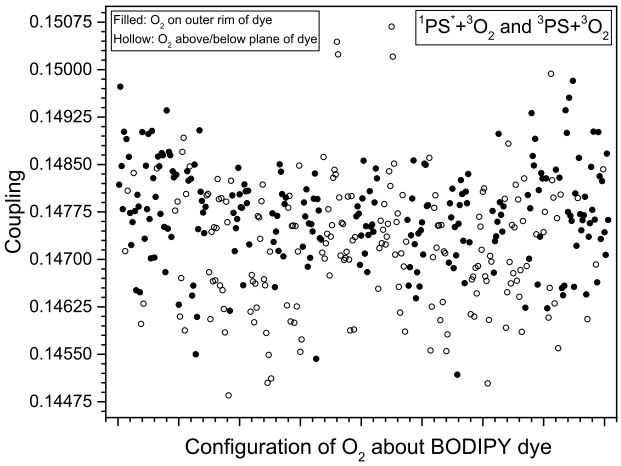

(d) $^1PS^*+^3O_2$ and $^3PS+^3O_2$

Figure 4.5: Plots of the absolute value of the couplings ($|V|$) between directly connected electronic states, pathways for forming singlet oxygen and competing against the formation are included.

Electronic couplings were computed for the sampled configurations in Figure 4.3a and are plotted in Figure 4.5. Looking closely at the figures in Figure 4.5, we can make a

few conclusions about how the configuration of the oxygen molecule affects the couplings between different electronic states. In plot 4.5a with the ^{1}PS+^{1}O$_2$ and ^{3}PS+^{3}O$_2$ couplings we see a very clear split of the couplings between the systems that contain side-on vs. face-on configurations of oxygen. The face-on configurations have the highest couplings, while the side-on configurations have lower couplings. Though the face-on configurations have higher couplings, the values span a wider range from 0.00eV to 0.22eV, while the side-on configurations all reside at around 0.00eV. From these observations we can conclude that the final step of energy transfer leading to the generation of singlet oxygen heavily favors the face-on configuration, giving a very low probability of taking the path towards singlet oxygen generation when the oxygen molecule adopts a side-on configuration. The other plots in Figure 4.5 do not show quite as valuable information. The plots 4.5d and 4.5b give little qualitative information. Plot 4.5d has an almost indistinguishable difference between the face-on vs. side-on configurations. All couplings are overlapping and there is no clear trend noticed. In the 4.5b plot there is a split of about 0.0005eV between the side-on vs. face-on configurations, but in relation to the difference seen in plot 4.5a where there is a 0.2eV difference, this value is rendered insignificant. We can make a few conclusions based on plot 4.5c. There exists a clear split between couplings of systems with face-on vs. side-on configurations, though the split is relatively small, spanning about 0.1eV. Nonetheless the face-on configurations exist, overall, at a higher coupling than the side-on configurations. There is a cluster of side-on configurations that have couplings higher than the face-on ones, these oxygen molecules could be interacting with the ethyl groups which gives them a higher coupling for this transition because the oxygen molecules maybe be close enough and position just correctly to allow for electron transfer to occur which would give these configurations higher coupling. More analysis of the orbitals would be required to confirm this, but for now we hypothesize that the relatively small difference in coupling is due to the oxygen molecule existing in just the right position to allow for electron transfer to occur.

To further examine how the configurations of the oxygen molecules about the BODIPY

dye affect the system's couplings, we will look at the angle each oxygen molecule makes relative to the dye and how it relates to the couplings between states.

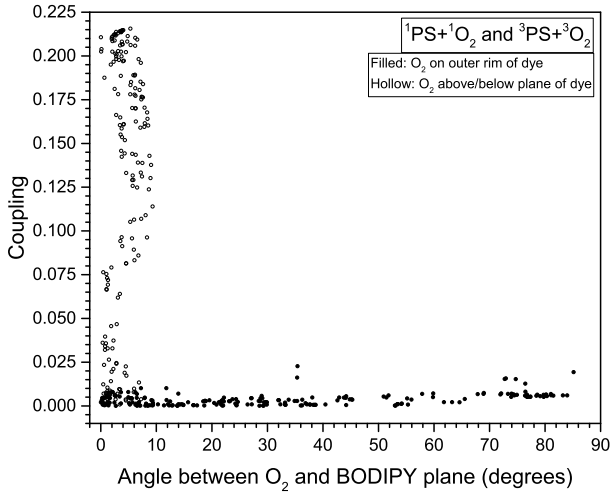

(a) $^1PS+^1O_2$ and $^3PS+^3O_2$

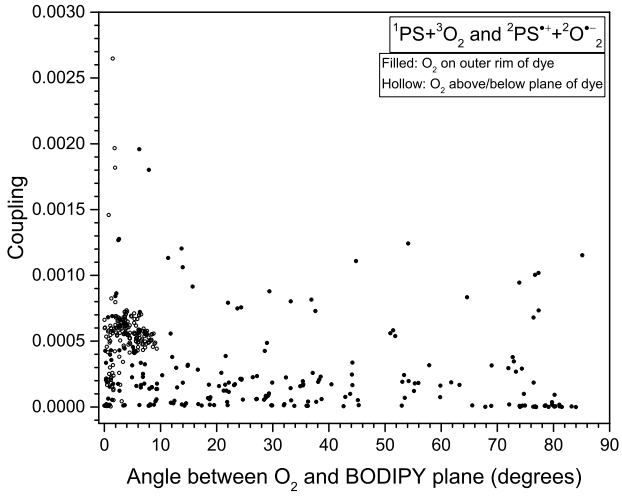

(b) $^1PS+^3O_2$ and $^2PS^{\bullet+}+^2O_2^{\bullet-}$

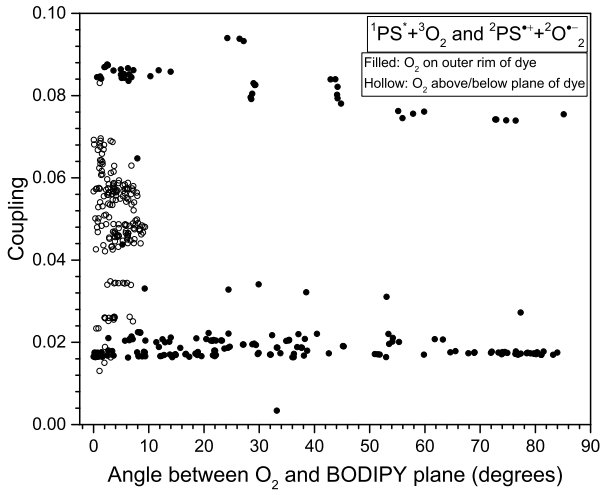

(c) $^1PS^*+^3O_2$ and $^2PS^{\bullet+}+^2O_2^{\bullet-}$

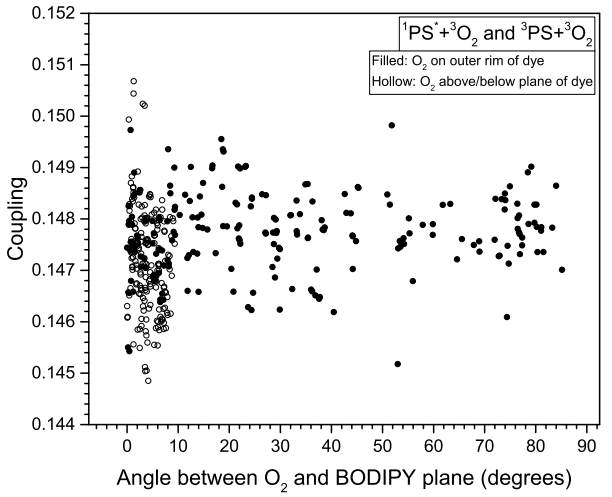

(d) $^1PS^*+^3O_2$ and $^3PS+^3O_2$

Figure 4.6: Plots of the couplings between directly connected electronic states, and the angles of the oxygen molecules in relation to the plane of the dye. Angles for the oxygen molecules are defined along the bond between two oxygen atoms.

Figure 4.6d shows the couplings between the $^1PS^*+^3O_2$ and $^3PS+^3O_2$ states, which is the first step after vertical excitation the complex takes towards generating singlet oxygen.

Looking at the plots in Figure 4.6d we can investigate the couplings with a deeper understanding of how they relate to the orientation of an oxygen molecule around the BODIPY dye. In the plot 4.6d, we see that the face-on configurations have oxygen molecules consistently residing at about 0° in relation to the plane of the dye, while the molecules with a side-on configuration span from 0-90° without a variation in the coupling. Plot 4.6b, which shows the couplings between the $^1PS^*+^3O_2$ and $^2PS^{\bullet+}+^2O_2^{\bullet-}$ states, has the same trend of oxygen molecules with a face-on configuration adopting a 0° angle to the plane, while the side-on configurations span from 0-90° rotation. We see this trend in all of the plots within Figure 4.6. The most distinguishable plot is 4.6a where we see the range of couplings for the face-on configurations almost equally spread from 0.0-0.225eV. This trend is seen more clearly in this plot due to all of the configurations adopting the same orientation within roughly 10° of each other, so we can see the data clustered together.

Taking a step back to look at the coupling values overall, regardless of the position of the molecules we can make some conclusions about which processes may be more favorable over others.

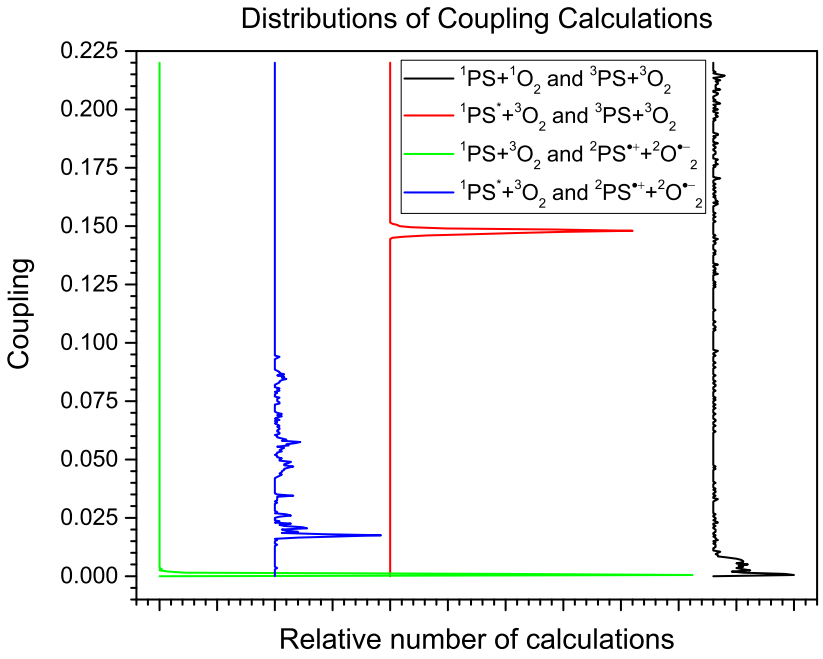

Figure 4.7: Distribution plot for all the electronic states involved in the process of PDT.

From Figure 4.7 we see that the couplings between $^1PS+^3O_2$ and $^2PS^{\bullet+}+^2O_2^{\bullet-}$ is < 0.01 eV, showing that the process of relaxing from $^2PS^{\bullet+}+^2O_2^{\bullet-}$ down to the ground $^1PS+^3O_2$ state would be very slow. The $^1PS^*+^3O_2$ to $^2PS^{\bullet+}+^2O_2^{\bullet-}$ electron transfer charge separation chances are slightly higher, having couplings that range from 0.015-0.09eV. The transition from $^3PS+^3O_2$ to $^1PS+^1O_2$ has consistent couplings from 0.0-0.225eV, having a significant amount of couplings around 0.0-0.01eV. Though the consistent couplings also give some of the highest couplings close to 0.225eV, due to the configuration of the oxygen molecules having a parallel and face-on configuration. These higher couplings give the system a better chance at crossing from the triplet state over to the singlet state via energy transfer, generating singlet oxygen. Finally we examine one of the most important transitions, from the excited state $^1PS^*+^3O_2$ over to the $^3PS+^3O_2$ state, which is the first step in generating singlet oxygen. This transition has consistently high coupling values, much larger than the transition from the excited state to the doublet state. The formation of a doublet state is the primary

competition to forming singlet oxygen (other than fluorescence/phosphorescence) that could negatively impact the photosensitizers performance. Since we see that the system has large coupling values between the excited state and triplet state, it shows that the formation of the triplet state is preferred over the doublet state. This shows that the specific photosensitizer we are investigating has a better chance of forming singlet oxygen than of forming superoxide because referring back to the Jablonski diagram in Figure 1.3 we see that the formation of the triplet state is the first step in forming singlet oxygen where the only other competition is to form the doublet radical ion.

Before we were successful in converging CDFT calculations of the PS+O_2 system to calculate the couplings, we attempted a method to calculate the couplings via an alternative "ad hoc" method, covered in Equation 4.10.

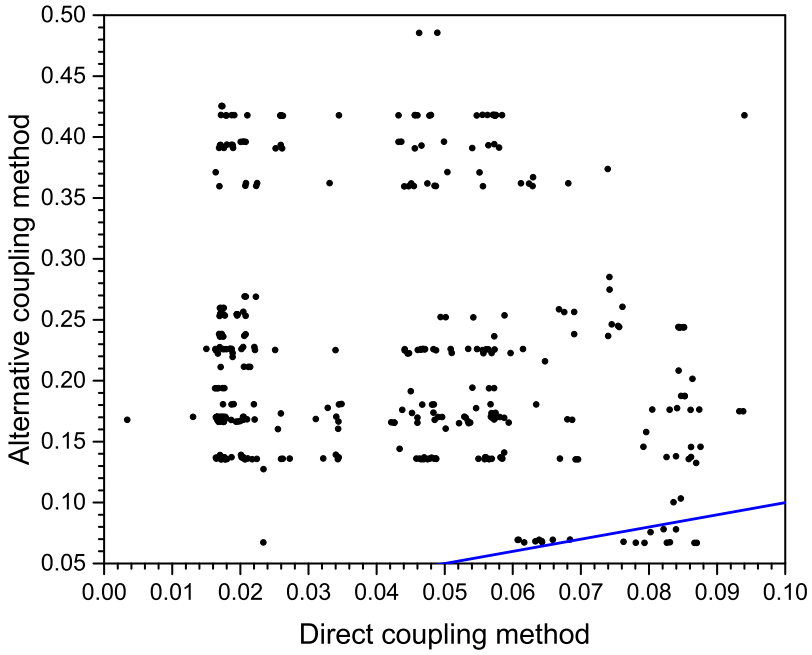

Figure 4.8: A plot of our alternative method of computing the electronic state couplings. The blue line is a x=y line, to show what a perfect 1:1 ratio would be. R^2 is 0.00705.

The results are presented in Figure 4.8. From this plot we can see almost no correlation between the values calculated via our alternative method and the values that were computed

in a single calculation on the PS+O_2 complex. This is clearly shown in the R^2 value of 0.00705 which essentially states there is no correlation. Also looking at the blue 1:1 line, the alternative couplings are not predictive of the corresponding direct couplings at a given configuration, and vice versa. The full details of our alternative method is laid out in the computational details section. From our findings we see that the alternative method we explored is not an accurate method to calculate the couplings between electronic states of a system containing different molecules. The discrepancies in the data could very well be due to the lack of coupling interactions between the BODIPY dye and the oxygen molecule. In the alternative method presenting the two molecules are in systems of their own, while the full coupling calculation includes both molecules within one system. It appears to be necessary to include intermolecular interactions directly within the CDFT-CI calculations rather than as a post-CDFT correction.

4.4 Conclusions

The major findings we gained from the coupling position and angular analysis is that overall the systems where the oxygen molecule adopts a face-on configuration, usually have the highest coupling values and those systems also have the oxygen molecule being nearly parallel to the plane of the dye. This could be due to the interaction of the molecular on the orbitals of the oxygen with the orbitals of the BODIPY dye which allow for easier intersystem crossing and energy transfer. As opposed to the systems where the oxygen molecule adopts a side-on configuration where there is little to no orbital overlap. However, with the side-on configurations we do see a higher coupling between the $^1PS^*+^3O_2$ and $^2PS^{\bullet+}+^2O_2^{\bullet-}$ states which could be due to the oxygen being in such close proximity to the dye that electron transfer was highly favorable. We also found that the distributions of couplings inferred that the more favorable process for this particular BODIPY dye is to form the triplet state photosensitizer as opposed to the doublet radical ion. This leads us to the believe that there is less competition between possible routes of electronic state transitions that could deter

the formation of singlet oxygen. We also found that the formation of singlet oxygen from the prior PS triplet state has a reasonably high likelihood of occuring if oxygen is nearby.

Our findings have shown that the particular photosensitizer in study could be a potentially useful scaffold for designing PS to be used in PDT due to the potential for singlet oxygen generation with little competition from other processes that could deter the quantum yield of singlet oxygen. In order to be a successful PS however, one would need to promote the formation of the triplet ^{3}PS via enhancing intersystem crossing to facilitate singlet oxygen generation. We also have provided accurate methods to compute the couplings between systems of two molecules where each exist in different electronic states and are not connected by any bonds or direct intermolecular interactions. Also, we have shown that the alternative method of combining and averaging the couplings between the individual molecules (i.e. coupling between $^3O_2$ and $^2O_2^{\bullet-}$, and $^1PS^*$ and $^2PS^{\bullet+}$) is not an accurate method to compute the couplings between states. It is highly suggested that one uses the approach of implementing the CDFT techniques described in here to compute the couplings between electronic states of different molecules.

5 Conclusion

In this thesis through the use of computational chemistry methods we were able to compute the excited state properties for a set of 26 derivatives of BODIPY dyes, as well as characterize how two excited state density functional based methods (TDDFT, and the ROKS method) describe the S_1 excited state PES for a particular derivative. Through these results we have found that in addition to the known overestimation of the vertical excitation energy by TDDFT, ROKS systematically underestimates the excitation energy, though to a lesser margin than TDDFT. There also exists a strong correlation between ROKS and TDDFT vertical excitation and emission energies, showing that both approaches predict similar shifts in absorption and emission spectra due to chemical substitution on the dye. Through molec-

ular dynamics samplings, we found that ROKS samples a region of the S_1 PES, where the ROKS and TDDFT PES are parallel but are offset by roughly 0.5eV. While TDDFT samples a region that is not as offset, but has substantial differences in the local shape of the PES. Also covered was the investigation of the interactions between an oxygen molecule and a particular BODIPY derivative, employing CDFT to compute the electronic states and couplings between the states. Through this study it was found that the oxygen molecules which adopted a face-on configuration have the highest couplings between all electronic states, while couplings with oxygen molecules in a side-on configuration had the lowest couplings. Oxygen molecules that were in a face-on configuration were nearly parallel in relation to the plane of the dye, which possibly allowed the orbitals to overlap between molecules and allow for higher couplings. The couplings between the $^1PS^*+^3O_2$ and $^2PS^{\bullet+}+^2O^{\bullet-}{}_2$ states showed that for the oxygen molecules that were in a side-on configuration the systems had high couplings (0.145-0.150eV). These higher couplings could be due to the proximity of the molecules to each other allowing for electron transfer to occur more easily. It was also found that if one can suppress the preference of this specific dye to fluoresce/phosphoresce, then the production of singlet oxygen is preferred with little competition from the formation of the doublet radical ions. Through this study we have provided useful information that may help others optimize the framework of a BODIPY dye to tailor their photophysical characteristics, give insight to users and developers of time-independent excited state DFT strategies, provided a scheme for computing the couplings between systems of multiple molecules existing in different electronic states, and shown that BODIPY dyes can be an efficient photosensitizer so long as their preference to radiatively relax is suppressed. In the future this work may benefit from the addition of solvent in calculations, expanding the on the excited state dynamics, and also applying our scheme to calculate the couplings on other BODIPY derivatives.

Bibliography

[1] R. R. Allison and C. H. Sibata. Oncologic photodynamic therapy photosensitizers: A clinical review. *Photodiagn. Photodyn. Ther.*, 7:61–75, 2010.

[2] National Cancer Institute. Cancer statistics. `https://www.cancer.gov/about-cancer/understanding/statistics`, 2016. [Online; accessed 04-January-2017].

[3] A. Molassiotis, B.M.C. Yam, H. Yung, F.Y.S. Chan, and T.S.K. Mok. Pretreatment factors predicting the development of postchemotherapy nausea and vomiting in chinese breast cancer patients. *Support Care Cancer*, 10:139–145, 2002.

[4] A. M. Griffin, P. N. Butow, A. S. Coates, A. M. Childs, P. M. Ellis, S. M. Dunn, and M.H.N. Tattersall. On the receiving end v: Patient perceptions of the side effects of cancer chemotherapy in 1993. *Annals of Oncology*, 7:189–195, 1996.

[5] R. R. Love, H. Leventhal, D. V. Easterling, and D. R. Nerenz. Side effects and emotional distress during cancer chemotherapy. *Cancer Chemotherapy*, 63:604–612, 1989.

[6] American Cancer Society. Chemotherapy side effects. `http://www.cancer.org/treatment/treatments-and-side-effects/treatment-types/chemotherapy/chemotherapy-side-effects.html`, 2016. [Online; accessed 23-January-2017].

[7] H. J. Yoo, S. H. Ahn, S. B. Kim, W. K. Kim, and O. S. Han. Efficacy of progressive muscle relaxation training and guided imagery in reducing chemotherapy side effects

in patients with breast cancer and in improving their quality of life. *Support Care Cancer*, 13:826–833, 2005.

[8] US News. Oncologists worry about rising costs of cancer treatment. http://health.usnews.com/health-news/patient-advice/articles/2015/07/01/oncologists-worry-about-rising-costs-of-cancer-treatment, 2016. [Online; accessed 23-January-2017].

[9] Cancer.net. Side effects of surgery. http://www.cancer.net/navigating-cancer-care/how-cancer-treated/surgery/side-effects-surgery, 2016. [Online; accessed 23-January-2017].

[10] American Cancer Society. How surgery is used for cancer. https://www.cancer.org/treatment/treatments-and-side-effects/treatment-types/surgery/how-surgery-is-used-for-cancer.html, 2016. [Online; accessed 23-January-2017].

[11] American Cancer Society. Risks of cancer surgery. https://www.cancer.org/treatment/treatments-and-side-effects/treatment-types/surgery/risks-of-cancer-surgery.html, 2016. [Online; accessed 23-January-2017].

[12] Early Breast Cancer Trialists' Collaborative Group. Effects of radiotherapy and surgery in early breast cancer. *The New England Journal of Medicine*, 333:1444–1455, 1995.

[13] B. C. Wilson. Photodynamic therapy for cancer: Principles. *Can J Gastroenterol*, 16:393–396, 2002.

[14] T. J. Dougherty, C. J. Gomer, B. W. Henderson, G. Jori, D. Kessel, M. Korbelik, J. Moan, and Q. Peng. Photodynamic therapy. *J Natl Cancer Inst.*, 90:889–905, 1998.

[15] M. B. Vrouenraets, G. W. Visser, G. B. Snow, and G. A. Van Dongen. Basic principles, applications in oncology and improved selectivity of photodnyamic therapy. *Anticancer Res.*, 23:505–522, 2003.

[16] American Cancer Society. Photodynamic therapy. http://www.cancer.org/treatment/treatmentsandsideeffects/treatmenttypes/photodynamic-therapy, 2015. [Online; accessed 12-January-2017].

[17] J. Moan and K. Berg. The photodegradation of porphyrins in cells can be used to estimate the lifetime of singlet oxygen. *Photochem. Photobiol.*, 53:549–553, 1991.

[18] M. J. Garland, C. M. Cassidy, D. Woolfson, and R. F. Donnelly. Designing photosensitizers for photodynamic therapy: Strategies, challenges and promising developments. *Future Med. Chem.*, 1:667–691, 2009.

[19] A. Kamkaew, S. H. Lim, H. B. Lee, L. V. Kiew, L. Y. Chung, and K. Burgess. Bodipy dyes in photodynamic therapy. *Chem. Soc. Rev.*, 42:77–88, 2013.

[20] M. J. Garland, C. M. Cassidy, D. Woolfson, and R. F. Donnelly. Designing photosensitizers for photodynamic therapy: strategies, challenges and promising developments. *Future Med. Chem.*, 1:667–691, 2009.

[21] R. R. Allison, V. S. Bagnato, R. Cuenca, G. H. Downie, and C. H. Sibata. The future of photodynamic therapy in oncology. *Future Oncol.*, 2:53–71, 2006.

[22] T. Kiesslich, J. Berlanda, K. Plaetzer, B. Krammer, and F. Berr. Comparative characterization of the efficiency and cellular pharmacokinetics of foscan- and foslip-based photodynamic treatment in human biliary tract cancer cell lines. *Photochem. Photobiol.*, 6:619–627, 2007.

[23] A. Cruess, G. Zlateva, A. Pleil, and B. Wirostko. Photodynamic therapy with verteporfin in age-related macular degeneration: a systematic review of efficacy, safety, treatment modifications and pharmacoeconomic properties. *Acta Opthalmol.*, 87:118–132, 2009.

[24] Y. Hongying, W. Fuyuan, and Z. Zhiyi. Photobleaching of chlorins in homogeneous and heterogeneous media. *Dyes Pigm.*, 43:109–117, 1999.

[25] E. D. Sternberg, D. Dolphin, and C. Bruckner. Porphyrin-based photosensitizers for use in photodynamic therapy. *Tetrahedron*, 54:4151–4202, 1998.

[26] E. S. Nyman and P. H. Hynninen. Research advances in the use of tetrapyrrolic photosensitizers for photodynamic therapy. *J. Photochem. Photobiol. B*, 73:1–28, 2004.

[27] M. Wainwright, D. A. Phoenix, L. Rice, S. M. Burrow, and J. Waring. Increased cytotoxicity and phototoxicity in the methylene blue series via chromophore methylation. *J. Photochem. Photobiol. B*, 40:233–239, 1997.

[28] A. Treibs and F. H. Kreuzer. Difluorboryl-komplexe von di- und tripyrrylmethenen. *Justus Liebigs Ann. Chem.*, 718:208–223, 1968.

[29] G. Ulrich, R. Ziessel, and A. Harriman. The chemistry of fluorescent bodipy dyes: Versatility unsurpassed. *Angew. Che. Int. Ed.*, 47:1184–1201, 2008.

[30] R. Ziessel, G. Ulrich, and A. Harriman. The chemistry bodipy: A new el dorado for fluorescence tools. *New J. Chem.*, 31:496–501, 2007.

[31] A. Loudet and K. Burgess. Bodipy dyes and their derivatives: Syntheses and spectroscopic properties. 107:4891–4932, 2007.

[32] Q. Zhang, Y. Cai, X. Wang, J. Xu, Z. Ye, S. Wang, P. H. Seeberger, and J. Yin. Targeted photodynamic killing of breast cancer cells employing heptamannosylated cyclodextrin-mediated nanoparticle formation of an adamantane-functionalized bodipy photosensitizer. *Appl. Mater. Interfaces*, 8:33405–33411, 2016.

[33] C. S. Kue, A. Kamkaew, H. B. Lee, L. Y. Chung, L. V. Kiew, and K. Burgess. Targeted pdt agent eradicates trkc expressing tumors via photodynamic therapy. *Mol. Pharmaceutics*, 12:212–222, 2015.

[34] P. Hohenberg and W. Kohn. Inhomogeneous electron gas. *Phys. Rev.*, 136:864–871, 1964.

[35] A. D. Dwyer and D. J. Tozer. Effects of chemical change on tddft accuracy: orbital overlap perspective of the hydrogenation of retinal. *Phys. Chem. Chem. Phys.*, 12:2816–2818, 2010.

[36] C. Adamo and V. Barone. Inexpensive and accurate predictions of optical excitations in transition-metal complexes: the tddft/pbe0 route. *Theor. Chem. Acc.*, 105:169–172, 2000.

[37] K. T. Komoto and T. Kowalczyk. How parallel are excited state potential energy surfaces from time-independent and time-dependent dft? a bodipy dye, case study. *J. Phys. Chem. A*, 120:8160–8168, 2016.

[38] E. K. U. Gross and W. Kohn. Time-dependent density-functional theory. *Adv. Quantum Chem.*, 21:255–291, 1990.

[39] M. A. L. Marques and E. K. U. Gross. Time-dependent density functional theory. *Annu. Rev. Phys. Chem.*, 55:427–455, 2004.

[40] R. Lincoln, L. E. Greene, K. Krumova, Z. Ding, and G. Cosa. Electronic excited state redox properties for bodipy dyes predicted from hammett constants: Estimating the driving force of photoinduced electron transfer. *J. Phys. Chem.*, 118:10622–10630, 2014.

[41] A. T. B. Gilbert, N. A. Besley, and P. M. W. Gill. Self-consistent Field Calculations of Excited States using the Maximum Overlap Method (MOM). *J. Phys. Chem. A*, 112:13164–13171, 2008.

[42] B. Kaduk, T. Kowalczyk, and T. Van Voorhis. Constrained density functional theory. *Chem. Rev.*, 112:321–370, 2012.

[43] L. Basabe-Desmonts, D. N. Reinhoudt, and M. Crego-Calama. Design of fluorescent materials for chemical sensing. *Chem. Soc. Rev.*, 36:993–1017, 2007.

[44] N. Dorh, S. Zhu, K. B. Dhungana, R. Pati, F.-T. Luo, H. Liu, and A. Tiwari. BODIPY-based fluorescent probes for sensing protein surface-hydrophobicity. *Sci. Rep.*, 5:18337, 2015.

[45] A. Hagfeldt, G. Boschloo, L. Sun, L. Kloo, and H. Pettersson. Dye-sensitized solar cells. *Chem. Rev.*, 110:6595–6663, 2010.

[46] S. Mathew, A. Yella, P. Gao, R. Humphry-Baker, B. F. E. Cuchod, N. Ashari-Astani, I. Tavernelli, U. Rothlisberger, K. Nazeeruddin, and M. Grätzel. Dye-sensitized solar cells with 13% efficiency achieved through the molecular engineering of porphyrin sensitizers. *Nature Chem.*, 6:242–247, 2014.

[47] A. Kamkaew, S. H. Lim, H. B. Lee, L. V. Kiew, L. Y. Chung, and K. Burgess. BODIPY dyes in photodynamic therapy. *Chem. Soc. Rev.*, 42:77–88, 2013.

[48] T. Kowalczyk, Z. Lin, and T. Van Voorhis. Fluorescence quenching by photoinduced electron transfer in the zn^{2+} sensor Zinpyr-1: A computational investigation. *J. Phys. Chem. A*, 114:10427–10434, 2010.

[49] N. Martsinovich and A. Troisi. High-throughput computational screening of chromophores for dye-sensitized solar cells. *J. Phys. Chem. C*, 115:11781–11792, 2011.

[50] E. O. Pyzer-Knapp, C. Suh, R. Gómez-Bombarelli, J. Aguilera-Iparraguirre, and A. Aspuru-Guzik. What is high-throughput virtual screening? A perspective from organic materials discovery. *Annu. Rev. Mat. Sci.*, 45:195–216, 2015.

[51] A. Loudet and K. Burgess. BODIPY dyes and their derivatives: Syntheses and spectroscopic properties. *Chem. Rev.*, 107:4891–4932, 2007.

[52] R. Ziessel, G. Ulrich, and A. Harriman. The chemistry of BODIPY: A new *el dorado* for fluorescence tools. *New J. Chem.*, 31:496–501, 2007.

[53] J. D. Spiegel, M. Kleinschmidt, A. Larbig, J. Tatchen, and C. M. Marian. Quantum-chemical studies on excitation energy transfer processes in BODIPY-based donor-acceptor systems. *J. Chem. Theory Comput.*, 11:4316–4327, 2015.

[54] X. Wu, W. Wu, X. Cui, J. Zhao, and M. Wu. Preparation of bodipyferrocene dyads and modulation of the singlet/triplet excited state of BODIPY via electron transfer and triplet energy transfer. *J. Mater. Chem. C*, 4:2843–2853, 2016.

[55] Wanhua Wu, Huimin Guo, Wenting Wu, Shaomin Ji, and Jianzhang Zhao. Organic triplet sensitizer library derived from a single chromophore (BODIPY) with long-lived triplet excited state for triplet-triplet annihilation based upconversion. *J. Org. Chem.*, 76:7056–7064, 2011.

[56] Y. Cakmak, S. Kolemen, S. Duman, Y. Dede, Y. Dolen, B. Kilic, Z. Kostereli, L. T. Yildirim, A. L. Dogan, D. Guc, and E. U. Akkaya. Designing excited states: Theory-guided access to efficient photosensitizers for photodynamic action. *Angew. Chem. Int. Ed*, 50:11937–11941, 2011.

[57] Y.-C. Lai, S.-Y. Su, and C.-C. Chang. Special reactive oxygen species generation by a highly photostable BODIPY-based photosensitizer for selective photodynamic therapy. *ACS Appl. Mater. Interfaces*, 5:12935–12943, 2013.

[58] H. Kang, Y. Si, J. Liu, L. Chen, Y. Li, H. Chen, J. Groeper, and B. Yang. An experimental and theoretical study of dimethylaminostyryl BODIPY-perylenetetracarboxylic derivative dyads: Synthesis, properties and DFT calculation. *RSC Adv.*, 6:23094–23101, 2016.

[59] R. Lincoln, L. E. Greene, K. Krumova, Z. Ding, and G. Cosa. Electronic excited state redox properties for BODIPY dyes predicted from Hammett constants: Estimating the

driving force of photoinduced electron transfer. *J. Phys. Chem. A*, 118:10622–10630, 2014.

[60] S. Mukherjee and P. Thilagar. Effect of alkyl substituents in BODIPYs: A comparative DFT computational investigation. *RSC Adv.*, 5:2706–2714, 2015.

[61] L. Jiao, C. Yu, J. Wang, E. A. Briggs, N. A. Besley, D. Robinson, M. J. Ruedas-Rama, A. Orte, L. Crovetto, E. M. Talavera, J. M. Alvarez-Pez, M. Van der Auweraer, and N. Boens. Unusual spectroscopic and photophysical properties of meso-*tert*-butylBODIPY in comparison to related alkylated BODIPY dyes. *RSC Adv.*, 5:89375–89388, 2015.

[62] E. Runge and E. K. U. Gross. Density-Functional Theory for Time-Dependent Systems. *Phys. Rev. Lett.*, 52:997–1000, 1984.

[63] A. Dreuw and M. Head-Gordon. Single-reference *ab initio* methods for the calculation of excited states of large molecules. *Chem. Rev.*, 105:4009–4037, 2005.

[64] A. D. Laurent and D. Jacquemin. TD-DFT benchmarks: A review. *Int. J. Quantum Chem.*, 113:2019–2039, 2013.

[65] S. Grimme and F. Neese. Double-hybrid density functional theory for excited electronic states of molecules. *J. Chem. Phys.*, 127:154116, 2007.

[66] D. Jacquemin, Y. Zhao, R. Valero, C. Adamo, I. Ciofini, and D. G. Truhlar. Verdict: Time-dependent density functional theory "Not Guilty" of large errors for cyanines. *J. Chem. Theory Comput.*, 8:1255–1259, 2012.

[67] M. R. Momeni and A. Brown. Why do TD-DFT excitation energies of BODIPY/aza-BODIPY families largely deviate from experiment? answers from electron correlated and multireference methods. *J. Chem. Theory Comput.*, 11:2619–2632, 2015.

[68] S. Chibani, A. D. Laurent, B. Le Guennic, and D. Jacquemin. Improving the accuracy of excited-state simulations of BODIPY and aza-BODIPY dyes with a joint SOS-CIS(D) and TD-DFT approach. *J. Chem. Theory Comput.*, 10:4574–4582, 2014.

[69] B. Kaduk and T. Van Voorhis. Communication: Conical intersections using constrained density functional theory-configuration interaction. *J. Chem. Phys.*, 133:061102, 2010.

[70] T. Ziegler, A. Rauk, and E. J. Baerends. Calculation of multiplet energies by the hartree-fock-slater method. *Theor. Chim. Acta*, 43:261–271, 1977.

[71] N. A. Besley, A. T. B. Gilbert, and P. M. W. Gill. Self-consistent-field Calculations of Core Excited States. *J. Chem. Phys.*, 130:124308, 2009.

[72] T. Kowalczyk, S. R. Yost, and T. Van Voorhis. Assessment of the ΔSCF density functional theory approach for electronic excitations in organic dyes. *J. Chem. Phys.*, 134:054128, 2011.

[73] M. Filatov and S. Shaik. Application of Spin-restricted Open-shell Kohn–Sham Method to Atomic and Molecular Multiplet States. *J. Chem. Phys.*, 110:116, 1999.

[74] T. Kowalczyk, T. Tsuchimochi, P.-T. Chen, L. Top, and T. Van Voorhis. Excitation energies and stokes shifts from a restricted open-shell kohn-sham approach. *J. Chem. Phys.*, 138:164101, 2013.

[75] J. Cullen, M. Krykunov, and T. Ziegler. The Formulation of a Self-consistent Constricted Variational Density Functional Theory for the Description of Excited States. *Chem. Phys.*, 391:11–18, 2011.

[76] M. Krykunov and T. Ziegler. Self-consistent formulation of constricted variational density functional theory with orbital relaxation. Implementation and applications. *J. Chem. Theory Comput.*, 9:2761–2773, 2013.

[77] F. A. Evangelista, P. Shushkov, and J. C. Tully. Orthogonality constrained density functional theory for electronic excited states. *J. Phys. Chem. A*, 117:7378–7892, 2013.

[78] D. Hait, T. Zhu, D. P. McMahon, and T. Van Voorhis. Prediction of excited-state energies and singlet-triplet gaps of charge-transfer states using a restricted open-shell kohnsham approach. *J. Chem. Theory Comput.*, 12:3353–3359, 2016.

[79] E. A. Briggs, N. A. Besley, and D. Robinson. QM/MM excited state molecular dynamics and fluorescence spectroscopy of BODIPY. *J. Phys. Chem. A*, 117:2644–2650, 2013.

[80] P. W. Ayers, M. Levy, and Á. Nagy. Time-independent density-functional theory for excited states of coulomb systems. *Phys. Rev. A*, 85:042518, 2012.

[81] P. W. Ayers, M. Levy, and Á. Nagy. Communication: Kohn-Sham theory for excited states of Coulomb systems. *J. Chem. Phys.*, 143:191101, 2015.

[82] C. Reichardt. Solvatochromic dyes as solvent polarity indicators. *Chem. Rev.*, 94:2319–2358, 1994.

[83] A. DeFusco, N. Minezawa, L. V. Slipchenko, F. Zahariev, and M. S. Gordon. Modeling solvent effects on electronic excited states. *J. Phys. Chem. Lett.*, 2:2184–2192, 2011.

[84] C. A. Guido, D. Jacquemin, C. Adamo, and B. Mennucci. Electronic excitations in solution: The interplay between state specific approaches and a time-dependent density functional theory description. *J. Chem. Theory Comput.*, 11:5782–5790, 2015.

[85] A. Filarowski, M. Lopatkova, P. Lipkowski, M. Van der Auweraer, V. Leen, and W. Dehaen. Solvatochromism of BODIPY-Schiff dye. *J. Phys. Chem. B*, 119:2576–2584, 2015.

[86] M. D. Hanwell, D. E. Curtis, D. C. Lonie, T. Vandermeersch, E. Zurek, and G. R. Hutchison. Avogadro: An advanced semantic chemical editor, visualization, and analysis platform. *J. Cheminf.*, 4:17, 2012.

[87] A. D. Becke. Density-functional thermochemistry .3. The role of exact exchange. *J. Chem. Phys.*, 98:5648–5652, 1993.

[88] I. Frank, J. Hutter, D. Marx, and M. Parrinello. Molecular Dynamics in Low-spin Excited States. *J. Chem. Phys.*, 108:4060, 1998.

[89] S. Grimm, C. Nonnenberg, and I. Frank. Restricted open-shell kohn–sham theory for π–π^* transitions. i. polyenes, cyanines, and protonated imines. *J. Chem. Phys.*, 119:11574, 2003.

[90] J. M. Wittbrodt and H. B. Schlegel. Some reasons not to use spin projected density functional theory. *J. Chem. Phys.*, 105:6574, 1996.

[91] S. Hirata and M. Head-Gordon. Time-dependent density functional theory within the Tamm-Dancoff approximation. *Chem. Phys. Lett.*, 314(3-4):291–299, 1999.

[92] Y. Shao, Z. Gan, E. Epifanovsky, A. T. B. Gilbert, M. Wormit, J. Kussmann, A. W. Lange, A. Behn, J. Deng, X. Feng, D. Ghosh, M. Goldey, P. R. Horn, L. D. Jacobson, I. Kaliman, R. Z. Khaliullin, T. Kus, A. Landau, J. Liu, E. I. Proynov, Y. M. Rhee, R. M. Richard, M. A. Rohrdanz, R. P. Steele, E. J. Sundstrom, H. L. Woodcock III, P. M. Zimmerman, D. Zuev, B. Albrecht, E. Alguire, B. Austin, G. J. O. Beran, Y. A. Bernard, E. Berquist, K. Brandhorst, K. B. Bravaya, S. T. Brown, D. Casanova, C.-M. Chang, Y. Chen, S. H. Chien, K. D. Closser, D. L. Crittenden, M. Diedenhofen, R. A. DiStasio Jr., H. Do, A. D. Dutoi, R. G. Edgar, S. Fatehi, L. Fusti-Molnar, A. Ghysels, A. Golubeva-Zadorozhnaya, J. Gomes, M. W. D. Hanson-Heine, P. H. P. Harbach, A. W. Hauser, E. G. Hohenstein, Z. C. Holden, T.-C. Jagau, H. Ji, B. Kaduk, K. Khistyaev, J. Kim, J. Kim, R. A. King, P. Klunzinger, D. Kosenkov, T. Kowalczyk,

C. M. Krauter, K. U. Lao, A. D. Laurent, K. V. Lawler, S. V. Levchenko, C. Y. Lin, F. Liu, E. Livshits, R. C. Lochan, A. Luenser, P. Manohar, S. F. Manzer, S.-P. Mao, N. Mardirossian, A. V. Marenich, S. A. Maurer, N. J. Mayhall, E. Neuscamman, C. M. Oana, R. Olivares-Amaya, D. P. O'Neill, J. A. Parkhill, T. M. Perrine, R. Peverati, A. Prociuk, D. R. Rehn, E. Rosta, N. J. Russ, S. M. Sharada, S. Sharma, D. W. Small, A. Sodt, T. Stein, D. Stueck, Y.-C. Su, A. J. W. Thom, T. Tsuchimochi, V. Vanovschi, L. Vogt, O. Vydrov, T. Wang, M. A. Watson, J. Wenzel, A. White, C. F. Williams, J. Yang, S. Yeganeh, S. R. Yost, Z.-Q. You, I. Y. Zhang, X. Zhang, Y. Zhao, B. R. Brooks, G. K. L. Chan, D. M. Chipman, C. J. Cramer, W. A. Goddard III, M. S. Gordon, W. J. Hehre, A. Klamt, H. F. Schaefer III, Michael W. Schmidt, C. D. Sherrill, D. G. Truhlar, A. Warshel, X. Xu, A. Aspuru-Guzik, R. Baer, A. T. Bell, N. A. Besley, J.-D. Chai, A. Dreuw, B. D. Dunietz, T. R. Furlani, S. R. Gwaltney, C.-P. Hsu, Y. Jung, J. Kong, D. S. Lambrecht, W. Liang, C. Ochsenfeld, V. A. Rassolov, L. V. Slipchenko, J. E. Subotnik, T. Van Voorhis, J. M. Herbert, A. I. Krylov, P. M. W. Gill, and M. Head-Gordon. Advances in molecular quantum chemistry contained in the Q-Chem 4 program package. *Mol. Phys.*, 113:184–215, 2015.

[93] C. Nonnenberg, S. Grimm, and I. Frank. Restricted open-shell kohn–sham theory for π–π^* transitions. ii. simulation of photochemical reactions. *J. Chem. Phys.*, 119(22):11585, 2003.

[94] A. Van Yperen-De Deyne, T. De Meyer, E. Pauwels, A. Ghysels, K. De Clerck, M. Waroquier, V. Van Speybroeck, and K. Hemelsoet. Exploring the vibrational fingerprint of the electronic excitation energy via molecular dynamics. *J. Chem. Phys.*, 140:134105, 2014.

[95] R. Peverati and D. G. Truhlar. Quest for a universal density functional: The accuracy of density functionals across a broad spectrum of databases in chemistry and physics. *Phil. Trans. Roy. Soc. (London) A*, 372:20120476, 2014.

[96] N. Mardirossian and M Head-Gordon. Mapping the genome of meta-generalized gradient approximation density functionals: The search for B97M-V. *J. Chem. Phys.*, 142:074111, 2015.

[97] F. Furche and R. Ahlrichs. Adiabatic Time-dependent Density Functional Methods for Excited State Properties. *J. Chem. Phys.*, 117:7433, 2002.

[98] M. Schulte and I. Frank. Restricted open-shell kohn–sham theory: n unpaired electrons. *Chem. Phys.*, 373:283–288, 2010.

[99] M. Tassi, I. Theophilou, and S. Thanos. Double excitations from modified hartree fock subsequent minimization scheme. *J. Chem. Phys.*, 138:124107, 2013.

[100] J. R. Lakowicz. *Principles of Fluorescence Spectroscopy.* Springer, 1983.

[101] McGlynn S. P., M. J. Reynolds, G. W. Daigre, and N. D. Christodoyleas. The external heavy-atom spin-orbital coupling effect. iii. phosphorescence spectra and lifetimes of externally perturbed naphthalenes. *J. Phys. Chem.*, 66:2499–2505, 1962.

[102] G. N. Lewis and M. Kasha. Phosphorescence and the triplet state. *J. Am. Chem. Soc.*, 66:2100–2116, 1944.

[103] C. S. Foote. Definition of type i and type ii photosensitized oxidation. *Photochem. Photobiol.*, 54:659, 1991.

[104] M. C. DeRosa and R. J. Crutchley. Photosensitized singlet oxygen and its applications. *Coord. Chem. Rev.*, 233–234:351–371, 2002.

[105] W. J. Royea, A. M. Fajardo, and N. S. Lewis. Fermi golden rule approach to evaluating outer-sphere electron-transfer rate constants at semiconductor/liquid interfaces. *J. Phys. Chem. B*, 101:11152–11159, 1997.

A Appendix

Table A1: Naming scheme for examined BODIPY dyes based on the positions of particular substituents. Placement of substituents are specified in Figure 1.7.

Substituents on positions 2,6	Substituent on position 8				
	CH_3	CH_2OH	H	CH_2OAc	CHO
CH_2CH_3, CH_2CH_3	2c	3c	4c	5c	8c
H, H	2d	3d	4d	5d	8d
H, Cl	2f	3f	4f	5f	8f
Cl, Cl	2g	3g	4g	5g	8g
H, CN		3i		5i	8i
CN, CN		3j		5j	8j

Optimized geometries in xyz file format:

```
48
2c
C         0.010776      -1.507885       0.134120
C        -1.216058      -0.817756       0.185172
C         1.232869      -0.808804       0.177075
N        -1.238574       0.568033       0.356265
B         0.001360       1.484589       0.555786
F        -0.004710       2.505277      -0.392186
F         0.002912       2.017175       1.845585
C        -2.517348       0.987392       0.373058
C        -3.382992      -0.120951       0.196813
C        -2.577249      -1.257817       0.075169
C        -3.103430      -2.646393      -0.158744
H        -2.621410      -3.138377      -1.010669
H        -4.176058      -2.616998      -0.367833
H        -2.967027      -3.300017       0.713370
C        -2.872184       2.428651       0.556224
H        -2.556707       3.019182      -0.310914
```

H	-2.349776	2.841337	1.424798
H	-3.948813	2.552783	0.694113
C	2.596367	-1.239094	0.057812
C	3.394855	-0.096656	0.175336
C	2.522527	1.005386	0.358050
N	1.246680	0.576941	0.349077
C	3.131209	-2.623676	-0.180339
H	4.201999	-2.585932	-0.397338
H	2.646856	-3.119257	-1.028843
H	3.006032	-3.278245	0.692718
C	2.868039	2.449250	0.538568
H	2.337713	2.861813	1.402238
H	2.555438	3.035137	-0.332899
H	3.943085	2.579926	0.682925
C	0.016305	-3.013285	0.029216
H	0.018112	-3.341727	-1.019104
H	-0.859386	-3.447764	0.507757
H	0.894925	-3.441086	0.508658
C	-4.885756	-0.049504	0.131613
C	-5.436656	0.199067	-1.284841
H	-5.242112	0.746964	0.796978
H	-5.318350	-0.975734	0.529106
H	-5.060823	1.143482	-1.694248
H	-6.532128	0.244968	-1.277539
H	-5.134814	-0.599653	-1.971845
C	4.896604	-0.015041	0.099193
C	5.435551	0.232155	-1.322015
H	5.338444	-0.936810	0.496990
H	5.252238	0.786326	0.759058
H	5.133065	-0.570364	-2.004274
H	6.530779	0.284210	-1.323020
H	5.051419	1.173167	-1.731499

```
36
2d
C       -0.037917      -1.522195       0.062784
C       -1.243998      -0.797395       0.028956
C        1.201696      -0.855805       0.034773
N       -1.229786       0.602254       0.013411
B        0.035261       1.507844       0.051467
F        0.056787       2.339094      -1.067410
F        0.052239       2.264289       1.221003
C       -2.497737       1.053351      -0.030904
C       -3.373490      -0.049012      -0.056594
C       -2.616930      -1.214629      -0.019049
C       -3.212796      -2.593023      -0.055459
H       -2.794933      -3.211911      -0.857368
H       -4.292018      -2.521228      -0.222619
H       -3.069327      -3.139696       0.885942
C       -2.841884       2.507355      -0.046746
H       -3.926450       2.641287      -0.069434
H       -2.399018       3.000463      -0.918330
H       -2.436575       3.008893       0.838683
C        2.552636      -1.339822      -0.005240
C        3.365497      -0.212558      -0.039974
C        2.544413       0.931352      -0.020520
N        1.255720       0.542779       0.017396
C        3.079143      -2.746278      -0.035822
H        4.161032      -2.729576      -0.200520
H        2.632175      -3.346496      -0.836209
H        2.905840      -3.281215       0.907309
C        2.958402       2.367185      -0.034968
H        2.579393       2.885811       0.852244
H        2.537651       2.882733      -0.904390
H        4.048080       2.448904      -0.059794
C       -0.073882      -3.029675       0.113120
H       -0.075760      -3.456987      -0.898739
H       -0.964691      -3.390653       0.624155
H        0.791041      -3.431954       0.637803
H       -4.453432       0.012939      -0.104566
H        4.447435      -0.203792      -0.082216
```

```
36
2f
C       -0.532093      -1.518123       0.056749
C       -1.756920      -0.830959       0.031028
C        0.690708      -0.813414       0.022339
N       -1.781176       0.570415       0.018036
B       -0.543906       1.514300       0.050212
F       -0.550769       2.342974      -1.068311
F       -0.542372       2.266579       1.220478
C       -3.059516       0.987446      -0.013983
C       -3.907103      -0.138635      -0.034511
C       -3.122536      -1.283500      -0.006266
C       -3.691232      -2.673731      -0.042514
H       -3.507766      -3.229003       0.886406
H       -3.288129      -3.272146      -0.867332
H       -4.776271      -2.620878      -0.174955
C       -3.444066       2.431042      -0.022284
H       -4.531894       2.534802      -0.036576
H       -3.021019       2.938848      -0.895153
H       -3.045941       2.940091       0.862033
C        2.045735      -1.273712      -0.019178
C        2.817962      -0.114088      -0.048093
C        1.979091       1.018949      -0.026028
N        0.705921       0.582968       0.010264
C        2.593908      -2.668493      -0.054790
H        3.670024      -2.637420      -0.242728
H        2.134364      -3.275670      -0.841622
H        2.445773      -3.197791       0.895352
C        2.351484       2.463547      -0.034619
H        1.958803       2.962468       0.857709
H        1.909290       2.966637      -0.900438
H        3.436787       2.577667      -0.063637
Cl       4.557970      -0.040416      -0.110060
C       -0.505229      -3.024634       0.117612
H       -0.269345      -3.454555      -0.864726
H       -1.455935      -3.438031       0.441891
H        0.259564      -3.372502       0.814231
H       -4.988544      -0.104089      -0.073166
```

```
36
2g
C       -0.009632      -1.505714       0.104086
C       -1.230142      -0.803501       0.079559
C        1.216735      -0.815507       0.043755
N       -1.243148       0.594632       0.072203
B        0.006742       1.526230       0.134220
F       -0.010386       2.404551      -0.941851
F        0.032758       2.216926       1.339848
C       -2.513942       1.032427       0.038404
C       -3.356860      -0.099899       0.007481
C       -2.588940      -1.260302       0.031988
C       -3.143684      -2.651932      -0.028172
H       -3.042852      -3.180960       0.928628
H       -2.653574      -3.260787      -0.794498
H       -4.210381      -2.613611      -0.262894
C       -2.885346       2.477063       0.030916
H       -3.964850       2.593702       0.144472
H       -2.569992       2.949058      -0.905819
H       -2.373995       3.003614       0.842555
C        2.568430      -1.287157      -0.039133
C        3.348058      -0.135113      -0.086474
C        2.518715       1.006334      -0.036166
N        1.244261       0.582327       0.031780
C        3.105360      -2.685161      -0.110094
H        4.164944      -2.660493      -0.376795
H        2.585189      -3.291287      -0.858495
H        3.026882      -3.209058       0.851662
C        2.905886       2.446761      -0.044449
H        2.526307       2.945687       0.853564
H        2.461106       2.957861      -0.904110
H        3.991878       2.549554      -0.082823
Cl       5.084306      -0.074272      -0.203695
Cl      -5.094666      -0.018634      -0.063691
C       -0.015136      -3.011228       0.194421
H       -0.019752      -3.469317      -0.803793
H       -0.892434      -3.373058       0.727449
H        0.863760      -3.378960       0.721241
```

```
49
3c
C        0.027438      -1.271513      -0.252148
C       -1.217358      -0.648116      -0.066026
C        1.226751      -0.561832      -0.077158
N       -1.285572       0.722407       0.190019
B       -0.074037       1.695280       0.290327
F       -0.106631       2.622800      -0.749750
F       -0.097167       2.345608       1.523215
C       -2.577979       1.075746       0.321490
C       -3.402720      -0.070371       0.178349
C       -2.558594      -1.157258      -0.066313
C       -3.008582      -2.582561      -0.217797
H       -3.041091      -2.899756      -1.269916
H       -4.021507      -2.706678       0.177367
H       -2.351285      -3.270640       0.321585
C       -2.986344       2.489786       0.583232
H       -2.555412       3.155759      -0.171569
H       -2.606250       2.829206       1.552922
H       -4.073456       2.593432       0.570771
C        2.600232      -0.975074      -0.095426
C        3.369285       0.167988       0.141088
C        2.467724       1.252803       0.297901
N        1.201631       0.809469       0.182692
C        3.148190      -2.364516      -0.255644
H        4.175115      -2.416082       0.119248
H        3.182671      -2.679801      -1.308259
H        2.552787      -3.097563       0.296300
C        2.776716       2.694643       0.545350
H        3.853207       2.859502       0.627456
H        2.287025       3.040041       1.461119
H        2.384304       3.311960      -0.270555
C        0.075875      -2.719243      -0.690996
C       -4.905389      -0.078175       0.261213
C       -5.596789       0.126699      -1.100317
H       -5.241165       0.702413       0.954949
H       -5.247348      -1.025735       0.695994
H       -5.304826       1.082988      -1.548340
H       -6.687738       0.120307      -0.991751
H       -5.320200      -0.665970      -1.804732
C        4.869572       0.263064       0.205163
C        5.530975       0.481652      -1.168733
H        5.279590      -0.648842       0.657511
H        5.159220       1.080331       0.876746
H        5.304107      -0.346379      -1.849868
```

H	6.620691	0.554716	-1.072973
H	5.167760	1.403414	-1.636790
O	0.109404	-3.565141	0.463569
H	0.959092	-2.877369	-1.317203
H	-0.799519	-2.936359	-1.310622
H	0.132987	-4.482597	0.147317

```
37
3d
C        0.254445      -1.272531      -0.289025
C       -1.082593      -0.862248      -0.173125
C        1.304433      -0.343807      -0.221983
N       -1.398727       0.497681      -0.086947
B       -0.383804       1.675976      -0.188026
F       -0.563457       2.366853      -1.383697
F       -0.542398       2.531537       0.899273
C       -2.733149       0.626379       0.042254
C       -3.317696      -0.656978       0.060917
C       -2.308855      -1.602532      -0.073937
C       -2.523096      -3.088695      -0.046602
H       -2.420900      -3.540076      -1.043337
H       -3.535701      -3.311377       0.303711
H       -1.812276      -3.587426       0.619977
C       -3.411426       1.952924       0.150865
H       -4.496486       1.825233       0.183022
H       -3.150081       2.590434      -0.700836
H       -3.083437       2.481703       1.051712
C        2.729884      -0.508658      -0.171885
C        3.260785       0.771720      -0.077793
C        2.196812       1.697634      -0.072110
N        1.031855       1.026077      -0.145359
C        3.540207      -1.772334      -0.149517
H        4.566221      -1.550726       0.160271
H        3.599280      -2.246190      -1.139242
H        3.122744      -2.505875       0.547396
C        2.267495       3.187782       0.005164
H        1.813493       3.549935       0.933553
H        1.704838       3.641376      -0.817714
H        3.306714       3.523342      -0.041046
C        0.568410      -2.738537      -0.497389
O        0.722695      -3.370578       0.777397
H        1.480419      -2.832138      -1.094701
H       -0.239714      -3.203311      -1.070549
H        0.924145      -4.305744       0.612618
H        4.310089       1.027838      -0.002346
H       -4.374806      -0.857947       0.180889
```

```
37
3f
C       -0.493788      -1.314466      -0.270993
C       -1.727592      -0.656193      -0.188051
C        0.714744      -0.605165      -0.146947
N       -1.780997       0.737725      -0.078780
B       -0.558970       1.702648      -0.131632
F       -0.561640       2.421675      -1.322763
F       -0.583929       2.560292       0.961541
C       -3.069260       1.116967       0.011951
C       -3.889446      -0.031601      -0.016360
C       -3.077457      -1.149884      -0.143588
C       -3.571736      -2.567069      -0.159358
H       -2.985921      -3.205971       0.508563
H       -3.532913      -3.007350      -1.165430
H       -4.616899      -2.600733       0.163578
C       -3.486823       2.546349       0.124283
H       -4.575829       2.629121       0.084124
H       -3.050449       3.138662      -0.686920
H       -3.128375       2.983173       1.062486
C        2.072333      -1.053623      -0.060600
C        2.825020       0.110201       0.062547
C        1.971211       1.235568       0.057164
N        0.706891       0.789199      -0.056838
C        2.617785      -2.449226      -0.023569
H        2.693611      -2.888867      -1.027936
H        1.991913      -3.103260       0.589630
H        3.626906      -2.442269       0.397261
C        2.325639       2.680667       0.156672
H        1.963349       3.101994       1.100669
H        1.846414       3.244893      -0.649681
H        3.407956       2.812177       0.098890
Cl       4.557051       0.195777       0.223553
C       -0.459872      -2.808371      -0.515505
O       -0.465725      -3.488272       0.742502
H        0.434801      -3.057809      -1.094958
H       -1.324955      -3.094569      -1.121627
H       -0.433639      -4.440574       0.556827
H       -4.968991      -0.027527       0.065503
```

37
3g

C	0.027039	-1.319665	-0.248085
C	-1.212760	-0.670231	-0.135043
C	1.230137	-0.602882	-0.144340
N	-1.273200	0.722539	-0.033303
B	-0.054791	1.698100	-0.098076
F	-0.078723	2.417012	-1.287145
F	-0.075676	2.548986	0.998089
C	-2.557575	1.106158	0.072540
C	-3.357820	-0.059871	0.060101
C	-2.550154	-1.184391	-0.065616
C	-3.027195	-2.604884	-0.044910
H	-2.376222	-3.232298	0.569859
H	-3.070669	-3.038772	-1.053573
H	-4.039963	-2.651533	0.364704
C	-2.982304	2.530908	0.182972
H	-4.068626	2.610752	0.111638
H	-2.519329	3.126955	-0.609686
H	-2.653353	2.956678	1.137101
C	2.593953	-1.042790	-0.088254
C	3.340274	0.123885	0.032729
C	2.477833	1.244356	0.053709
N	1.215290	0.791128	-0.041057
C	3.149006	-2.434700	-0.074938
H	3.210207	-2.862447	-1.085353
H	2.537870	-3.099175	0.541770
H	4.165186	-2.425121	0.328307
C	2.825296	2.690334	0.159336
H	2.466209	3.103621	1.108068
H	2.337434	3.256519	-0.640568
H	3.906302	2.828465	0.095222
Cl	5.072872	0.221200	0.164140
Cl	-5.091749	-0.054794	0.208115
C	0.067511	-2.810937	-0.509716
O	0.099902	-3.503393	0.740516
H	0.949364	-3.045507	-1.114369
H	-0.810454	-3.097291	-1.097088
H	0.126062	-4.454070	0.545334

```
38
3i
C       -0.387924      -1.315103      -0.286608
C       -1.623819      -0.670579      -0.213836
C        0.817205      -0.586265      -0.183579
N       -1.694208       0.727008      -0.140894
B       -0.483802       1.708201      -0.220418
F       -0.494977       2.390877      -1.430200
F       -0.525471       2.591794       0.850167
C       -2.984119       1.091635      -0.054029
C       -3.793143      -0.069265      -0.047048
C       -2.971624      -1.179329      -0.148376
C       -3.447028      -2.602174      -0.120168
H       -2.847616      -3.213176       0.561443
H       -3.408601      -3.069581      -1.113768
H       -4.489246      -2.640267       0.211074
C       -3.420003       2.517281       0.023943
H       -4.509507       2.586479      -0.022074
H       -2.986043       3.095882      -0.798227
H       -3.069459       2.977991       0.953619
C        2.170323      -1.013055      -0.086609
C        2.931076       0.164850       0.021657
C        2.048167       1.274522      -0.010511
N        0.793750       0.812887      -0.120714
C        2.746109      -2.396214      -0.036544
H        3.770584      -2.359379       0.344846
H        2.792766      -2.856306      -1.033249
H        2.155872      -3.049524       0.612268
C        2.393931       2.724290       0.054120
H        3.476801       2.854227       0.114426
H        1.922084       3.193558       0.922961
H        2.016317       3.244517      -0.832941
C        4.340720       0.244311       0.160000
C       -0.333120      -2.814803      -0.489783
N        5.498940       0.302189       0.273177
O       -0.305580      -3.454614       0.787922
H        0.556080      -3.064635      -1.077504
H       -1.202556      -3.133964      -1.072401
H       -0.238103      -4.410531       0.632656
H       -4.872000      -0.073572       0.042259
```

39
3j

C	-0.024074	-1.348302	0.319100
C	-1.234482	-0.638775	0.265455
C	1.206804	-0.673080	0.329753
N	-1.241322	0.761865	0.341644
B	0.011827	1.669141	0.578059
F	0.050084	2.670404	-0.378102
F	-0.012998	2.191257	1.861573
C	-2.500353	1.205550	0.248199
C	-3.360749	0.084209	0.083053
C	-2.581665	-1.080614	0.092587
C	-3.122024	-2.463333	-0.110738
H	-3.173950	-3.021321	0.834029
H	-2.502229	-3.033129	-0.808730
H	-4.139466	-2.411151	-0.508085
C	-2.879406	2.645956	0.314802
H	-3.966192	2.753630	0.308969
H	-2.457201	3.193185	-0.534262
H	-2.473821	3.103863	1.223113
C	2.548239	-1.153277	0.228540
C	3.359398	-0.010875	0.259775
C	2.523533	1.134537	0.379015
N	1.249312	0.726791	0.405856
C	3.058737	-2.551033	0.054393
H	4.095805	-2.529166	-0.291928
H	2.458516	-3.104839	-0.672828
H	3.048188	-3.108022	1.001206
C	2.937380	2.564300	0.463920
H	2.487575	3.037731	1.342869
H	2.584201	3.117964	-0.412088
H	4.024932	2.642921	0.525635
C	4.775237	0.017871	0.167460
C	-4.768464	0.153121	-0.082796
N	5.937393	0.035356	0.091869
N	-5.924205	0.204755	-0.217854
C	-0.046844	-2.861979	0.376924
O	-0.015561	-3.371843	-0.956569
H	-0.946765	-3.188394	0.907146
H	0.811916	-3.213105	0.957437
H	-0.030829	-4.341045	-0.900338

```
45
4c
C        0.016137      -1.585872      -0.002560
C       -1.198073      -0.915919       0.100099
C        1.220752      -0.913159      -0.173563
N       -1.243327       0.475486       0.038313
B       -0.007183       1.413111      -0.173476
F       -0.156346       2.126428      -1.359642
F        0.128149       2.279525       0.907800
C       -2.528984       0.858208       0.172365
C       -3.359422      -0.286198       0.329259
C       -2.522841      -1.404461       0.281316
C       -2.919469      -2.846491       0.380713
H       -2.081823      -3.479397       0.692072
H       -3.283049      -3.234584      -0.580325
H       -3.726155      -2.988258       1.108793
C       -2.922355       2.300411       0.147651
H       -2.673566       2.746012      -0.822011
H       -2.361657       2.861831       0.902284
H       -3.992315       2.421907       0.330697
C        2.554815      -1.397663      -0.287581
C        3.376029      -0.277746      -0.442972
C        2.526677       0.863471      -0.421343
N        1.245359       0.477257      -0.260896
C        2.971783      -2.836429      -0.227973
H        3.793292      -3.041791      -0.923527
H        2.148167      -3.510580      -0.485429
H        3.322656      -3.117497       0.774262
C        2.898402       2.305343      -0.550334
H        3.962409       2.421143      -0.769165
H        2.664736       2.845157       0.374350
H        2.313193       2.779466      -1.344927
C       -4.855598      -0.277550       0.486725
C       -5.620501      -0.294077      -0.849703
H       -5.163612       0.602868       1.065033
H       -5.161307      -1.147094       1.082899
H       -5.373405       0.583342      -1.457952
H       -6.703784      -0.294796      -0.680649
H       -5.368597      -1.183758      -1.437967
C        4.874777      -0.255812      -0.573420
C        5.606411      -0.020107       0.762173
H        5.175801       0.521602      -1.287706
H        5.215515      -1.205637      -1.004065
H        5.320750       0.941523       1.202622
H        6.693296      -0.018332       0.618619
```

H	5.360083	-0.802214	1.488954
H	0.024307	-2.669812	0.055939

```
33
4d
C       -0.017437      -1.663854       0.000118
C       -1.226487      -0.981810      -0.001367
C        1.208101      -1.006450       0.000114
N       -1.255259       0.415416      -0.001194
B        0.014636       1.342052      -0.001281
F        0.020550       2.133085      -1.143251
F        0.021550       2.132131       1.141340
C       -2.543086       0.806453      -0.001259
C       -3.378791      -0.339143      -0.001778
C       -2.568759      -1.465303      -0.002074
C       -2.995649      -2.902510      -0.005341
H       -2.600603      -3.446864       0.861655
H       -2.648051      -3.428008      -0.903893
H       -4.086309      -2.981280       0.022776
C       -2.969208       2.239811      -0.000765
H       -3.575993       2.457399      -0.888282
H       -2.115034       2.915860       0.009445
H       -3.592490       2.451351       0.876653
C        2.538846      -1.515635       0.001412
C        3.372568      -0.403078       0.000352
C        2.560063       0.754856      -0.001954
N        1.262259       0.389124      -0.002124
C        2.940351      -2.960195       0.002937
H        3.541232      -3.206569      -0.881058
H        2.073786      -3.628496       0.007962
H        3.548380      -3.202551       0.883100
C        3.012577       2.180558      -0.003768
H        3.623786       2.387789       0.883122
H        2.171316       2.872622      -0.014014
H        3.638844       2.380094      -0.881829
H       -4.461480      -0.318763      -0.001776
H       -0.031188      -2.749576       0.001292
H        4.455471      -0.400896       0.000756
```

```
33
4f
C       -0.494545      -1.653779       0.006282
C       -1.735535      -1.035311       0.033513
C        0.695043      -0.928268      -0.022794
N       -1.836453       0.358082       0.035783
B       -0.626503       1.353675       0.010627
F       -0.689004       2.144504      -1.130338
F       -0.630364       2.135554       1.158834
C       -3.142425       0.683443       0.063998
C       -3.918257      -0.502307       0.080328
C       -3.052753      -1.587004       0.061592
C       -3.406754      -3.043252       0.066060
H       -2.965344      -3.566651       0.923509
H       -3.052948      -3.550278      -0.840624
H       -4.491038      -3.176568       0.118422
C       -3.615516       2.099752       0.074177
H       -3.252583       2.630758      -0.812422
H       -3.214666       2.631235       0.944114
H       -4.707159       2.142169       0.097780
C        2.046331      -1.368892      -0.056165
C        2.800604      -0.199730      -0.078359
C        1.937368       0.921073      -0.058653
N        0.668645       0.466250      -0.025357
C        2.549494      -2.776669      -0.069748
H        3.089435      -2.994569      -0.999558
H        1.735983      -3.502011       0.023391
H        3.252080      -2.949941       0.753929
C        2.281457       2.371790      -0.067102
H        1.911302       2.855112       0.843743
H        1.795062       2.871131      -0.911541
H        3.362196       2.510673      -0.135370
Cl       4.538598      -0.115970      -0.123769
H       -5.000147      -0.535466       0.103394
H       -0.448638      -2.738347       0.006745
```

```
33
4g
C       -0.000544      -1.592044      -0.021061
C       -1.216160      -0.919195       0.033580
C        1.216691      -0.920897      -0.053224
N       -1.251413       0.475536       0.058250
B        0.002691       1.419311       0.024673
F       -0.039621       2.218927      -1.108664
F        0.047159       2.187455       1.179536
C       -2.537099       0.872667       0.113073
C       -3.351728      -0.286436       0.124934
C       -2.548527      -1.419754       0.075102
C       -2.989194      -2.848176       0.070423
H       -3.521607      -3.099599       0.995933
H       -2.144667      -3.536135      -0.028209
H       -3.681402      -3.041778      -0.757477
C       -2.944863       2.305922       0.148914
H       -2.588771       2.823236      -0.748470
H       -2.487146       2.808497       1.007526
H       -4.030901       2.395419       0.211685
C        2.548085      -1.423173      -0.107634
C        3.353953      -0.290811      -0.118757
C        2.541761       0.869422      -0.073254
N        1.255221       0.473891      -0.033733
C        2.984748      -2.852491      -0.138445
H        3.640618      -3.043411      -0.995812
H        2.134672      -3.537568      -0.204595
H        3.555061      -3.110228       0.762598
C        2.953648       2.301943      -0.066166
H        2.594212       2.794816       0.843488
H        2.502244       2.829773      -0.912902
H        4.040271       2.389840      -0.120683
Cl       5.091977      -0.283773      -0.180547
Cl      -5.089502      -0.277712       0.193470
H       -0.001994      -2.676956      -0.038414
```

54
5c2
C 0.129452 -0.709529 0.164014
C -1.172713 -0.202047 0.012827
C 1.253476 0.130780 0.087699
N -1.376648 1.170724 -0.136397
B -0.269676 2.265480 -0.129537
F -0.340759 3.015568 -1.302706
F -0.413402 3.087686 0.986004
C -2.697341 1.405581 -0.251181
C -3.405166 0.176190 -0.206163
C -2.458794 -0.838352 -0.038097
C -2.780894 -2.304688 0.011670
H -2.124373 -2.890307 -0.638594
H -3.809210 -2.477839 -0.317863
H -2.699187 -2.718691 1.025683
C -3.239056 2.791288 -0.394270
H -4.327294 2.784492 -0.484706
H -2.807154 3.283204 -1.271517
H -2.959883 3.398768 0.473827
C 2.664078 -0.136335 0.117173
C 3.311151 1.095340 -0.013273
C 2.302691 2.089258 -0.114184
N 1.089292 1.508233 -0.067861
C 3.361106 -1.463632 0.208490
H 4.415862 -1.358817 -0.061183
H 2.919871 -2.203151 -0.466019
H 3.335733 -1.882623 1.223713
C 2.460324 3.569392 -0.249523
H 1.951460 4.080153 0.575321
H 1.990471 3.922815 -1.172921
H 3.513622 3.858107 -0.248175
C 4.793877 1.353771 -0.031886
C 0.320458 -2.175719 0.467211
C -4.899463 0.018723 -0.300696
O 0.475529 -2.896850 -0.782124
C 0.617720 -4.241570 -0.650421
H -0.528431 -2.588033 1.008562
H 1.202377 -2.344221 1.082867
O 0.613627 -4.809181 0.418981
C 0.787448 -4.914028 -1.993337
H 0.656715 -4.214247 -2.819952
H 0.065162 -5.731400 -2.074806
H 1.788147 -5.355971 -2.043534
C 5.406919 1.540318 1.368545

H	5.003974	2.244519	-0.636251
H	5.307089	0.527526	-0.539884
H	4.944412	2.385035	1.891331
H	6.484555	1.730226	1.301986
H	5.256923	0.647648	1.986226
C	-5.596254	-0.087964	1.068613
H	-5.139166	-0.873359	-0.894055
H	-5.326193	0.862498	-0.855426
H	-5.215487	-0.943561	1.637414
H	-6.678636	-0.213811	0.948332
H	-5.423399	0.811703	1.669910

```
42
5d2
C        0.565273       0.003230      -0.512475
C       -0.169652       1.168884      -0.241948
C       -0.032281      -1.266238      -0.449461
N       -1.535539       1.087597       0.048931
B       -2.390436      -0.214185       0.085172
F       -2.977536      -0.359962       1.339640
F       -3.364496      -0.177654      -0.909409
C       -2.007747       2.327414       0.277779
C       -0.949549       3.250836       0.151663
C        0.207295       2.554639      -0.173346
C        1.551667       3.197416      -0.358293
H        2.327181       2.712005       0.242956
H        1.503151       4.247765      -0.055141
H        1.885215       3.179810      -1.404131
C       -3.438343       2.597452       0.611527
H       -3.613392       3.671919       0.707434
H       -3.714877       2.101249       1.547773
H       -4.094964       2.191132      -0.164946
C        0.499335      -2.592741      -0.602263
C       -0.571199      -3.458261      -0.419811
C       -1.727654      -2.693296      -0.163181
N       -1.398610      -1.387471      -0.173878
C        1.909417      -3.041292      -0.857943
H        1.979823      -4.125453      -0.727732
H        2.621329      -2.575622      -0.168677
H        2.244383      -2.818429      -1.879612
C       -3.118207      -3.175449       0.089098
H       -3.814605      -2.730526      -0.629511
H       -3.457805      -2.871325       1.084987
H       -3.166048      -4.264445       0.009931
H       -0.533812      -4.539677      -0.456092
C        2.019792       0.118793      -0.897647
H       -1.035357       4.320442       0.295822
O        2.818158       0.063958       0.310966
C        4.158166       0.172297       0.116833
H        2.225100       1.053466      -1.416107
H        2.326318      -0.687119      -1.561901
O        4.663300       0.304190      -0.975527
C        4.913238       0.104728       1.424351
H        4.242830       0.010637       2.279697
H        5.524212       1.006778       1.527901
H        5.597026      -0.749579       1.395354
```

```
42
5f2
C        0.622838       0.421488      -0.459771
C       -0.048007       1.629146      -0.220011
C       -0.044284      -0.814830      -0.367224
N       -1.417841       1.630686       0.066583
B       -2.344739       0.381363       0.127301
F       -2.943564       0.295797       1.379171
F       -3.305356       0.443597      -0.876939
C       -1.821923       2.898930       0.264564
C       -0.713184       3.760349       0.122410
C        0.404014       2.995632      -0.180739
C        1.781323       3.561422      -0.372953
H        2.526227       3.056683       0.250858
H        1.785091       4.621934      -0.103476
H        2.121585       3.492591      -1.414208
C       -3.235851       3.255413       0.586063
H       -3.536727       2.810928       1.540793
H       -3.913512       2.854137      -0.174670
H       -3.354805       4.340296       0.641009
C        0.424680      -2.164340      -0.491286
C       -0.703918      -2.954233      -0.295875
C       -1.827984      -2.132896      -0.056678
N       -1.414551      -0.853370      -0.095660
C        1.809141      -2.687677      -0.729942
H        1.837737      -3.761861      -0.530214
H        2.543614      -2.203588      -0.080048
H        2.133206      -2.544857      -1.769158
C       -3.241645      -2.531155       0.199984
H       -3.910897      -2.022427      -0.501061
H       -3.547686      -2.229524       1.207629
H       -3.358985      -3.611528       0.097298
Cl      -0.756104      -4.694243      -0.323426
C        2.082226       0.448850      -0.843822
H       -0.740031       4.835822       0.243066
O        2.870648       0.336716       0.365952
C        4.217243       0.411041       0.182392
H        2.346129       1.370395      -1.357639
H        2.334903      -0.372190      -1.513119
O        4.729644       0.568572      -0.902285
C        4.945582       0.258770       1.496352
H        4.553582       0.963091       2.236325
H        6.011347       0.428533       1.340423
H        4.789117      -0.750483       1.892461
```

42
5g

C	-0.030110	-0.734454	-0.235781
C	-1.101914	0.170820	-0.164465
C	1.295673	-0.311930	-0.044573
N	-0.856680	1.537115	-0.003177
B	0.549345	2.215046	0.048338
F	0.763678	2.955359	-1.107060
F	0.647049	3.012369	1.179372
C	-2.025367	2.199810	0.038150
C	-3.064564	1.247240	-0.078866
C	-2.523207	-0.026769	-0.204330
C	-3.315720	-1.296206	-0.282685
H	-2.925180	-2.056318	0.399848
H	-3.327296	-1.716788	-1.297762
H	-4.355597	-1.100093	-0.009384
C	-2.124221	3.679424	0.187503
H	-3.158703	4.006390	0.067895
H	-1.494582	4.177901	-0.556307
H	-1.760242	3.989398	1.172807
C	2.528277	-1.042831	0.043389
C	3.501918	-0.075593	0.263109
C	2.902954	1.204956	0.311000
N	1.580125	1.044788	0.133935
C	2.777941	-2.519938	-0.010529
H	3.792530	-2.735445	0.333325
H	2.695488	-2.915246	-1.032221
H	2.080461	-3.070617	0.627423
C	3.549444	2.531842	0.518755
H	3.200687	2.983092	1.453377
H	3.275500	3.218732	-0.288809
H	4.635119	2.425546	0.551960
Cl	5.204242	-0.362352	0.472179
Cl	-4.757324	1.643468	-0.045678
C	-0.305855	-2.186199	-0.557971
O	-0.493518	-2.903425	0.677271
H	0.531396	-2.607365	-1.115228
H	-1.196062	-2.266502	-1.182007
C	-0.769042	-4.249212	0.676720
O	-0.890232	-4.803857	1.738132
C	-0.907783	-4.944048	-0.663232
H	0.009740	-4.862477	-1.256429
H	-1.722401	-4.511440	-1.254501
H	-1.120749	-5.996593	-0.476231

```
43
5i
C        0.375785      -0.585105      -0.496132
C       -0.745508      -1.386814      -0.269290
C        0.298788       0.823021      -0.405120
N       -1.990605      -0.802916       0.001798
B       -2.298232       0.724066       0.068794
F       -3.185190       1.078173      -0.940236
F       -2.810199       1.048578       1.319053
C       -2.897556      -1.776002       0.186016
C       -2.259920      -3.031617       0.053272
C       -0.921825      -2.819402      -0.230875
C        0.084852      -3.918203      -0.409669
H        0.967477      -3.777177       0.222638
H        0.431789      -4.002879      -1.447468
H       -0.366774      -4.878196      -0.142602
C       -4.333407      -1.498796       0.484549
H       -4.901637      -2.430556       0.535567
H       -4.764271      -0.851975      -0.286764
H       -4.431114      -0.962798       1.434701
C        1.292423       1.836466      -0.521209
C        0.615667       3.053243      -0.326476
C       -0.755762       2.774145      -0.097322
N       -0.928058       1.445018      -0.140576
C        2.769390       1.732007      -0.758830
H        3.241952       2.703775      -0.590770
H        3.001842       1.433871      -1.789360
H        3.237776       1.006091      -0.087699
C       -1.861406       3.742730       0.156161
H       -2.303120       3.567060       1.142517
H       -2.662089       3.606032      -0.578043
H       -1.490090       4.768489       0.102948
C        1.193771       4.348893      -0.340346
C        1.690736      -1.229238      -0.861677
N        1.672536       5.410978      -0.350770
O        2.439426      -1.445813       0.358021
H        2.271713      -0.597888      -1.532437
H        1.547650      -2.181427      -1.367669
C        3.638771      -2.070402       0.190145
O        4.050286      -2.428444      -0.889332
C        4.345002      -2.234674       1.514112
H        4.523275      -1.254720       1.968855
H        5.294036      -2.747975       1.356682
H        3.720736      -2.806049       2.208511
H       -2.747779      -3.991110       0.168236
```

```
44
5j
C       -0.279974      -0.624837      -0.438500
C       -1.060408       0.542264      -0.376619
C        1.100279      -0.588266      -0.175580
N       -0.458784       1.783425      -0.120971
B        1.073827       2.045941       0.046859
F        1.552569       2.769243      -1.034307
F        1.308316       2.704792       1.242837
C       -1.396005       2.737946      -0.098473
C       -2.661048       2.129426      -0.327264
C       -2.468865       0.752985      -0.506412
C       -3.581926      -0.222378      -0.740653
H       -3.527079      -1.074278      -0.056637
H       -3.576357      -0.614634      -1.765571
H       -4.545438       0.272135      -0.590249
C       -1.102601       4.181375       0.130085
H       -2.012751       4.776589       0.029962
H       -0.355299       4.533238      -0.588694
H       -0.679283       4.331740       1.128703
C        2.076158      -1.628553      -0.075921
C        3.281519      -0.985207       0.233879
C        3.039835       0.413974       0.318508
N        1.741067       0.632491       0.082142
C        1.931028      -3.114375      -0.208492
H        2.838208      -3.609107       0.149217
H        1.787045      -3.422007      -1.252175
H        1.084742      -3.492373       0.372028
C        4.020228       1.495021       0.621695
H        3.763879       1.987252       1.565742
H        3.991104       2.264541      -0.156731
H        5.030371       1.085813       0.691186
C        4.538124      -1.609483       0.447145
C       -3.902835       2.816405      -0.351574
N        5.566452      -2.127358       0.622539
N       -4.924441       3.375348      -0.369539
C       -0.930075      -1.935260      -0.813905
O       -1.397700      -2.570368       0.397319
H       -0.230582      -2.597062      -1.321672
H       -1.768423      -1.783354      -1.491647
C       -2.030599      -3.765129       0.203772
O       -2.183895      -4.254291      -0.890802
C       -2.487742      -4.348141       1.517891
H       -1.635224      -4.478705       2.192207
H       -2.969990      -5.309273       1.337677
```

H	-3.189884	-3.666220	2.008657

```
47
8c
C        0.013489      -1.343655       0.068258
C       -1.228765      -0.691949       0.165608
C        1.226356      -0.641878       0.104675
N       -1.286133       0.691737       0.309371
B       -0.059785       1.645583       0.418508
F       -0.101111       2.597930      -0.594552
F       -0.048194       2.259631       1.669935
C       -2.579524       1.067433       0.350336
C       -3.412982      -0.075388       0.225280
C       -2.572788      -1.184726       0.099628
C       -3.024069      -2.606238      -0.082823
H       -2.870323      -3.211289       0.821328
H       -2.499939      -3.108793      -0.903058
H       -4.092374      -2.644203      -0.312547
C       -2.976941       2.499285       0.507477
H       -2.641442       3.087095      -0.353973
H       -2.495781       2.934298       1.389650
H       -4.060227       2.598395       0.604879
C        2.601476      -1.061254       0.068110
C        3.373688       0.094829       0.187884
C        2.475666       1.192074       0.301527
N        1.207153       0.747867       0.257742
C        3.145524      -2.452924      -0.071174
H        2.913548      -2.879648      -1.051109
H        2.729090      -3.138478       0.675401
H        4.231543      -2.452150       0.054448
C        2.795534       2.644441       0.448793
H        2.278416       3.059602       1.319592
H        2.439962       3.204354      -0.423302
H        3.870255       2.802839       0.558318
C       -4.918344      -0.059367       0.203278
C       -5.515508       0.173238      -1.197500
H       -5.286017       0.720478       0.882219
H       -5.302009      -1.003777       0.607315
H       -5.184373       1.131327      -1.613353
H       -6.611037       0.180452      -1.159433
H       -5.204447      -0.612707      -1.894818
C        4.874785       0.202323       0.176318
C        5.468442       0.404625      -1.230371
H        5.313354      -0.697092       0.624986
H        5.187499       1.033516       0.820382
H        5.215314      -0.434406      -1.887894
H        6.560794       0.485052      -1.185709
```

H	5.079735	1.317617	-1.695341
C	-0.003508	-2.839758	-0.055971
O	0.521884	-3.461016	-0.953939
H	-0.553256	-3.366694	0.749308

35
8d

C	-0.106098	-1.379873	-0.189890
C	-1.273406	-0.607323	-0.119316
C	1.175260	-0.800063	-0.153007
N	-1.166629	0.785192	-0.005230
B	0.154755	1.613924	0.061374
F	0.208137	2.504316	-1.007022
F	0.232224	2.295397	1.272328
C	-2.404259	1.313584	0.006375
C	-3.350295	0.271943	-0.112858
C	-2.674482	-0.936074	-0.197667
C	-3.349845	-2.267388	-0.343872
H	-3.212818	-2.890908	0.544064
H	-2.962270	-2.841437	-1.192517
H	-4.421831	-2.116426	-0.502957
C	-2.655743	2.780175	0.123340
H	-3.727920	2.982547	0.183697
H	-2.237191	3.310417	-0.739285
H	-2.158823	3.183730	1.011539
C	2.488131	-1.381439	-0.158108
C	3.375717	-0.316802	-0.063617
C	2.632967	0.880268	0.007639
N	1.318804	0.582944	-0.040500
C	2.890992	-2.826846	-0.225701
H	2.708376	-3.263854	-1.216218
H	2.362184	-3.446312	0.507352
H	3.962293	-2.920729	-0.023979
C	3.137762	2.280489	0.124366
H	2.774780	2.742410	1.048859
H	2.762876	2.894384	-0.701334
H	4.230448	2.296809	0.118721
C	-0.180628	-2.871028	-0.331423
O	-0.854570	-3.596080	0.368024
H	0.445143	-3.293291	-1.141100
H	-4.424201	0.406427	-0.133269
H	4.455970	-0.382874	-0.037745

```
35
8f
C       -0.519218      -1.366441      -0.123127
C       -1.754743      -0.700747      -0.108826
C        0.699998      -0.672955      -0.065904
N       -1.805455       0.691513      -0.026798
B       -0.576249       1.646000       0.051753
F       -0.562579       2.501693      -1.043268
F       -0.608426       2.362868       1.241794
C       -3.096477       1.075868       0.005947
C       -3.918499      -0.070962      -0.046039
C       -3.104653      -1.193238      -0.112379
C       -3.596829      -2.611009      -0.156983
H       -3.125638      -3.243821       0.603585
H       -3.416779      -3.082229      -1.132033
H       -4.676585      -2.633889       0.018181
C       -3.509723       2.507964       0.087823
H       -4.598960       2.593327       0.077412
H       -3.094503       3.076416      -0.751201
H       -3.120680       2.967911       1.002690
C        2.065564      -1.113824      -0.128502
C        2.815366       0.054275      -0.063161
C        1.955435       1.175342       0.027139
N        0.689516       0.724433       0.016888
C        2.627398      -2.496771      -0.248299
H        3.706624      -2.442657      -0.409040
H        2.189035      -3.047086      -1.087685
H        2.437265      -3.087016       0.652579
C        2.309726       2.620497       0.113748
H        1.831930       3.075240       0.987270
H        1.936947       3.155247      -0.766637
H        3.391706       2.746942       0.181675
Cl       4.551122       0.165227      -0.088908
C       -0.545245      -2.865717      -0.209837
O        0.023786      -3.602997       0.564633
H       -1.144033      -3.276225      -1.046112
H       -5.000788      -0.062512      -0.027004
```

```
35
8g
C       -0.006474      -1.357733      -0.070900
C       -1.242633      -0.687932      -0.077549
C        1.212066      -0.667601      -0.018284
N       -1.289294       0.705123      -0.036981
B       -0.054519       1.660030       0.029184
F       -0.026595       2.480149      -1.090435
F       -0.101180       2.407529       1.197544
C       -2.574223       1.105294      -0.031391
C       -3.387005      -0.052620      -0.059828
C       -2.585130      -1.188518      -0.079774
C       -3.072522      -2.606015      -0.075254
H       -2.534497      -3.227944       0.647459
H       -2.972192      -3.078570      -1.061335
H       -4.133327      -2.632725       0.187810
C       -2.983868       2.537764       0.003913
H       -4.070891       2.626313      -0.036020
H       -2.542081       3.079763      -0.838725
H       -2.613905       3.015140       0.917592
C        2.578546      -1.114434      -0.057136
C        3.331116       0.051224      -0.007691
C        2.473150       1.177774       0.049709
N        1.206292       0.731907       0.035415
C        3.135956      -2.501631      -0.140568
H        4.218284      -2.455426      -0.281067
H        2.711007      -3.064887      -0.978256
H        2.924846      -3.074025       0.766971
C        2.832490       2.622750       0.109061
H        3.913607       2.746631       0.191083
H        2.342019       3.099285       0.963723
H        2.475329       3.137963      -0.789372
Cl       5.066082       0.157405      -0.015117
Cl      -5.125299      -0.025268      -0.057059
C       -0.034600      -2.858839      -0.144800
O        0.517905      -3.589410       0.647179
H       -0.616859      -3.273495      -0.990654
```

```
36
8i
C       -0.511461      -1.358334      -0.114346
C       -1.702738      -0.627082      -0.062030
C        0.748684      -0.741650       0.015633
N       -1.675795       0.757982       0.121437
B       -0.397860       1.629390       0.323959
F       -0.321136       2.595096      -0.669557
F       -0.413675       2.207615       1.586379
C       -2.937686       1.221991       0.098243
C       -3.823543       0.138999      -0.114680
C       -3.079260      -1.023793      -0.222318
C       -3.651020      -2.387782      -0.477934
H       -3.552262      -3.048268       0.393238
H       -3.174472      -2.890952      -1.326716
H       -4.718556      -2.304382      -0.701454
C       -3.270966       2.665584       0.273788
H       -4.352016       2.817810       0.233655
H       -2.790612       3.266542      -0.505719
H       -2.890295       3.032415       1.233328
C        2.077618      -1.262245       0.040377
C        2.908974      -0.149078       0.240927
C        2.097792       1.012801       0.341761
N        0.815764       0.646090       0.210927
C        2.579702      -2.666207      -0.104645
H        3.657225      -2.693330       0.078220
H        2.383671      -3.057221      -1.106632
H        2.099639      -3.351010       0.602839
C        2.536334       2.421217       0.557215
H        2.093833       2.819963       1.476270
H        2.188782       3.056958      -0.263460
H        3.624991       2.476528       0.624924
C        4.324862      -0.159480       0.336881
C       -0.620329      -2.844300      -0.310563
N        5.486745      -0.167005       0.419441
O       -0.030366      -3.462580      -1.168364
H       -1.301051      -3.360038       0.393746
H       -4.900029       0.222805      -0.190079
```

```
37
8j
C       -0.093473      -1.375361      -0.018199
C       -1.288100      -0.640355       0.073818
C        1.162687      -0.757477       0.041864
N       -1.254735       0.748418       0.238403
B        0.034842       1.624652       0.370002
F        0.062215       2.573757      -0.637385
F        0.080128       2.210316       1.624931
C       -2.507806       1.220582       0.270129
C       -3.404196       0.126517       0.111892
C       -2.652642      -1.049125      -0.018555
C       -3.234629      -2.413737      -0.231281
H       -3.117891      -3.050792       0.654910
H       -2.773707      -2.934357      -1.077399
H       -4.306407      -2.332556      -0.432188
C       -2.840815       2.663013       0.441286
H       -3.922383       2.802648       0.496976
H       -2.441737       3.245792      -0.395854
H       -2.373993       3.053361       1.351543
C        2.496922      -1.279944       0.007751
C        3.333299      -0.166905       0.144115
C        2.525790       1.000873       0.266261
N        1.240833       0.635387       0.208385
C        2.987292      -2.686933      -0.138838
H        4.072990      -2.714134      -0.015414
H        2.734889      -3.094630      -1.121502
H        2.544698      -3.356481       0.606577
C        2.979428       2.409679       0.437122
H        2.600239       2.816709       1.380752
H        2.576132       3.037763      -0.363575
H        4.069937       2.464197       0.430929
C        4.752719      -0.174023       0.165252
C       -4.819457       0.229021       0.082123
C       -0.207700      -2.868766      -0.168568
N        5.916972      -0.177082       0.186398
O        0.316329      -3.500153      -1.057704
H       -0.824251      -3.369817       0.602412
N       -5.981098       0.307509       0.056953
```

Electronic states and coupling calculations Q-Chem input file for ^{1}PS+^{1}O$_2$ state. Note that all subsequent example calculation inputs will be using this same set of xyz coordinates as this first example but will use "XYZ" as a placeholder.

```
$rem
  Unrestricted  TRUE
  exchange      omegaB97X-D
  basis         6-31G(d)
  scf_convergence    6
  thresh       14
  max_scf_cycles       200
  !geom_opt_max_cycles  100
  !SCF_ALGORITHM        DIIS_GDM
  !THRESH_DIIS_SWITCH   6
$end
$molecule
0   1
C        0.222728      -1.490455      -0.073732
C       -0.947463      -0.734001      -0.250214
C        1.461899      -0.860527       0.104457
N       -0.908665       0.653375      -0.168442
B        0.337810       1.509928       0.167649
F        0.539752       2.469687      -0.820348
F        0.185342       2.116872       1.413746
C       -2.142125       1.135152      -0.364148
C       -3.035226       0.069133      -0.596236
C       -2.293318      -1.108901      -0.532844
C       -2.863706      -2.479314      -0.741917
H       -2.254106      -3.086369      -1.416579
H       -3.865678      -2.417037      -1.173517
H       -2.954122      -3.026122       0.205126
C       -2.430888       2.599008      -0.329498
H       -1.968592       3.098559      -1.186002
H       -2.008516       3.046319       0.574186
H       -3.507222       2.783349      -0.351425
C        2.795594      -1.367102       0.189312
C        3.632912      -0.268894       0.356824
C        2.814654       0.883246       0.352493
N        1.536870       0.526290       0.196750
C        3.274970      -2.783520       0.070863
H        4.363500      -2.807768      -0.022991
H        2.860558      -3.279363      -0.812546
H        3.015232      -3.389375       0.947418
C        3.241691       2.309277       0.453854
H        2.569021       2.874929       1.101972
```

```
H        3.217349       2.780098      -0.534024
H        4.258756       2.375742       0.847026
C        0.138912      -2.991662      -0.086360
H        0.153232      -3.373916      -1.114194
H       -0.782010      -3.338323       0.381083
H        0.968403      -3.445764       0.449724
C       -4.499923       0.201279      -0.899089
C       -4.783121       0.319673      -2.401909
H       -4.909364       1.078441      -0.384815
H       -5.039140      -0.660570      -0.489212
H       -4.306892       1.213961      -2.817408
H       -5.858993       0.381273      -2.598708
H       -4.384567      -0.548292      -2.938529
C        5.130221      -0.253434       0.465069
C        5.820991       0.028710      -0.874463
H        5.488758      -1.207055       0.867605
H        5.433376       0.504762       1.197329
H        5.561998      -0.737217      -1.613327
H        6.910655       0.046193      -0.767297
H        5.501117       0.995667      -1.277534
O       -2.626873      -0.625388       2.679067
O       -1.648812       0.056300       2.860184
$end
```

Q-Chem input file for ^{1}PS+^{3}O$_2$ state

```
$rem
  CDFT      TRUE
  Unrestricted  TRUE
  exchange      omegaB97X-D
  basis         6-31G(d)
  scf_convergence      8
  thresh       14
  max_scf_cycles       200
  !geom_opt_max_cycles  100
  !SCF_ALGORITHM        DIIS_GDM
  !THRESH_DIIS_SWITCH   6
$end

$cdft
2
1   49  50  s
$end


$molecule
```

```
0   3
XYZ
$end
```

Q-Chem input file for $^1PS^*+^1O_2$ state

```
$rem
  Unrestricted  false
  ROKS      True
  exchange      omegaB97X-D
  basis         6-31G(d)
  scf_convergence       5
  thresh       10
  max_scf_cycles       200
  !geom_opt_max_cycles  100
  !SCF_ALGORITHM        DIIS_GDM
  !THRESH_DIIS_SWITCH   6
$end


$molecule
0   1
XYZ
$end
```

Q-Chem input file for $^1PS^*+^3O_2$ state

```
$rem
  Unrestricted  TRUE
  exchange      omegaB97X-D
  basis         6-31G(d)
$end

$molecule
1   2
XYZ
$end


@@@

$rem
  Unrestricted  TRUE
  exchange      omegaB97X-D
  basis         6-31G(d)
  MOM_START     1
```

```
  SCF_GUESS     READ
$end

$swap_occupied_virtual
alpha 94 95
$end

$molecule
0   3
XYZ
$end
```

Q-Chem input file for ^{3}PS+^{3}O$_2$ state

```
$rem
  CDFT      TRUE
  Unrestricted  TRUE
  exchange      omegaB97X-D
  basis         6-31G(d)
  scf_convergence    6
  thresh       10
  max_scf_cycles       200
  !geom_opt_max_cycles  100
  !SCF_ALGORITHM        DIIS_GDM
  !THRESH_DIIS_SWITCH   6
$end

$cdft
2
1   49  50  s
$end


$molecule
0   5
XYZ
$end
```

Q-Chem input file for ^{2}PS$^{\bullet+}$+^{2}O$^{\bullet-}{}_2$ state

```
$rem
  CDFT      TRUE
  Unrestricted  TRUE
  exchange      omegaB97X-D
  basis         6-31G(d)
  scf_convergence      8
```

```
  thresh       14
  max_scf_cycles       200
  !geom_opt_max_cycles  100
  !SCF_ALGORITHM        DIIS_GDM
  !THRESH_DIIS_SWITCH   6
$end

$cdft
1
1   49  50  s
$end


$molecule
0   3
XYZ
$end
```

Q-Chem input file for coupling between ^{1}PS+^{1}O$_2$ and ^{3}PS+^{3}O$_2$

```
$rem
  CDFT          TRUE
  CDFTCI        TRUE
  CDFTCI_STOP   1
  CDFTCI_COUPLING  2
  Unrestricted  TRUE
  exchange      omegaB97X-D
  basis         6-31G(d)
  scf_convergence    5
  thresh       14
  max_scf_cycles       200
  !geom_opt_max_cycles  100
  !SCF_ALGORITHM        DIIS_GDM
  !THRESH_DIIS_SWITCH   6
$end

$cdft
0
1       1      50      s
----------
2
1       49      50      s
$end


$molecule
```

```
0   1
XYZ
$end



@@@


$rem
  CDFT           TRUE
  CDFTCI         TRUE
  CDFTCI_RESTART         1
  CDFTCI_COUPLING  2
  Unrestricted  TRUE
  exchange       omegaB97X-D
  basis          6-31G(d)
  scf_convergence    5
  thresh       14
  max_scf_cycles       200
  !geom_opt_max_cycles  100
  !SCF_ALGORITHM        DIIS_GDM
  !THRESH_DIIS_SWITCH   6
$end

$cdft
0
1       1      50      s
----------
2
1       49      50      s
$end


$molecule
0   5
XYZ
$end
```

Q-Chem input file for coupling between $^1\mathrm{PS}^* + {}^3\mathrm{O}_2$ and $^2\mathrm{PS}^{\bullet+} + {}^2\mathrm{O}^{\bullet-}{}_2$

```
$rem
  Unrestricted  TRUE
  exchange       omegaB97X-D
  basis          6-31G(d)
$end
```

```
$molecule
1   2
XYZ
$end


@@@




$rem
  CDFT           TRUE
  CDFTCI         TRUE
  CDFTCI_STOP    1
  CDFTCI_COUPLING  2
  Unrestricted   TRUE
  exchange       omegaB97X-D
  MOM_START      1
  SCF_GUESS      READ
  basis          6-31G(d)
  scf_convergence    6
  thresh       14
  max_scf_cycles       200
$end

$swap_occupied_virtual
alpha 94 95
$end

$cdft
0
1       1      50      s
----------
1
1       49      50
1       49      50     s
$end

$molecule
0   3
XYZ
$end
```

```
@@@



$rem
  CDFT           TRUE
  CDFTCI         TRUE
  CDFTCI_RESTART         1
  CDFTCI_COUPLING  2
  scf_guess  read
  cdftci_skip_promolecules   true
  Unrestricted  TRUE
  exchange       omegaB97X-D
  basis          6-31G(d)
  scf_convergence    6
  thresh       14
  max_scf_cycles       200
  !geom_opt_max_cycles  100
  !SCF_ALGORITHM        DIIS_GDM
  !THRESH_DIIS_SWITCH   6
$end

$cdft
0
1       1      50      s
----------
1
1      49      50
1      49      50      s
$end


$molecule
0   3
XYZ
$end
```

Q-Chem input file for coupling between ^{1}PS+^{3}O$_2$ and ^{2}PS$^{\bullet+}$+^{2}O$^{\bullet-}{}_2$

```
$rem
  exchange  omegaB97X-D
  basis  6-31G(d)
  unrestricted  true
$end
```

```
$molecule
0   3
XYZ
$end


@@@


$rem
  CDFT           TRUE
  CDFTCI         TRUE
  CDFTCI_STOP    1
  CDFTCI_SKIP_PROMOLECULES    TRUE
  CDFTCI_PRINT  3
  scf_guess  read
  scf_guess_mix  10
  CDFTCI_COUPLING  1
  Unrestricted  TRUE
  exchange      omegaB97X-D
  basis         6-31G(d)
  scf_convergence    5
  thresh       10
  max_scf_cycles       250
  !geom_opt_max_cycles  100
  !SCF_ALGORITHM        DIIS_GDM
  !THRESH_DIIS_SWITCH   6
$end

$cdft
0
0       1      50      s
----------
1
1       49      50
1       49      50      s
$end


$molecule
0   3
XYZ
$end

@@@
```

```
$rem
  CDFT           TRUE
  CDFTCI         TRUE
  CDFTCI_RESTART   1
  CDFTCI_COUPLING  1
  CDFTCI_SKIP_PROMOLECULES   TRUE
  Unrestricted  TRUE
  exchange      omegaB97X-D
  basis         6-31G(d)
  scf_convergence    5
  scf_guess  read
  scf_guess_mix  10
  thresh       10
  max_scf_cycles       250
  !geom_opt_max_cycles  100
  !SCF_ALGORITHM        DIIS_GDM
  !THRESH_DIIS_SWITCH   6
$end

$cdft
0
0       1      50      s
----------
1
1       49      50
1       49      50      s
$end


$molecule
0   3
XYZ
$end
```

Q-Chem input file for coupling between ^{1}PS*+^{3}O$_2$ and ^{3}PS+^{3}O$_2$

```
$rem
  Unrestricted  TRUE
  exchange      omegaB97X-D
  basis         6-31G(d)
$end

$molecule
1   2
XYZ
$end
```

```
@@@



$rem
  CDFT           TRUE
  CDFTCI         TRUE
  CDFTCI_STOP    1
  CDFTCI_COUPLING  2
  Unrestricted  TRUE
  exchange       omegaB97X-D
  SCF_GUESS      READ
  basis          6-31G(d)
  scf_convergence    6
  thresh       14
  max_scf_cycles       200
$end


$cdft
0
1       1      50      s
----------
2
1       49      50      s
$end

$molecule
0   3
XYZ
$end

@@@



$rem
  CDFT           TRUE
  CDFTCI         TRUE
  CDFTCI_RESTART        1
  CDFTCI_COUPLING  2
  Unrestricted  TRUE
```

```
  exchange      omegaB97X-D
  basis         6-31G(d)
  scf_convergence    6
  thresh       14
  max_scf_cycles       200
  !geom_opt_max_cycles  100
  !SCF_ALGORITHM        DIIS_GDM
  !THRESH_DIIS_SWITCH   6
$end

$cdft
0
1       1       50      s
----------
2
1       49       50      s
$end


$molecule
0   5
XYZ
$end
```

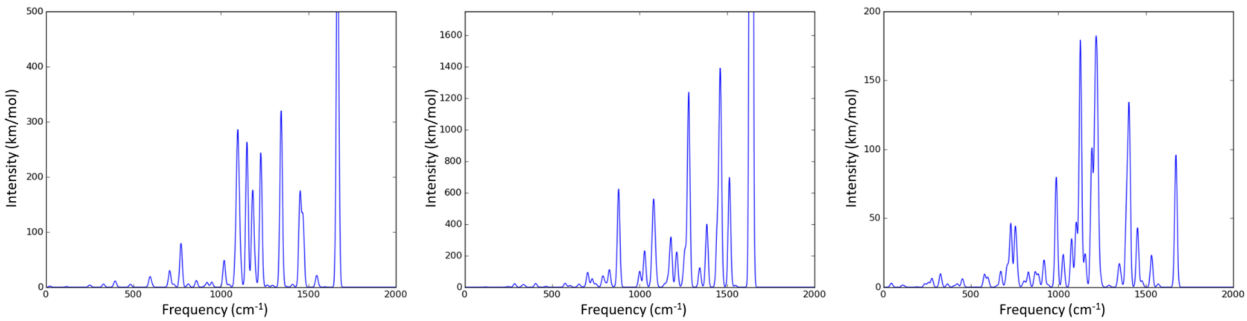

Figure A1: Simulated vibrational spectra for molecule 2c in the S_0 ground state (left), S_1 excited state using ROKS (center) and TDDFT (right). Lineshapes are approximated via uniform Lorentzian broadening of each absorption peak, with scale parameter y= 0.4cm^{-1}.

Table A2: Excitation and Emission Energies for BODIPY derivatives

	ROKS		TDDFT	
	Excitation (eV)	Emission (eV)	Excitation (eV)	Emission (eV)
2c	2.3265648262	2.1691204892	2.916	2.6904
2d	2.4014377803	2.2367761858	3.0608	2.9091
2f	2.3614554315	2.1973839644	2.9584	2.2836
2g	2.3007578689	2.1437104924	2.8613	2.2995
3c	2.1958718756	2.0126138435	2.7856	2.0294
3d	2.2790184005	2.0921167921	2.9412	2.7516
3f	2.2282097144	2.0479652232	2.8323	2.0721
3g	2.1729844458	1.9836422818	2.7381	2.0449
3i	2.2881629833	2.0989830898	2.8947	2.2565
3j	2.2424471005	2.0669765254	2.8312	2.1733
4c	2.3069469907	2.205148412	2.911	2.3198
4d	2.4113619325	2.2594537133	3.1084	2.3869
4f	2.3311471359	2.2221813159	2.9412	2.3368
4g	2.2918894013	2.1690209092	2.8557	2.3132
5c	2.1901334595	2.0460072389	2.7975	2.0506
5d	2.2784489798	2.1135047747	2.9518	2.784
5f	2.2421596558	2.0754177338	2.841	2.0931
5g	2.1588320109	1.9530407011	2.7248	1.9833
5i	2.295658158	2.1256988984	2.9096	2.2756
5j	2.248869192	2.0725921444	2.8371	2.618
8c	2.074733482	1.3605294123	2.5745	1.3028
8d	2.1044591383	1.4391190434	2.6642	1.4847
8f	2.0871535587	1.4000179702	2.6108	1.361
8g	2.046402361	1.3583134695	2.5373	1.3426
8i	2.1311671808	1.4352242067	2.6691	1.4778
8j	2.1271977725	1.4277424205	2.6561	1.485

Details on computing individual electronic states:

- ^{1}PS + ^{3}O$_2$ → Used CDFT with 2 spin constraints, one on each oxygen atom. No charge and an overall multiplicity of 3
- ^{1}PS* + ^{3}O$_2$ → Initial ground state calculation with overall charge of 1 and multiplicity of 2, followed by a MOM calculation swapping orbitals 94 and 95 and using an overall charge of 0 and multiplicity of 3
- ^{3}PS + ^{3}O$_2$ → CDFT with 2 spin constraints on the oxygen molecule, 0 charge and a multiplicity of 5
- ^{1}PS* + ^{1}O$_2$ → Used ROKS with overall charge of 0 and multiplicity of 1
- ^{1}PS + ^{1}O$_2$ → Charge of 0 and multiplicity of 1
- ^{2}PS$^{\bullet+}$ + ^{2}O$_2^{\bullet-}$ → CDFT with one spin constraint on the oxygen molecule, 0 charge and a multiplicity of 3

Details on computing couplings between electronic states:

- ^{1}PS* + ^{3}O$_2$ and ^{2}PS$^{\bullet+}$ + ^{2}O$_2^{\bullet-}$ → Initial ground state calculation with charge of 1 and multiplicity of 2. CDFT and CDFT-CI constraining 1 spin and 1 charge constraint on the oxygen molecule. Also used MOM and swapped orbitals 94 and 95. Overall charge of 0 and multiplicity of 3
- ^{1}PS + ^{3}O$_2$ and ^{2}PS$^{\bullet+}$ + ^{2}O$_2^{\bullet-}$ → Initial ground state calculation with charge of 0 and multiplicity of 3. CDFT, CDFT-CI, and skipping promolecules, constraining a spin and charge of 1 on the oxygen molecule with same charge and multiplicity overall
- ^{1}PS* + ^{3}O$_2$ and ^{3}PS + ^{3}O$_2$ → Initial ground state calculation with charge of 1 and multiplicity of 2. CDFT, CDFT-CI with 2 spin constraints on the oxygen molecule. Overall charge of 0 and multiplicity of 3 for the first part of the calculation and overall charge of 0 and multiplicity of 5 for the second

- ^{1}PS + $^1O_2$ and ^{3}PS + $^3O_2$ $\rightarrow$ CDFT, and CDFT-CI with 2 spin constraints on the oxygen molecule, overall charge of 0 and multiplicity of 1 for the first part, followed by an overall charge of 0 and multiplicity of 5 for the second part of the calculation